2014

Phenomenological studies of neutrino physics

Jiajun Liao
Iowa State University

Phenomenological studies of neutrino physics

by

Jiajun Liao

A dissertation submitted to the graduate faculty

in partial fulfillment of the requirements for the degree of

DOCTOR OF PHILOSOPHY

Major: High Energy Physics

Program of Study Committee:

Kerry Whisnant, Major Professor

German Valencia

Mayly Sanchez

James Evans

Stephen Willson

Iowa State University

Ames, Iowa

2014

TABLE OF CONTENTS

LIST OF TABLES

LIST OF FIGURES

ACKNOWLEDGEMENTS

This thesis would not have been possible if not for the help of many people. In particular, I would like to thank my advisor, Kerry Whisnant, for his advice, guidance, and encouragement throughout my Ph.D. program. I was lucky to be introduced to the field of neutrino physics by reading the manuscripts of his book before publication. His constant support and insightful knowledge have been crucial to the progression of my research, especially during difficult times. In addition, I am grateful that I can find him in his office ready for discussion at almost any time. I believe these interesting discussions that are related or unrelated to physics would be a great source of inspiration in the future.

I would also like to give special thanks to my collaborators, Danny Marfatia and Vernon Barger, for their valuable collaboration and helpful recommendations. I am also grateful to the rest of committee, German Valencia, Mayly Sanchez, James Evans, Stephen Willson for reading the thesis and helpful suggestions, and especially I would like to thank German Valencia for writing recommendation letters and Mayly Sanchez for teaching me experimental knowledge of neutrinos.

Last but not least, I am thankful to my friends and family members for their help and support over the past years. I would like to dedicate this thesis to my parents, Yueguang Liao and Guilian Ning, for their sacrifice and faith in raising me.

ABSTRACT

In this thesis, we studied the phenomenological results of several classes of neutrino models. We begin with an investigation of the effect of small perturbations on the $\mu - \tau$ symmetrical models. We found that since m_1 and m_2 are nearly degenerate, $\mu-\tau$ symmetry mixing scenarios are able to explain the experimental data with about the same size perturbation for most values of θ_{12}. This suggests that the underlying unperturbed mixing need not have θ_{12} close to the experimentally preferred value.

Then we studied a simple case of type I seesaw model that have four texture zeros in the Yukawa couplings matrix, which is equivalent to a single texture or cofactor zero for an off-diagonal element of the light neutrino mass matrix M in the context of low energy phenomenology. Furthermore we studied a variety of neutrino models that have one or two texture and/or cofactor zeros. We determined the constraints in the space of the CP phase and lightest neutrino mass using a global fit to neutrino parameters, including recent data on θ_{13}. We used leptogenesis to further constrain the parameter space for the seesaw models with four zeros in the Yukawa matrix, and made predictions on neutrinoless double beta decay for these models.

Finally we showed that any neutrino model with a homogeneous relationship among elements of the light neutrino mass matrix with one mass hierarchy predicts oscillation parameters and Majorana phases similar to those of models with the same homogeneous relationship among cofactors of the mass matrix with the opposite mass hierarchy if the lightest mass is not too small, e.g., less than about 20 meV. This general result applies to texture and/or cofactor zero models, scaling models, and models that have two equal mass matrix elements or cofactors, e.g. $\mu - \tau$ symmetric models.

CHAPTER 1. INTRODUCTION TO NEUTRINO PHYSICS

1.1 The Standard Model

Since the beginning of particle physics, physicists have had a strong desire to find an underlying symmetry that can describe all the fundamental particles and their interactions. This goal is partially accomplished by the building of the standard model (SM), which took a lot of hard work by many particle physicists in the last five decades. The building of the SM started in 1961, when Glashow [1] first proposed $SU(2) \otimes U(1)$ as the underlying symmetry to unify the electromagnetic and weak interactions. After that, three groups [2, 3, 4] in 1964 independently proposed the Higgs mechanism to explain the non-zero masses of the gauge bosons via spontaneous symmetry breaking. Applying the Higgs mechanism, Weinberg [5] in 1967 and Salam [6] in 1968 proposed the $SU(2)_L \otimes U(1)_Y$ theory of leptons in its modern form. In 1970, Glashow, Iliopoulos and Maiani [7] extended the $SU(2)_L \otimes U(1)_Y$ theory to the quark sector. They explained why flavor-changing neutral currents (FCNCs) are highly suppressed and predicted the existence of charm quarks. In 1972, 't Hooft and Veltman [8] proved that this theory can be renormalized under spontaneous symmetry breaking. In 1973, Gross, Wilczek [9] and Politzer [10] discovered asymptotic freedom of the strong interactions under the symmetry of $SU(3)_C$. Based on the gauge group $SU(3)_C \otimes SU(2)_L \otimes U(1)_Y$ the standard model was born and achieved enormous success in both theoretical and experimental physics. It is one of the most successful theories in history because many of its predictions have been verified by experiments, which includes the gluon [11], W [12] and Z [13] bosons; the charm [14], bottom [15], and top [16] quarks; and most recently the Higgs boson [17].

The standard model is a quantum field theory that is under the symmetry of the SM gauge group: $SU(3)_C \otimes SU(2)_L \otimes U(1)_Y$. It contains three different classes of fields: the gauge fields,

the fermionic fields and a complex scalar field. The gauge fields mediate the strong and electroweak interactions and are related to the SM gauge group; see Table 1.1. The fermionic fields generate matter particles, and can be separated into two types: the quarks q_L, u_R, d_R and the leptons l_L, e_R, where L(R) indicates the left (right) chiral projections $\psi_{L(R)} \equiv (1 \mp \gamma_5)\psi/2$. Each fermionic field also contains three generations, e.g., $u = (u, c, t)^T$, $d = (d, s, b)^T$ and $e = (e, \mu, \tau)^T$ respectively. The complex scalar field ϕ is responsible for the masses of all particles via the Higgs mechanism [2, 3, 4], hence it is also called the Higgs field. Both the Higgs field and the fermionic fields are assigned into an irreducible representation of the SM gauge group as shown in Table 1.2.

Table 1.1 Notations for the SM gauge group $SU(3)_C \otimes SU(2)_L \otimes U(1)_Y$. λ_i are the Gell-Mann matrices, τ_j are the Pauli matrices and q_Y is $U(1)$ hypercharge.

gauge group	coupling constant	generator	gauge field
$SU(3)_C$	g_s	$\frac{\lambda_i}{2}$ $(i = 1, ..., 8)$	G^i_μ
$SU(2)_L$	g	$\frac{\tau_j}{2}$ $(j = 1, 2, 3)$	W^j_μ
$U(1)_Y$	g'	q_Y	B_μ

Table 1.2 The Higgs and fermionic fields of the SM with their corresponding representations of the gauge group $SU(3)_C \otimes SU(2)_L$ and charges of $U(1)_Y$.

gauge group	ϕ	$q_L = \binom{u_L}{d_L}$	u_R	d_R	$l_L = \binom{\nu_{eL}}{e_L}$	e_R
$SU(3)_C$	**1**	**3**	**3**	**3**	**1**	**1**
$SU(2)_L$	**2**	**2**	**1**	**1**	**2**	**1**
q_Y	$+1$	$+\frac{1}{3}$	$+\frac{4}{3}$	$-\frac{2}{3}$	-1	-2

The dynamics of the SM fields is determined by the SM Lagrangian density, which can be written in three parts

$$\mathcal{L}_{SM} = \mathcal{L}_{YM} + \mathcal{L}_{Higgs} + \mathcal{L}_{Yukawa}. \tag{1.1}$$

The Yang-Mills (YM) Lagrangian is

$$\mathcal{L}_{YM} = \overline{\psi} i\gamma^\mu D_\mu \psi - \frac{1}{4} F^i_{\mu\nu} F_i^{\mu\nu}, \tag{1.2}$$

where ψ includes all fermionic fields, D_μ is the gauge-covariant derivative and F includes all field strength tensors. The Higgs Lagrangian is

$$\mathcal{L}_{Higgs} = (D^\mu \phi)^\dagger D_\mu \phi - V(\phi), \tag{1.3}$$

where $\phi = \begin{pmatrix} \phi^+ \\ \phi^0 \end{pmatrix}$ and $V(\phi)$ is the Higgs potential. The Yukawa Lagrangian is

$$\mathcal{L}_{Yukawa} = -\overline{u_R} Y_u \tilde{\phi}^\dagger q_L - \overline{d_R} Y_d \phi^\dagger q_L - \overline{e_R} Y_e \tilde{\phi}^\dagger l_L + h.c., \tag{1.4}$$

where $\tilde{\phi} = i\tau_2 \phi^*$ is the charge conjugate of ϕ; Y_u, Y_d and Y_e are all 3×3 matrices because both the quarks and the leptons contain three generations.

In order for the vector bosons to acquire mass, spontaneous symmetry breaking is introduced in the Higgs sector. The Higgs potential $V(\phi)$ can have the following most general renormalizable form

$$V(\phi) = \mu^2(\phi^\dagger \phi) + \lambda(\phi^\dagger \phi)^2, \tag{1.5}$$

where the sign of μ^2 is not restricted, but $\lambda > 0$ is required by vacuum stability. Consider $\mu^2 < 0$, minimization of the Higgs potential Eq. 1.5 yields the vacuum expectation value (VEV) of the complex scalar field to be $\langle \phi \rangle_0 = \begin{pmatrix} 0 \\ v/\sqrt{2} \end{pmatrix}$ with $v = \sqrt{-\mu^2/\lambda}$.

The spontaneous symmetry breaking, $\phi \to \phi' = \frac{1}{\sqrt{2}} \begin{pmatrix} 0 \\ v+H \end{pmatrix}$, leads to three main consequences. Firstly, the Higgs Lagrangian becomes

$$\mathcal{L}_{Higgs} \to M_W^2 W^{\mu+} W_\mu^- + \frac{1}{2} M_Z^2 Z^\mu Z_\mu - \frac{\mu^4}{4\lambda} + H \text{ terms}, \tag{1.6}$$

where $W^\pm = \frac{1}{\sqrt{2}}(W^1 \mp iW^2)$ and $Z = -\sin\theta_W B + \cos\theta_W W^3$ are the W and Z gauge bosons, respectively; the Weinberg angle θ_W is defined by $\tan\theta_W \equiv \frac{g'}{g}$. The W and Z bosons gain masses $M_W = \frac{gv}{2}$ and $M_Z = \sqrt{g^2 + g'^2}\frac{v}{2}$ after the spontaneous symmetry breaking, while the photon field $A = \cos\theta_W B + \sin\theta_W W^3$ remain massless.

Secondly, the gauge interactions in the $\mathcal{L}_{YM}$ are transformed into the quantum electrodynamics (QED) interactions that involve photons, the weak charge current (CC) interactions that involve W bosons and the weak neutral current (NC) interactions that involve Z bosons. The Lagrangian density of the QED interaction is

$$\mathcal{L}_{QED} = -\frac{gg'}{\sqrt{g^2 + g'^2}} J_Q^\mu A_\mu, \tag{1.7}$$

where

$$J_Q^\mu = \frac{2}{3}(\bar{u}\ \bar{c}\ \bar{t})\gamma^\mu \begin{pmatrix} u \\ c \\ t \end{pmatrix} - \frac{1}{3}(\bar{d}\ \bar{s}\ \bar{b})\gamma^\mu \begin{pmatrix} d \\ s \\ b \end{pmatrix} - (\bar{e}\ \bar{\mu}\ \bar{\tau})\gamma^\mu \begin{pmatrix} e \\ \mu \\ \tau \end{pmatrix}. \tag{1.8}$$

The weak CC and NC interactions are given by

$$\mathcal{L}_{CC} = -\frac{g}{2\sqrt{2}} J_W^\mu W_\mu^- + h.c., \tag{1.9}$$

and

$$\mathcal{L}_{NC} = -\frac{g}{4\cos\theta_W} J_Z^\mu Z_\mu, \tag{1.10}$$

where

$$J_W^\mu = (\bar{\nu}_e\ \bar{\nu}_\mu\ \bar{\nu}_\tau)\gamma^\mu(1-\gamma^5)\begin{pmatrix} e \\ \mu \\ \tau \end{pmatrix} + (\bar{u}\ \bar{c}\ \bar{t})\gamma^\mu(1-\gamma^5)V_q\begin{pmatrix} d \\ s \\ b \end{pmatrix}, \tag{1.11}$$

$$\begin{aligned} J_Z^\mu = {} & (\bar{u}\ \bar{c}\ \bar{t})\gamma^\mu(1-\gamma^5)\begin{pmatrix} u \\ c \\ t \end{pmatrix} - (\bar{d}\ \bar{s}\ \bar{b})\gamma^\mu(1-\gamma^5)\begin{pmatrix} d \\ s \\ b \end{pmatrix} \\ & + (\bar{\nu_e}\ \bar{\nu_\mu}\ \bar{\nu_\tau})\gamma^\mu(1-\gamma^5)\begin{pmatrix} \nu_e \\ \nu_\mu \\ \nu_\tau \end{pmatrix} - (\bar{e}\ \bar{\mu}\ \bar{\tau})\gamma^\mu(1-\gamma^5)\begin{pmatrix} e \\ \mu \\ \tau \end{pmatrix} - 4\sin^2\theta_W J_Q^\mu, \end{aligned} \tag{1.12}$$

and V_q is the Cabibbo-Kobayashi-Maskawa (CKM) matrix.

Thirdly, the fermionic fields also obtain masses through the Yukawa interaction,

$$\mathcal{L}_{Yukawa} \to -\overline{u_R} M_u u_L - \overline{d_R} M_d d_L - \overline{e_R} M_e e_L + h.c. + H \text{ terms}, \tag{1.13}$$

where the mass matrices are

$$M_u = \frac{v}{\sqrt{2}} Y_u,\ M_d = \frac{v}{\sqrt{2}} Y_d, \text{ and } M_e = \frac{v}{\sqrt{2}} Y_e. \tag{1.14}$$

Because the right-handed (RH) neutrinos do not exist in the SM, neutrinos has no mass in the standard model.

1.2 Beyond the Standard Model: Neutrino Oscillations

The three known neutrinos ν_e, ν_μ and ν_τ are called the flavor eigenstates because they are always produced and measured together with their corresponding partners e, μ, and τ via the charged current interactions. If all neutrinos are massless, then the flavor eigenstates ν_α are also the mass eigenstates, which means the lepton flavors will be conserved and there is no neutrino flavor oscillations. However, as we will discuss later, the existence of neutrino oscillations has been strongly supported by many experiments with solar, atmospheric, accelerator and reactor neutrinos in the last two decades.

1.2.1 Neutrino Oscillations in Vacuum

The propagation of a neutrino in the mass eigenstate $|\nu_i\rangle$ is determined by the Schrödinger's equation $i\frac{d}{dt}|\nu_i\rangle = H|\nu_i\rangle$, where $H \approx p + \frac{m^2}{2E}$ for extremely relativistic neutrinos. However, when a neutrino is produced via a CC interaction process with flavor eigenstate $|\nu_\alpha\rangle$, it is a coherent superposition of the mass eigenstates $|\nu_i\rangle$:

$$|\nu_\alpha\rangle = \sum_i U^*_{\alpha i}|\nu_i\rangle \tag{1.15}$$

where U is a unitary matrix, and is often called the PMNS matrix after the authors of Ref. [18]. Similarly, for an antineutrino produced in a CC interaction process with a flavor eigenstate $|\bar{\nu}_\alpha\rangle$, we have

$$|\bar{\nu}_\alpha\rangle = \sum_i U_{\alpha i}|\bar{\nu}_i\rangle \tag{1.16}$$

Then, after a time t, the evolution of the initial flavor eigenstate has

$$|\nu_\alpha(t)\rangle = \sum_i U^*_{\alpha i}e^{-iE_it}|\nu_i\rangle \approx e^{-ipt}\sum_i U^*_{\alpha i}e^{-i\frac{m_i^2}{2E}t}|\nu_i\rangle. \tag{1.17}$$

When a neutrino is observed by a neutrino detector, it is also measured by a CC interaction process with a flavor eigenstate $|\nu_\beta\rangle$. The amplitude of observing a neutrino with flavor eigenstate $|\nu_\beta\rangle$ at time t in the original neutrino beam with flavor eigenstate $|\nu_\alpha\rangle$ is

$$\langle\nu_\beta|\nu_\alpha(t)\rangle = \sum_{ij}\langle\nu_j|U_{\beta j}U^*_{\alpha i}e^{-i\frac{m_i^2}{2E}t}|\nu_i\rangle = \sum_i U_{\beta i}U^*_{\alpha i}e^{-i\frac{m_i^2}{2E}t}. \tag{1.18}$$

Since neutrinos are extremely relativistic, the distance traveled by the neutrinos $L \approx t$, hence the probability of finding $|\nu_\beta\rangle$ at a distance L in an originally $|\nu_\alpha\rangle$ beam is

$$\begin{aligned}
P(\nu_\alpha \to \nu_\beta) &= \left|\sum_i U_{\beta i}U^*_{\alpha i}e^{-i\frac{m_i^2}{2E}L}\right|^2 = \sum_{ij} U^*_{\alpha i}U_{\beta i}U_{\alpha j}U^*_{\beta j}e^{-i\frac{\delta m_{ij}^2}{2E}L} \\
&= \sum_i |U^*_{\alpha i}U_{\beta i}|^2 + \sum_{i\neq j}\mathrm{Re}\left(U^*_{\alpha i}U_{\beta i}U_{\alpha j}U^*_{\beta j}\right)\cos\left(\frac{\delta m_{ij}^2 L}{2E}\right) \\
&+ \sum_{i\neq j}\mathrm{Im}\left(U^*_{\alpha i}U_{\beta i}U_{\alpha j}U^*_{\beta j}\right)\sin\left(\frac{\delta m_{ij}^2 L}{2E}\right) \\
&= \delta_{\alpha\beta} - 2\sum_{i\neq j}\mathrm{Re}\left(U^*_{\alpha i}U_{\beta i}U_{\alpha j}U^*_{\beta j}\right)\sin^2\Delta_{ij} + 2\sum_{i\neq j}\mathrm{Im}\left(U^*_{\alpha i}U_{\beta i}U_{\alpha j}U^*_{\beta j}\right)\sin^2\Delta_{ij},
\end{aligned} \tag{1.19}$$

where $\delta m^2_{ij} = m^2_i - m^2_j$ are the mass-squared differences, and $\Delta_{ij} = \frac{\delta m^2_{ij} L}{4E}$ are the oscillation arguments. The probabilities for antineutrino channels can be obtained by CPT conjugation. Assuming no CPT violation in ordinary neutrino oscillation, the antineutrino oscillation probabilities are $P(\bar{\nu}_\alpha \to \bar{\nu}_\beta) = P(\nu_\beta \to \nu_\alpha)$.

1.2.2 Three-neutrino Oscillations

In the SM, there are three types of neutrino flavors: ν_e, ν_μ, and ν_τ. Also, the total number of light active neutrino species is determined by studying the invisible width of the Z boson at the Large Electron Positron (LEP) collider, and the experimental value of the total number of active neutrinos is $N_\nu = 2.9840 \pm 0.0082$ [19]. So in general, we consider three-neutrino mixing and the PMNS matrix is a 3×3 unitary matrix. In the standard parametrization, the PMNS matrix can be described by

$$U = V \cdot \mathrm{diag}\left(1, e^{i\frac{\phi_2}{2}}, e^{i\frac{\phi_3}{2}}\right), \tag{1.20}$$

where

$$\begin{aligned} V &= \begin{bmatrix} 1 & 0 & 0 \\ 0 & c_{23} & s_{23} \\ 0 & -s_{23} & c_{23} \end{bmatrix} \begin{bmatrix} c_{13} & 0 & s_{13}e^{-i\delta} \\ 0 & 1 & 0 \\ -s_{13}e^{i\delta} & 0 & c_{13} \end{bmatrix} \begin{bmatrix} c_{12} & s_{12} & 0 \\ -s_{12} & c_{12} & 0 \\ 0 & 0 & 1 \end{bmatrix} \\ &= \begin{bmatrix} c_{13}c_{12} & c_{13}s_{12} & s_{13}e^{-i\delta} \\ -s_{12}c_{23} - c_{12}s_{23}s_{13}e^{i\delta} & c_{12}c_{23} - s_{12}s_{23}s_{13}e^{i\delta} & s_{23}c_{13} \\ s_{12}s_{23} - c_{12}c_{23}s_{13}e^{i\delta} & -c_{12}s_{23} - s_{12}c_{23}s_{13}e^{i\delta} & c_{23}c_{13} \end{bmatrix}, \end{aligned} \tag{1.21}$$

c_{ij}, s_{ij} denotes $\cos\theta_{ij}$, $\sin\theta_{ij}$ respectively, δ is the Dirac CP phase and ϕ_2, ϕ_3 are the two Majorana phases. Using the standard parametrization and the probability in Eq. (1.19), we can obtain the vacuum oscillation probabilities in terms of the oscillation arguments Δ_{ij}, the three mixing angles θ_{12}, θ_{23}, θ_{13} and the Dirac CP phase δ. The two Majorana phases do not affect the vacuum oscillation probabilities.

Experimental results show $|\delta m^2_{31}| \gg |\delta m^2_{21}|$, hence for the same neutrino energy and travel distance, $|\Delta_{31}| \gg |\Delta_{21}|$. For atmospheric and long-baseline neutrino oscillations, Δ_{31} is dominant, Δ_{21} is negligible, and the vacuum oscillation probabilities in the leading order approxi-

mation are [20]

$$P(\nu_e \to \nu_e) \simeq 1 - \sin^2 2\theta_{13} \sin^2 \Delta_{31}, \tag{1.22}$$

$$P(\nu_e \to \nu_\mu) \simeq s_{23}^2 \sin^2 2\theta_{13} \sin^2 \Delta_{31}, \tag{1.23}$$

$$P(\nu_\mu \to \nu_\mu) \simeq 1 - (c_{13}^4 \sin^2 2\theta_{23} + s_{23} \sin^2 2\theta_{13}) \sin^2 \Delta_{31}, \tag{1.24}$$

$$P(\nu_\mu \to \nu_\tau) \simeq c_{13}^4 \sin^2 2\theta_{23} \sin^2 \Delta_{31}. \tag{1.25}$$

For reactor neutrinos, the $\bar{\nu}_e$ survival probability is approximately

$$P(\bar{\nu}_e \to \bar{\nu}_e) \simeq 1 - \sin^2 2\theta_{13} \sin^2 \Delta_{31} - c_{13}^4 \sin^2 2\theta_{12} \sin^2 \Delta_{21}. \tag{1.26}$$

From the above oscillation probabilities, we can see in the limit $\theta_{13} \to 0$, the atmospheric/long-baseline neutrino oscillation and the solar/reactor neutrino oscillation completely decouple and each is reduced to the form of 2-neutrino oscillation. Also, if θ_{13} is very small, it is difficult to resolve the sign of δm_{31}^2 and the quadrant of θ_{23}.

1.2.3 Neutrino Oscillations in Matter

When neutrinos travel through matter, ν_e interacts with the matter constituents via both neutral and charged currents, whereas ν_μ and ν_τ interact only via the neutral currents (NC), therefore their propagation in matter is affected by coherent forward scattering, as first shown by Wolfenstein [21]. Barger, Whisnant, Pakvasa and Phillips [22] studied the matter effect in long-base neutrino experiments on earth, and found the oscillation amplitude and wavelength in matter could be resonantly enhanced by the matter effect. Mikheyev and Smirnov [23] applied the enhancement to the propagation of solar neutrinos in the Sun, and provided the most likely solution to the solar neutrino puzzle. The matter effect due to coherent forward scattering can be described by an effective potential [24]. For the CC process, the low-energy Hamiltonian density can be described by the effective four-fermion interaction term

$$\begin{aligned} \mathcal{H}_{CC} &= \frac{G_F}{\sqrt{2}} [\bar{\nu}_e(x)\gamma^\mu(1-\gamma^5)e(x)][\bar{e}(x)\gamma_\mu(1-\gamma^5)\nu_e(x)] \\ &= -\frac{G_F}{\sqrt{2}} [\bar{\nu}_e(x)\gamma^\mu(1-\gamma^5)\nu_e(x)][\bar{e}(x)\gamma_\mu(1-\gamma^5)e(x)], \end{aligned} \tag{1.27}$$

where we used a Fierz transformation in the above equation. For simplicity, we assume that the background electrons are thermally distributed and unpolarized, then the electron degrees of freedom can be integrated out as

$$\begin{aligned}\overline{\mathcal{H}}_{CC} &= \frac{G_F}{\sqrt{2}}[\bar{\nu}_e(x)\gamma^\mu(1-\gamma^5)\nu_e(x)] \\ &\times \frac{1}{2}\sum_s \int \frac{d^3\mathbf{p}}{(2\pi)^3} g_e f(p,T)\langle e(\mathbf{p},s)|\bar{e}(x)\gamma_\mu(1-\gamma^5)e(x)|e(\mathbf{p},s)\rangle \\ &= \frac{G_F}{\sqrt{2}}N_e[\bar{\nu}_e(x)\gamma^0(1-\gamma^5)\nu_e(x)] = \sqrt{2}G_F N_e \bar{\nu}_e(x)\gamma^0 P_L \nu_e(x), \end{aligned} \tag{1.28}$$

where g_e is the internal degree of freedom, $f(p,T)$ is the distribution function of electrons and N_e is the electron number density. Therefore, the left-handed electron neutrinos propagating in matter receive an extra effective potential:

$$\mathcal{V}_{CC} = \int \frac{d^3\mathbf{p}}{(2\pi)^3}\frac{d^3\mathbf{x}}{2E_\mathbf{p}}\langle \nu_{eL}(\mathbf{p},s)|\overline{\mathcal{H}}_{CC}|\nu_{eL}(\mathbf{p},s)\rangle = \sqrt{2}G_F N_e. \tag{1.29}$$

Note that for electron anti-neutrinos, the integral above will differ by a sign, i.e., the effective potential for $\bar{\nu}_e$ is $-\sqrt{2}G_F N_e$.

For the NC, we can find the effective potential in a similar way for ν_x $(x = e, \mu, \tau)$, which is [25]

$$\mathcal{V}_{NC} = \sqrt{2}G_F \sum_f n_f \left[I_{3L}^f - 2\sin^2\theta_W Q^f\right], \tag{1.30}$$

where f stands for electron, proton and neutron, Q^f is the charge of f and I_{3L}^f is the third component of the weak isospin of left-chiral projection of f. Since for protons, $Q = 1$ and $I_{3L} = \frac{1}{2}$, whereas for electrons, $Q = -1$ and $I_{3L} = -\frac{1}{2}$, the NC potential of neutrinos with electrons and protons cancel and only the neutron contribution is left in ordinary neutral matter,

$$\mathcal{V}_{NC} = -\sqrt{2}G_F N_n/2, \tag{1.31}$$

where N_n is the neutron number density. Therefore, for three-neutrino propagating in matter, the Hamiltonian in the flavor basis can be written as

$$\mathcal{H} = p + \frac{1}{2E}UM^2U^\dagger + \mathcal{V}_{CC} + \mathcal{V}_{NC}, \tag{1.32}$$

where $M = \mathrm{diag}(m_1, m_2, m_3)$, E is the energy of neutrinos and U is the neutrino vacuum mixing matrix. Note that the NC contributions are the same for all active neutrino flavors and

the CC contribution only affects electron neutrinos, therefore for three-neutrino oscillations, the matter effect can be represented by adding an extra term

$$A = 2\sqrt{2}G_F N_e E, \tag{1.33}$$

to the $\nu_e - \nu_e$ element of $UM^2U^\dagger$. For anti-neutrinos, a term of

$$A = -2\sqrt{2}G_F N_e E \tag{1.34}$$

is added to the $\nu_e - \nu_e$ element of $UM^2U^\dagger$.

1.3 Neutrino Oscillation Experiments

There are many neutrino oscillation experiments that have been done in the last five decades, here I will focus on some recent experiments, especially those that contribute to the latest global-fit data.

1.3.1 Solar Neutrino Experiments

The first indication of neutrino oscillations came from the measurement of solar neutrinos. Solar neutrinos are an essential byproduct in the chains of fusion reactions in the Sun. The main process is called the *pp* chain, which accounts for 86% of the solar neutrinos. The *pp* chain contains two reactions that produce neutrinos: the *pp* reaction and the *pep* reaction, which are

$$\begin{aligned} p + p &\rightarrow ({}^2\mathrm{H})^+ + e^+ + \nu_e (\leq 0.42 \text{ MeV}) \\ p + e^- + p &\rightarrow ({}^2\mathrm{H})^+ + \nu_e (1.44 \text{ MeV}), \end{aligned} \tag{1.35}$$

where the neutrino energy is shown in the parentheses. A secondary process is called the *hep* chain that contributes about 14% of the neutrino flux. In the *hep* chain, the reactions that producing neutrinos are

$$\begin{aligned} {}^3\mathrm{He} + p &\rightarrow {}^4\mathrm{He} + e^+ + \nu_e (\leq 18.77 \text{ MeV}) \\ {}^7\mathrm{Be} + e^- &\rightarrow {}^7\mathrm{Li} + \nu_e (0.861 \text{ MeV}). \end{aligned} \tag{1.36}$$

A tertiary process that produce 0.11% of solar neutrinos are using ^{8}B produced in the *hep* chain:

$$^8\mathrm{B} \to {}^8\mathrm{Be} + e^+ + \gamma + \nu_e (\leq 14.06 \text{ MeV}) \tag{1.37}$$

Also, there are neutrinos created in the CNO cycle:

$$\begin{aligned} ^{13}\mathrm{N} &\to {}^{13}\mathrm{C} + e^+ + \nu_e (\leq 1.2 \text{ MeV}) \\ ^{15}\mathrm{O} &\to {}^{15}\mathrm{N} + e^+ + \nu_e (\leq 1.73 \text{ MeV}) \\ ^{17}\mathrm{F} &\to {}^{17}\mathrm{O} + e^+ + \nu_e (\leq 1.74 \text{ MeV}). \end{aligned} \tag{1.38}$$

The CNO cycle dominates over the *pp* chain only if the temperature exceeds 1.8×10^7K, which is not met in the Sun, thus the CNO cycle only accounts for 1.5% of the solar neutrino fluxes.

Based on the above nuclear reactions, the solar neutrino fluxes can be calculated in the Standard Solar Model (SSM) [26]. The first experiment to detect the solar neutrinos was proposed by Raymond Davis, Jr. [27] in 1964 at the Homestake Mine in South Dakota, USA. The result shows that the observed number of neutrinos is a factor of two to three times below the predictions of the SSM [28]. This surprising result kicked off decades long experiments of exploring solar neutrinos. Up to now, the ^{37}Cl [29], Super-K [30] and SNO [31] experiments measured the high energy neutrinos ($E \gtrsim 5$ MeV) from the ^{8}B process; the Borexino [32] and ^{37}Cl experiment measured the intermediate energy neutrinos from the ^{7}Be process, the *pep* process and the CNO cycle; the SAGE[33], GALLEX [34] and GNO [35] experiments mainly measured the low energy neutrinos from the *pp* reaction. They all confirm that there was a deficiency of 1/3 to 1/2 in the measured solar neutrino fluxes relative to the SSM predictions. Especially, the SNO experiment measured both the combined flux of all three neutrinos from the NC process and the ν_e flux from the CC process, a comparison between them show that the discrepancies of solar neutrinos exist without the calculations in the SSM [36].

The deficiency of solar neutrino fluxes can be explained by neutrino oscillation in the Sun. Consider two-neutrino propagation in matter [22]

$$i\frac{d}{dt}\begin{pmatrix}\nu_e \\ \nu_\mu\end{pmatrix} = \frac{1}{2E}\begin{pmatrix} m_1^2\cos^2\theta + m_2^2\sin^2\theta + A & \delta m^2 \sin\theta\cos\theta \\ \delta m^2\sin\theta\cos\theta & m_1^2\sin^2\theta + m_2^2\cos^2\theta \end{pmatrix}\begin{pmatrix}\nu_e \\ \nu_\mu\end{pmatrix}, \tag{1.39}$$

where $\delta m^2 = m_2^2 - m_1^2$, θ is the vacuum mixing angle, and the matter effect term $A = 2\sqrt{2}G_F N_e E$. The instantaneous eigenstates in matter is related with the flavor eigenstates by a unitary mixing matrix,

$$\begin{pmatrix} \nu_{1m} \\ \nu_{2m} \end{pmatrix} = \begin{pmatrix} \cos\theta_m & -\sin\theta_m \\ \sin\theta_m & \cos\theta_m \end{pmatrix} \begin{pmatrix} \nu_e \\ \nu_\mu \end{pmatrix} \tag{1.40}$$

where the effective mixing angle can be obtained by diagonalizing the Hamiltonian in Eq. (1.39),

$$\sin^2 2\theta_m = \frac{\delta m^2 \sin^2 2\theta}{(\delta m^2 \cos 2\theta - A)^2 + \delta m^2 \sin^2 2\theta}. \tag{1.41}$$

Note that the oscillation amplitude above can be enhanced if $\delta m^2 \cos 2\theta > 0$ and a resonance can occur at a critical density. The instantaneous states depend on the electron density N_e and therefore change as the solar neutrinos propagate through the Sun. Since the electron density in the Sun changes very slowly, an electron neutrino created in the Sun can undergo an adiabatic transition, the oscillation probability measured on Earth is

$$\langle P(\nu_e \to \nu_e) \rangle = \frac{1}{2}(1 + \cos 2\theta \cos 2\theta_m^0), \tag{1.42}$$

where θ_m^0 is dependent on the electron density N_e^0 when the neutrino is created, i.e.,

$$\cos 2\theta_m^0 = \frac{\delta m^2 \cos 2\theta - A}{\sqrt{(\delta m^2 \cos 2\theta - A)^2 + \delta m^2 \sin^2 2\theta}}. \tag{1.43}$$

From Eq. (1.42), we can see even for a small vacuum mixing angle, a large depletion is still possible if the neutrinos are created above the resonance density. This is known as MSW effect [23], and can explain the results of solar neutrino experiments very well; see Fig. 1.1.

1.3.2 Atmospheric/Accelerator Neutrino Experiments

The atmospheric neutrinos came from the decay products of pions and kaons, which are produced when the cosmic rays collide with the atmosphere:

$$\begin{aligned} &\pi^+, K^+ \to \mu^+ \nu_\mu \to e^+ \nu_e \bar{\nu}_\mu \nu_\mu \\ &\pi^-, K^- \to \mu^- \bar{\nu}_\mu \to e^- \bar{\nu}_e \nu_\mu \bar{\nu}_\mu. \end{aligned} \tag{1.44}$$

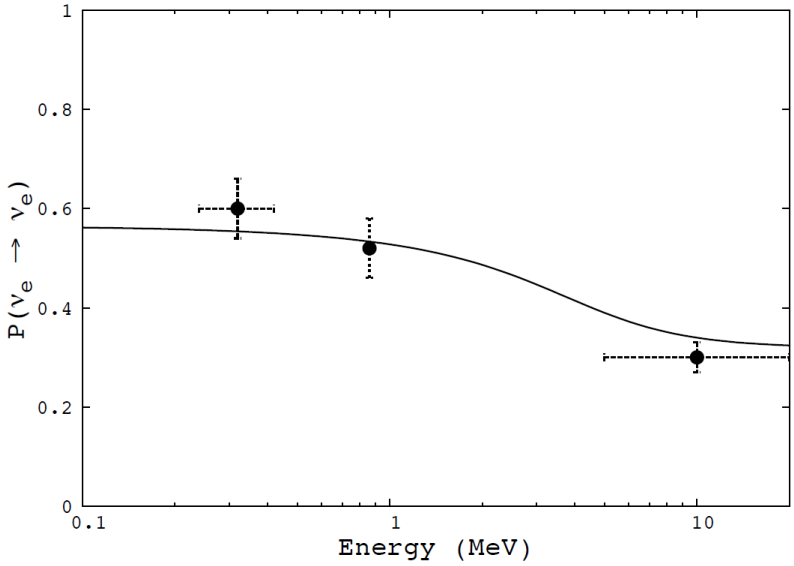

Figure 1.1 ν_e survival probability versus energy from solar neutrino experiments. The rightmost data point comes from SNO, the central data point comes from Borexino, and leftmost data point is infered from combined data of SNO and Borexino. The solid line corresponds to best-fit with $\delta m^2 = 7.6 \times 10^{-5}$ eV^2 and $\sin^2 2\theta_{12} = 0.87$. From Ref. [20].

The atmospheric neutrino flux has been well studied. The ν_μ flux in atmospheric neutrinos is about twice as large as the ν_e flux at $E_\nu = 1$ GeV, and there are much less neutrinos for $E_\nu \gtrsim 1$ GeV.

It is the study of atmospheric neutrinos by the Super-Kamiokande (Super-K) experiment in 1998 that provides the first compelling evidence for neutrino oscillations [30]. They measured the ν_e and ν_μ fluxes at different zenith angles that correspond to different path lengths L varying from 10-30 km for downward neutrinos to 12000 km for upward neutrinos, and found there was significant depletion of muon neutrinos. In 2004, the Super-K collaboration shows the result of the muon neutrino survival probability versus L/E; see Fig. 1.2. They found a dip at $L/E \approx 500$ km/GeV in the L/E distribution, which favors the explanation of neutrino oscillation when compared to neutrino decay and neutrino decoherence [37].

Since the pions and kaons are also produced in an accelerator when protons are smashed into a fixed target, the neutrino oscillations seen in the atmospheric experiments should be also observed independently in accelerator neutrino experiments. This has been confirmed

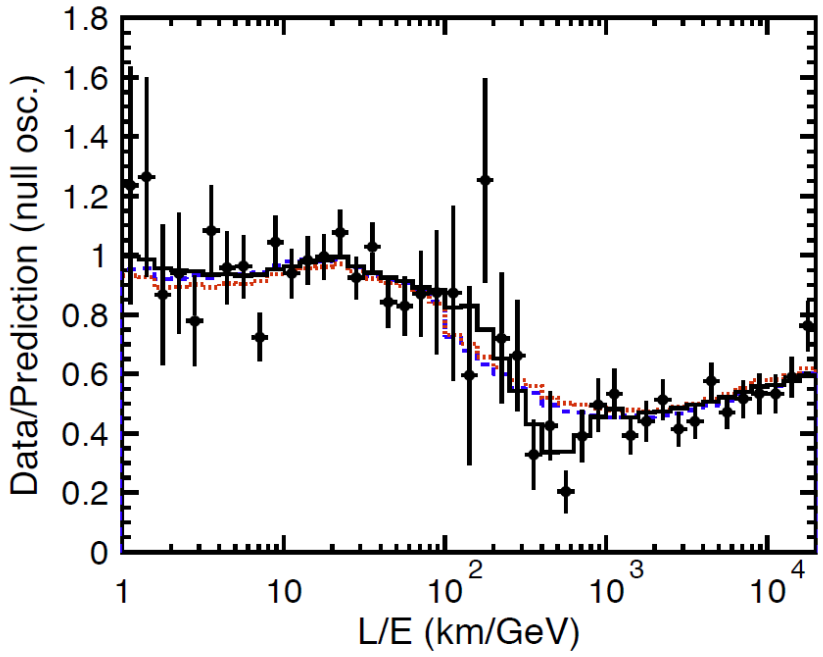

Figure 1.2 Atomospheric Muon neutrino survival propobility versus L/E in the Super-K experiment. The solid line corrsponds to the best-fit expection for two-neutrino oscillation, and the dashed (dotted) line conrresponds to the best-fits for neutrino decay (decoherence). From Ref. [37].

by three different accelerator neutrino experiments: K2K [38] and T2K [39] in Japan and MINOS [40] in the United States. The results of the three accelerator experiments are not only consistent with that of the atmospheric neutrino Super-K experiment, but also complementary to it. The long-baseline experiments, especially the MINOS experiment, have a more precise measurement of δm^2_{31}, while the atmospheric experiment Super-K has a better constraint on $\sin^2 2\theta_{23}$. A recent results from MINOS is shown in Fig. 1.3. Assuming CPT invariance, the neutrino and antineutrino oscillation parameters are identical in the leading order. The best-fits for two-neutrino oscillation parameters to the MINOS data are [41]:

$$|\Delta m^2| = (2.41^{+0.09}_{-0.10}) \times 10^{-3}\text{eV}^2, \;\; \sin^2(2\theta) = 0.950^{+0.035}_{-0.036}. \tag{1.45}$$

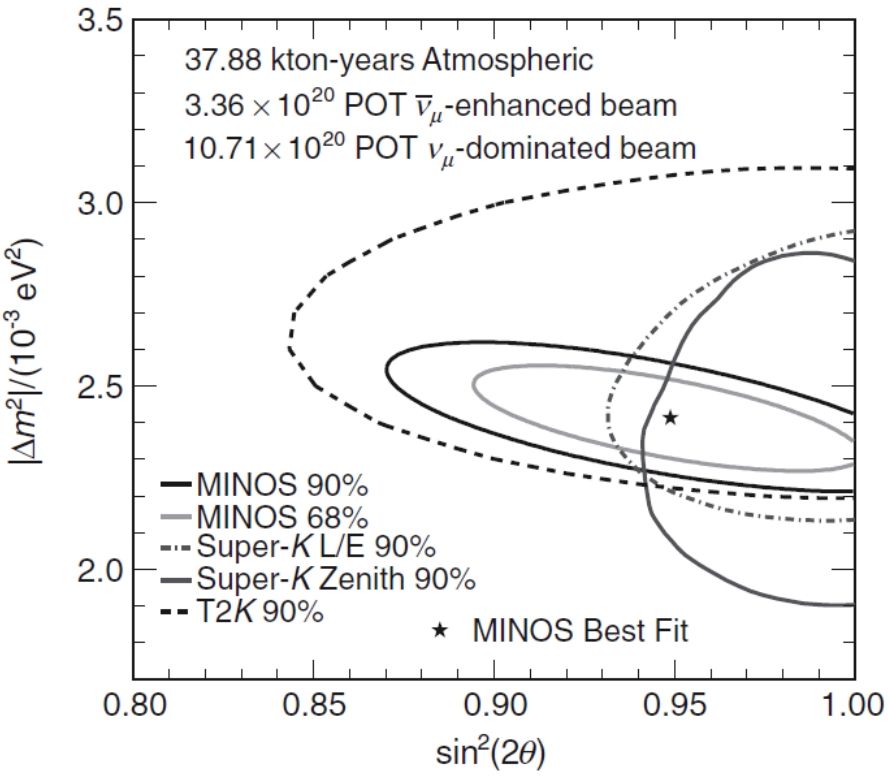

Figure 1.3 Allowed regions of Δm^2 and $\sin^2(2\theta)$ for two-neutrino oscillation. The neutrino and antineutrino oscillations are assumed to be identical. From Ref. [41].

1.3.3 Reactor Neutrino Experiments

The fission process in nuclear reactors is always accompanied by a large amount of low energy $\bar{\nu}_e$ through beta decays, e.g., a thermal power reactor with 1-MW produces about 2×10^{17} $\bar{\nu}_e$ per second. The energies of these antineutrinos peaks at 2 MeV and extend up to about 9 MeV, thus the reactors can be used as natural and cheap sources for studying the oscillation of $\bar{\nu}_e$. The measured reaction used most often is inverse beta decay:

$$\bar{\nu}_e + p \rightarrow e^+ + n. \tag{1.46}$$

Thus the reactor experiments always measure $\bar{\nu}_e$ disappearance, i.e., the measured $\bar{\nu}_e$ flux compared to the expected flux from the reactor at the detector's location. In the context of three neutrino oscillations, the $\bar{\nu}_e$ survival probability is given in Eq. 1.26.

According to the average distance from the reactors, the reactor neutrino oscillation exper-

iments can be classified into two types. For short-baseline experiments where the detectors are close to the reactor, since $|\Delta_{31}| \gg |\Delta_{21}|$, the survival probability becomes sensitive to θ_{13}, i.e.,

$$P(\bar{\nu}_e \to \bar{\nu}_e) \simeq 1 - \sin^2 2\theta_{13} \sin^2 \Delta_{31}. \tag{1.47}$$

Most short-baseline experiments observed no oscillation signal [42], which placed an upper bound on θ_{13}. A recent null result is the CHOOZ reactor experiment, which has $L \sim 1000$m and $E_\nu \sim 3$ MeV, it placed a 90% C.L. upper bound of $\sin^2 2\theta_{13} < 0.16$ for $\delta m^2_{31} = 2.4 \times 10^{-3}$ eV^2 [43].

For long-baseline experiment, such as KamLAND experiment, the terms involving Δ_{31} average $\frac{1}{2}$ over a complete cycle, in the case when θ_{13} is very small, the survival probability is similar to that of two-neutrino oscillation,

$$P(\bar{\nu}_e \to \bar{\nu}_e) \simeq 1 - \sin^2 2\theta_{12} \sin^2 \Delta_{21}. \tag{1.48}$$

The results from KamLAND show a spectral distortion in the energy spectrum and exhibit a spectacular oscillatory behavior; see Fig. 1.4. The best-fit oscillation parameters to the KamLAND data are consistent with the solar result. The solar data provides a very good measurement of θ_{12}, while KamLAND does better in determining δm^2_{21}. Combining KamLAND and solar data, we can get the best-fit of parameters [45]

$$\delta m^2_{21} = 7.59^{+0.20}_{-0.21} \times 10^{-5}\text{eV}^2, \;\; \tan^2\theta_{12} = 0.457^{+0.041}_{-0.028}. \tag{1.49}$$

Because of the null oscillation results from short baseline experiments, θ_{13} is believed to be very small compared to the large mixing angle θ_{12} and θ_{23}. Some theorists even believed $\theta_{13} = 0$ because many models predict a zero mixing angle. The situation has changed rapidly in the last three years. First in 2011, a nonzero value of θ_{13} is indicated from three different collaborations: T2K [39], MINOS [46], and Double Chooz [47] experiments. Then in early 2012, two reactor experiments Daya Bay [48] and RENO [49] conformed a nonzero measurement of θ_{13} independently. Especially, Daya Bay results show $\theta_{13} \neq 0$ at the 5.2σ level. A recent result from Daya Bay experiments exhibits a spectral distortion in the $\bar{\nu}_e$ survival probability; see Fig. 1.5. The best-fit to the Daya Bay data yields the first direct measurement of the $\bar{\nu}_e$

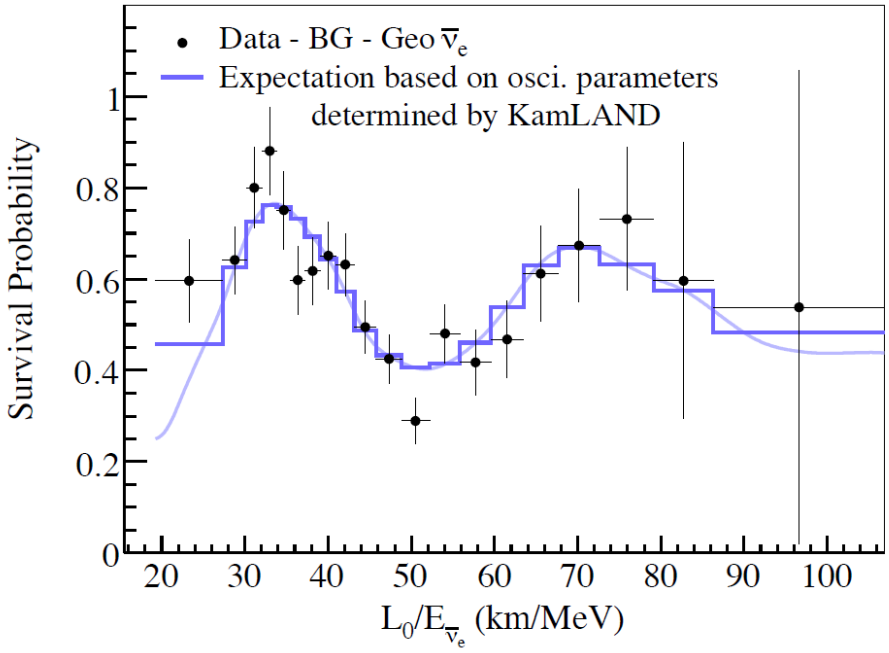

Figure 1.4 $\bar{\nu}_e$ survival probability versus $L_0/E_{\bar{\nu}}$ in KamLAND experiment. From Ref. [44].

mass-squared difference and the most precise estimate of θ_{13} [50]:

$$\Delta m^2_{ee} = 2.59^{+0.19}_{-0.20} \times 10^{-3}\text{eV}^2, \;\; \sin^2 2\theta_{13} = 0.090^{+0.008}_{-0.009}, \tag{1.50}$$

where Δm^2_{ee} comes from the definition $\sin^2 \Delta_{ee} \equiv \cos^2\theta_{12} \sin^2 \Delta 31 + \sin^2\theta_{12} \sin^2 \Delta_{32}$, and is consistent with the effective mass-squared difference $\Delta m^2_{\mu\mu}$ measured in ν_μ disappearance of MINOS experiment [51].

1.3.4 Global Three-neutrino Fits

As we discussed before, there are six parameters that can be measured in three-neutrino oscillation experiments: three mixing angles θ_{12}, θ_{23}, θ_{13}, two mass-squared differences δm^2_{21}, δm^2_{31} and a Dirac CP phase δ. Because of some special features among these parameters, e.g., $|\delta m^2_{31}| \gg \delta m^2_{21}$ and a relatively small θ_{13}, many neutrino oscillation experiments are governed by separate parameters in the leading order. Meanwhile, each type of neutrino oscillation experiment has its speciality in determining a particular parameter, namely solar neutrino experiments in determining θ_{12}; short-baseline reactor experiments such as Double Chooz,

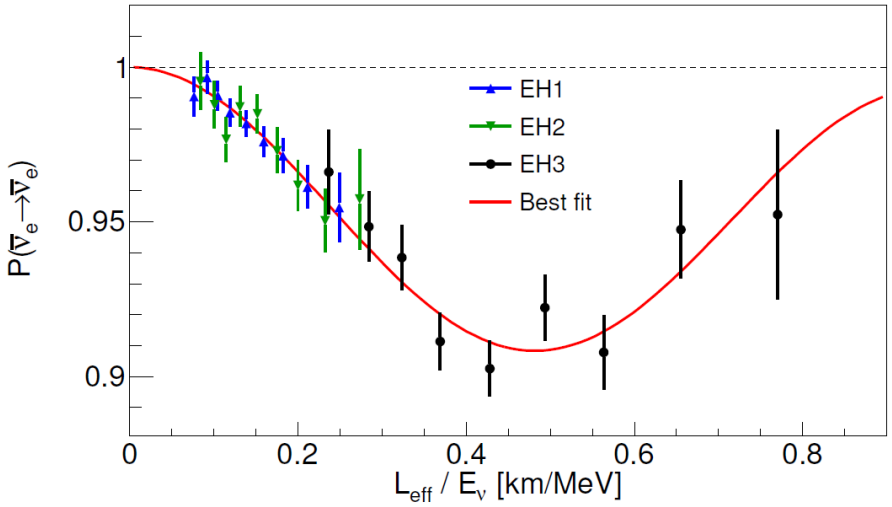

Figure 1.5 $\bar{\nu}_e$ survival probability versus $L_0/E_{\bar{\nu}}$ in Daya Bay experiment. From Ref. [50].

Daya Bay and RENO in determining θ_{13}; atmospheric neutrino experiments such as Super-K in determining θ_{23}; long-baseline reactor experiments such as KamLAND in determining δm^2_{21} and long-baseline accelerator experiments such as MINOS in determining δm^2_{31}. Therefore, a global fit to all the reliable experiments is necessary.and useful to further constrain the known parameter space. It can also provide a guidance about the unknown oscillation parameters before their experimental measurement. For example, a hint of $\sin^2\theta_{13} \sim 0.02$ was indicated by the global fit in 2008 [52], which is four years before the discovery of θ_{13} by the Daya Bay experiment.

Up to now, there is still not enough data to determine the sign of δm^2_{31}, to discriminate the octant of θ_{23} and to discover the Dirac phase δ. Since the sign of δm^2_{31} is undetermined, there are two possible mass hierarchies: the normal hierarchy (NH) and the inverted hierarchy (IH), as shown in Fig. 1.6. The normal (inverted) hierarchy is also sometimes called the normal (inverted) mass ordering. Since $|\delta m^2_{31}| \gg \delta m^2_{21}$, m_1 and m_2 are approximately degenerate, thus $\Delta m^2 = m^2_3 - (m^2_1 + m^2_2)/2$ instead of δm^2_{31} is used more often in global fits. The most recent three-neutrino global fits are shown in Table 1.3.

The three unknown quantities, the sign of Δm^2, θ_{23} octant and the Dirac phase δ, will be the main goal of the next-generation neutrino oscillation experiments. In the last section, we

will discuss the potential of future neutrino oscillation experiments, such as NOνA, LBNE and JUNO experiments.

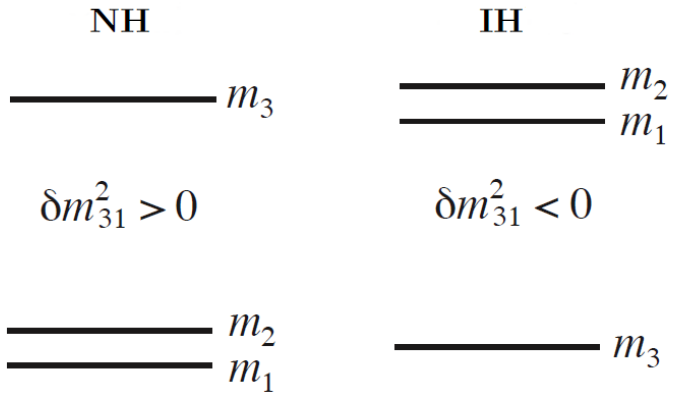

Figure 1.6 The neutrino mass spectrum in the normal mass hierarchy (left) and the inverted mass hierarchy (right).

Table 1.3 Global three-neutrino fits to the neutrino oscillation parameters. Here $\delta m^2 = m_2^2 - m_1^2$ and $\Delta m^2 = m_3^2 - (m_1^2 + m_2^2)/2$, with $\Delta m^2 > 0$ for NH and $\Delta m^2 < 0$ for IH. From Ref. [53].

Parameter	Best-fit	1σ range	2σ range	3σ range
$\delta m^2/10^{-5}\text{eV}^2$	7.54	7.32-7.80	7.15-8.00	6.99-8.18
$\sin^2\theta_{12}/10^{-1}$	3.08	2.91-3.25	2.75-3.42	2.59-3.59
$\lvert\Delta m^2\rvert/10^{-3}\text{eV}^2$ (NH)	2.43	2.37-2.49	2.30-2.55	2.23-2.61
$\lvert\Delta m^2\rvert/10^{-3}\text{eV}^2$ (IH)	2.38	2.32-2.44	2.25-2.50	2.19-2.56
$\sin^2\theta_{23}/10^{-1}$ (NH)	4.37	4.14-4.70	3.93-5.52	3.74-6.26
$\sin^2\theta_{23}/10^{-1}$ (IH)	4.55	4.24-5.94	4.00-6.20	3.80-6.41
$\sin^2\theta_{13}/10^{-2}$ (NH)	2.34	2.15-2.54	1.95-2.74	1.76-2.95
$\sin^2\theta_{13}/10^{-2}$ (IH)	2.40	2.18-2.59	1.98-2.79	1.78-2.98
δ/π (NH)	1.39	1.12-1.77	0.00-0.16 $\oplus$ 0.86-2.00	0-2.00
δ/π (IH)	1.31	0.98-1.60	0.00-0.02 $\oplus$ 0.70-2.00	0-2.00

1.4 Massive Neutrino Models

Neutrino oscillation experiments have confirmed that neutrinos are massive. However, neutrino oscillation experiments only measure the mass-squared differences, and the absolute scale of neutrino masses is still unknown, although we can get a upper bound on the sum of all

neutrinos mass from cosmology. The current 95 % C.L. upper bound on $\sum m_\nu$ from the Planck data is 0.66 eV [54]. The nonzero masses of neutrinos can be addressed by introducing right-handed neutrinos into the SM, while the smallness of the neutrino masses can be explained by the Seesaw Mechanism.

1.4.1 Dirac vs. Majorana Masses

As we know, a fermion is described by a Dirac field ψ that satisfies the Dirac equation $(i\gamma^\mu\partial_\mu - m)\psi = 0$, which can be derived from the Lagrangian density:

$$\mathcal{L} = \bar{\psi} i\gamma^\mu \partial_\mu \psi - m\bar{\psi}\psi. \tag{1.51}$$

Since the SM is based on chiral fields, we can rewrite the mass term above in terms of the chiral fields $\psi_{L,R} = \frac{1\pm\gamma^5}{2}\psi$:

$$\begin{aligned} m\bar{\psi}\psi &= m(\bar{\psi}_R\psi_L + \bar{\psi}_L\psi_R) \\ &= m(\bar{\psi}_R\psi_L + h.c.). \end{aligned} \tag{1.52}$$

This is the usual mass term that appears in Eq. 1.13 that yields the masses for quarks and charged-leptons, and it is called the Dirac mass term.

Now can we find additional possible mass terms? Since the Lagrangian has to be Lorentz-invariant, we consider multiplying one of the fields $\psi_L, \psi_R, (\psi^c)_L, (\psi^c)_R$ by one of the fields $\bar{\psi}_L, \bar{\psi}_R, \overline{(\psi^c)}_L, \overline{(\psi^c)}_R$, where $\psi^c \equiv \mathcal{C}^\dagger\psi\mathcal{C} = \mathcal{C}\bar{\psi}^T$. Note that a product with the same chiralities always vanish, and $(\psi_{L,R})^c = (\psi^c)_{R,L}$, which means $\overline{(\psi^c)_L}(\psi^c)_R = \bar{\psi}_L\psi_R$ and $\overline{(\psi^c)_R}(\psi^c)_L = \bar{\psi}_R\psi_L$, there are only six Lorentz-invariant mass terms that remain [55]: $\bar{\psi}_L\psi_R, \overline{\psi^c}_R\psi_L, \overline{\psi^c}_L\psi_R$, and $\bar{\psi}_R\psi_L, \bar{\psi}_L(\psi^c)_R, \bar{\psi}_R(\psi^c)_L$, Since for any two spinors χ and φ, $(\bar{\chi}\varphi)^\dagger = \bar{\varphi}\chi$, the six Lorentz-invariant mass terms are just $\bar{\psi}_L\psi_R, \overline{\psi^c}_R\psi_L, \overline{\psi^c}_L\psi_R$ and their hermitian conjugates. We can use them to build the most general form of the mass terms in the Lagrangian,

$$\begin{aligned} -\mathcal{L}_m &= M_D\left[\bar{\psi}_L\psi_R + h.c.\right] + \frac{M_L}{2}\left[\overline{\psi^c}_R\psi_L + h.c.\right] + \frac{M_R}{2}\left[\overline{\psi^c}_L\psi_R + h.c.\right] \\ &= M_D\left[\bar{\psi}_L\psi_R + h.c.\right] + \frac{M_L}{2}\left[\overline{(\psi_L)^c}\psi_L + h.c.\right] + \frac{M_R}{2}\left[\overline{(\psi_R)^c}\psi_R + h.c.\right], \end{aligned} \tag{1.53}$$

where we have used $(\psi_{L,R})^c = (\psi^c)_{R,L}$, M_D is the usual Dirac mass, M_L and M_R are two Majorana masses. The physical meaning of the two Majorana masses can be easily seen if we

rewrite the Lagrangian in terms of $\chi \equiv \frac{\psi_L + (\psi_L)^c}{\sqrt{2}}$ and $\eta \equiv \frac{\psi_R + (\psi_R)^c}{\sqrt{2}}$. We can verify that

$$\begin{aligned}
\bar{\chi}\chi &= \frac{1}{2}\left[\overline{(\psi_L)^c}\psi_L + h.c.\right] \\
\bar{\eta}\eta &= \frac{1}{2}\left[\overline{(\psi_R)^c}\psi_R + h.c.\right] \\
\bar{\chi}\eta &= \bar{\eta}\chi = \frac{1}{2}\left[\bar{\psi}_L\psi_R + h.c.\right].
\end{aligned} \tag{1.54}$$

Therefore, the mass terms in the Lagrangian become

$$\begin{aligned}
-\mathcal{L}_m &= M_D(\bar{\chi}\eta + \bar{\eta}\chi) + M_L\bar{\chi}\chi + M_R\bar{\eta}\eta \\
&= [\bar{\chi}\ \bar{\eta}] \begin{bmatrix} M_L & M_D \\ M_D & M_R \end{bmatrix} \begin{bmatrix} \chi \\ \eta \end{bmatrix}.
\end{aligned} \tag{1.55}$$

Since both χ and η satisfy the Majorana condition $\chi^c = \chi$ and $\eta^c = \eta$, they are called the Majorana fields and M_L and M_R are their corresponding Majorana masses. Notice that Majorana mass does not exist for quarks and charged leptons because their electric charge is not zero and their fields cannot satisfy the Majorana condition, but since neutrinos do not have any electric charge, they could have both Dirac and Majorana masses.

1.4.2 The Seesaw Mechanism

In order for the neutrinos to have Dirac masses, we introduce the RH neutrino field ν_R to the SM. Since there are three generations for the LH neutrino field, we also consider $\nu_R = (\nu_{eR}, \nu_{\mu R}, \nu_{\tau_R})^T$. The Yukawa Lagrangian in the SM is then extended by the following terms

$$\mathcal{L} = -\overline{\nu_R} Y_\nu \phi^\dagger l_L + h.c.. \tag{1.56}$$

After the spontaneous symmetry breaking $\phi \to \frac{1}{\sqrt{2}}\begin{pmatrix} 0 \\ v \end{pmatrix}$, like the quarks and charged leptons, the neutrino sector also obtain a Dirac mass term

$$\mathcal{L} \to -\overline{\nu_R} M_D \nu_L + h.c., \tag{1.57}$$

where $M_D = \frac{v}{\sqrt{2}} Y_\nu$. The only problem is that we know $m_\nu < 1$ eV from cosmology, and $v \approx 246$ GeV, which indicates the Yukawa couplings of neutrinos $Y_\nu < 6 \times 10^{-12}$. Such a small Yukawa coupling seems very unnatural.

The tiny masses of active neutrinos can be elegantly explained by the seesaw mechanism [56]. We consider the neutrinos are Majorana particles and add the Majorana mass terms in the SM. Firstly, since $q_Y(\nu_L) = -1$, the $\overline{(\nu_L)^c}\nu_L$ term violates the hypercharge number by 2 units, thus the Majorana masses for the LH neutrinos are forbidden by the SM gauge group. However, the RH neutrinos have $q_Y(\nu_R) = 0$ and are singlets of the entire gauge group, we can add a Majorana mass term for ν_R into the SM Lagrangian:

$$\mathcal{L} = -\frac{M_R}{2}\overline{(\nu_R)^c}\nu_R + h.c.. \tag{1.58}$$

Since ν_R are singlets of the SM gauge group, the Majorana term for ν_R alone does not produce neutrino oscillations. Thus, we have to consider both the Dirac and Majorana masses. Combining Eqs. 1.57 and 1.58, we can get

$$\begin{aligned}\mathcal{L} &= -\overline{\nu_R}M_D\nu_L - \frac{M_R}{2}\overline{(\nu_R)^c}\nu_R + h.c.,\\ &= \begin{bmatrix}\bar{\nu}_L & \overline{(\nu_R)^c}\end{bmatrix}\begin{bmatrix}0 & M_D\\ M_D^T & M_R\end{bmatrix}\begin{bmatrix}(\nu_L)^c\\ \nu_R\end{bmatrix}\end{aligned} \tag{1.59}$$

Assuming $M_D \ll M_R$, the neutrino mass matrix $M = \begin{bmatrix}0 & M_D\\ M_D^T & M_R\end{bmatrix}$ can be block-diagonalized as

$$D = U^T M U \simeq \begin{bmatrix}-M_D M_R^{-1} M_D^T & 0\\ 0 & M_R\end{bmatrix}, \tag{1.60}$$

where

$$U \simeq \begin{bmatrix}1 & M_D M_R^{-1}\\ -M_R^{-1}M_D^T & 1\end{bmatrix}. \tag{1.61}$$

In order to see the meaning of the masses more clearly, let us define

$$\begin{pmatrix}\nu'\\ N'\end{pmatrix} \equiv U^\dagger \begin{pmatrix}(\nu_L)^c\\ \nu_R\end{pmatrix}, \text{ and } \begin{pmatrix}\nu\\ N\end{pmatrix} \equiv \frac{1}{\sqrt{2}}\begin{pmatrix}\nu' + (\nu')^c\\ N' + (N')^c\end{pmatrix}. \tag{1.62}$$

Then Eq. 1.59 becomes

$$\mathcal{L} \simeq M_D M_R^{-1} M_D^T \bar{\nu}\nu - M_R \bar{N} N. \tag{1.63}$$

From the above equation, we can see there are two Majorana fields: the light neutrinos ν with a mass matrix

$$M_\nu \simeq -M_D M_R^{-1} M_D^T = -Y_\nu M_R^{-1} Y_\nu^T v^2/2, \tag{1.64}$$

and the heavy neutrinos N with $M_N \simeq M_R$. If $M_R \gtrsim 10^{14-15}$ GeV, we can get $M_\nu < 1$ eV with $Y_\nu \simeq 1$. This mechanism is usually called the Type I seesaw mechanism or canonical seesaw mechanism. It is the simplest and most popular model to explain the smallness of the observed neutrino masses. Based on the similar idea of extending the SM by some heavy particles, there exist other seesaw-like models that can yield small neutrino masses like the Type I seesaw mechanism. At the tree level, besides the type I seesaw mechanism, there are the Type II seesaw mechanism [57] that extends the SM content by a scalar triplet and the Type III seesaw mechanism [58] that extends the SM content by a fermion triplet.

1.4.3 Neutrinoless Double Beta Decay and Leptogenesis

The Majorana nature of the neutrinos implied by the seesaw mechanism has several implications. Here we will discuss two of them: the neutrinoless double beta decay ($0\nu\beta\beta$) and leptogenesis.

1.4.3.1 Neutrinoless double beta decay

The neutrinoless double beta decay only occurs when neutrinos are Majorana particles; See Fig. 1.7. The rate for $0\nu\beta\beta$ depends on the effective Majorana mass [59], which is equal to the magnitude of the $\nu_e - \nu_e$ element of the neutrino mass matrix. In the three-neutrino context, the effective Majorana mass is

$$|M_{ee}| = \left| \sum_i U_{ei}^2 m_i \right| = \left| m_1 c_{12}^2 c_{13}^2 + m_2 e^{i\phi_2} s_{12}^2 c_{13}^2 + m_3 e^{i\phi_3} s_{13}^2 e^{-2i\delta} \right|. \tag{1.65}$$

Note that $|M_{ee}|$ can be written in a form that is independent of the Dirac CP phase δ by redefining ϕ_3. $0\nu\beta\beta$ has not been observed in experiments yet. The latest experimental result from EXO-200 [60] shows that the effective mass is less than $140 - 380$ meV at 90% C.L. In the foreseeable future, experiments such as KamLAND-Zen will reach a sensitivity of about 50 meV or below [61]. It is worth pointing out that $|M_{ee}|$ could vanish even for nonzero neutrino

masses [62], thus a null signal in $0\nu\beta\beta$ experiments cannot rule out that neutrinos are Majorana particles.

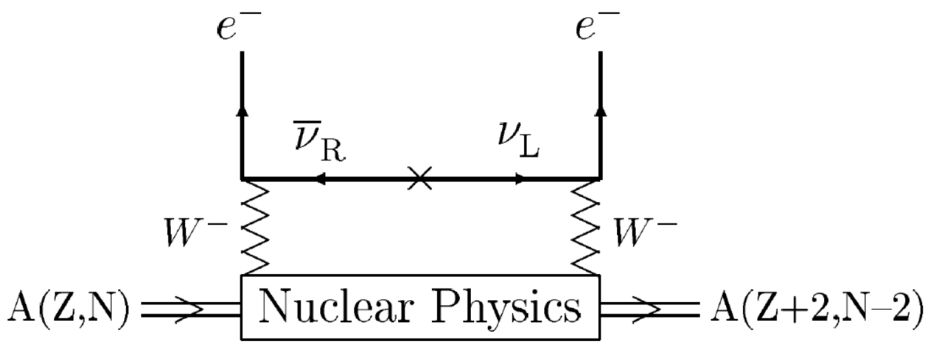

Figure 1.7 The diagram for neutrinoless double beta in the case of Majorana neutrino exchange. From Ref.[62].

1.4.3.2 Leptogenesis

We still do not understand why matter dominates over antimatter in our universe. The observed baryon asymmetry is $\eta_{B0} = \frac{n_B}{n_\gamma} = (6.19 \pm 0.15) \times 10^{-10}$ at 68% CL [63]. If we assume the universe began from a symmetric state with equal baryon number and anti-baryon number, then a baryon asymmetry can be generated only if all the three Sakharov's conditions [64] are met: (i) violation of baryon number in fundamental processes; (ii) the existence of CP violation and (iii) a departure from thermal equilibrium when the baryon number violation processes occurred. However, the SM provides neither sufficient CP violation nor the equilibrium condition to explain the origin of the baryon asymmetry of our universe. Other scenarios such as GUT baryogenesis, electroweak baryogenesis, the Affleck-Dine mechanism have been proposed to explain this puzzle; for a recent review, see Ref. [65].

As a product of the seesaw mechanism, the heavy RH neutrinos will play an important role at the early times of the universe. In a process called thermal leptogenesis [66], the decay of these heavy RH neutrinos can lead to the observed baryon asymmetry. One can easily check that all of Sakharov's conditions are satisfied in the process: (i) the heavy RH neutrinos can decay both into lepton-Higgs pair and into their CP conjugate pair, thus violating lepton number, and can lead to a baryon number violation via the sphaleron process [67]; (ii) the complex phases in

the neutrino Yukawa couplings result in CP violation, and (iii) the cosmological expansion rate during the heavy RH neutrinos decay process is faster than the decay lifetime, which yields the departure from thermal equilibrium.

There are many scenarios of leptogenesis that can explain the observed baryon asymmetry. In what follows, we adopt a minimal version of leptogenesis [68]. We assume the RH neutrinos to be hierarchical, $M_2, M_3 \gg M_1$, thus the final lepton asymmetry only depends on the decay of the lightest RH neutrino, which can be written as

$$\begin{aligned}\epsilon_1 &= \sum_{\alpha=e,\mu,\tau} \frac{\Gamma(N_1 \to \phi \bar{l}_\alpha) - \Gamma(N_1 \to \phi^\dagger l_\alpha)}{\Gamma(N_1 \to \phi \bar{l}) + \Gamma(N_1 \to \phi^\dagger l)} \\ &= -\frac{3}{16\pi} \frac{1}{(Y_\nu Y_\nu^\dagger)_{11}} \sum_{j\neq 1} \mathrm{Im}(Y_\nu Y_\nu^\dagger)_{1j}^2 \frac{M_1}{M_j}. \end{aligned} \tag{1.66}$$

We also work in the single flavor approximation in which $M_1 > 10^{12}$ GeV, so that the flavor composition of the leptons does not affect the baryon asymmetry of the universe. Then in the standard model the baryon asymmetry is given by [68]

$$\eta_{B0} = -9.72 \times 10^{-3} \times \epsilon_1 \times \eta, \tag{1.67}$$

where η is the wash out efficiency factor, which can be obtained by solving the Boltzmann equation. A very simple analytic fit yields [68]

$$\eta \simeq \left(\frac{0.55 \times 10^{-3}\ \mathrm{eV}}{\tilde{m}_1} \right)^{1.16}, \tag{1.68}$$

where $\tilde{m}_1$ is the so-called effective neutrino mass that is related to the decay rate of the lightest RH neutrino,

$$\tilde{m}_1 = \sum_{\alpha=e,\mu,\tau} |Y_{\nu\alpha 1}|^2 \frac{v^2}{2M_1}. \tag{1.69}$$

Equation (1.68) is valid for $M_1 \ll 10^{14}$ GeV and $\tilde{m}_1 \geq 0.01$ eV. With these constraints, the baryon asymmetry is

$$\eta_{B0} = \frac{n_B}{n_\gamma} \simeq -3.4 \times 10^{-4} \times \epsilon_1 (\frac{0.01\mathrm{eV}}{\tilde{m}_1})^{1.16}, \tag{1.70}$$

For $M_1 > 10^{12}$ GeV with appropriate structure of the Yukawa coupling matrix, we can produce the observed baryon asymmetry in our universe. On the other hand, successful leptogenesis may provide hints of the mass of the lightest RH neutrino and the structure of the Yukawa coupling matrix; see Ref. [69] for a recent review.

CHAPTER 2. PERTURBATIONS TO $\mu - \tau$ SYMMETRICAL MODELS

2.1 The $\mu - \tau$ Symmetry in Neutrino Mixing

There are numerous neutrino mixing scenarios existing in the literature [70]. Several of them have $\mu - \tau$ symmetry, such as tri-bimaximal mixing (TBM) [71], bimaximal mixing (BM) [72], hexagonal mixing (HM) [73] and two scenarios of Golden ratio mixing (GRM) [74, 75]. In these scenarios, $\theta_{23} = 45^\circ$, $\theta_{13} = 0$, and only θ_{12} depends on the particular model. The predictions on three mixing angles can be obtained with a choice of an appropriate discrete flavor symmetry group; see Table 2.1. Among them, TBM is most popular because the value of θ_{12} predicted by TBM is close to that preferred by the current experimental data. However, the latest results from the T2K [39], MINOS [46], and Double Chooz [47] experiments suggest a nonzero value of θ_{13}, and the recent Daya Bay [48] and RENO [49] experiments find $\theta_{13} \neq 0$ at the 5.2σ and 4.9σ level, respectively. Various corrections may reconcile such models with nonzero θ_{13}, such as vacuum misalignment corrections [76], renormalization group corrections [77], canonical normalization corrections [78], and charged lepton corrections [79].

Table 2.1 $\mu - \tau$ symmetrical models with their predictions on three mixing angles and their corresponding flavor symmetries.

Models	θ_{23}	θ_{12}	θ_{13}	Flavor group
TBM	45°	35.3°	0	A_4
BM	45°	45°	0	S_4
GRM1	45°	31.7°	0	A_5
GRM2	45°	36°	0	D_{10}
HM	45°	60°	0	D_{12}

We work in the basis in which the charged lepton mass matrix is diagonal. The mass matrix

for Majorana neutrinos is

$$M = U^* M^{\rm diag} U^\dagger \,, \tag{2.1}$$

where $M^{\rm diag} = {\rm diag}(m_1, m_2, m_3)$, U is the Pontecorvo-Maki-Nakagawa-Sakata (PMNS) mixing matrix [80]. The masses m_2 and m_3 are complex and m_1 can be taken to be real and non-negative.

The general condition describing $\mu - \tau$ symmetry (also sometimes called $\mu - \tau$ universality) is [81]

$$|U_{\mu i}| = |U_{\tau i}| \,, \text{ for } i = 1, 2, 3. \tag{2.2}$$

From the standard form of the mixing matrix these conditions are equivalent to

$$\theta_{23} = 45^\circ \,, \quad {\rm Re}(\cos\theta_{12} \sin\theta_{12} \sin\theta_{13} e^{i\delta}) = 0 \,. \tag{2.3}$$

Hence, there are four classes of $\mu - \tau$ symmetry: (a) $\theta_{23} = 45^\circ, \theta_{13} = 0$; (b) $\theta_{23} = 45^\circ, \theta_{12} = 0$; (c) $\theta_{23} = 45^\circ, \theta_{12} = 90^\circ$; (d) $\theta_{23} = 45^\circ, \delta = \pm 90^\circ$. Class (a) contains models with tri-bimaximal, bimaximal, hexagonal, and golden ratio symmetries, while class (d) includes tetramaximal symmetry [82], which predicts $\theta_{23} = 45^\circ$, $\theta_{12} = 30.4^\circ$, $\theta_{13} = 8.4^\circ$, and $\delta = 90^\circ$. Classes (b) and (c) have not been studied before because the unperturbed θ_{12} angle is far from the experimentally preferred value, but, as we show below, small perturbations can have a large effect on θ_{12}, and therefore these models should not be ignored.

2.2 Perturbations to Class (a) Symmetry

We consider small perturbations acting on Majorana mass matrices with $\mu - \tau$ symmetry and estimate the size of perturbations required to explain the experimental data. We first examine the effect of small perturbations on models in class (a). The initial (unperturbed) mixing matrix can be written as

$$U_0 = \begin{pmatrix} \cos\theta_{12}^0 & \sin\theta_{12}^0 & 0 \\ -\frac{\sin\theta_{12}^0}{\sqrt{2}} & \frac{\cos\theta_{12}^0}{\sqrt{2}} & \frac{1}{\sqrt{2}} \\ \frac{\sin\theta_{12}^0}{\sqrt{2}} & -\frac{\cos\theta_{12}^0}{\sqrt{2}} & \frac{1}{\sqrt{2}} \end{pmatrix} , \tag{2.4}$$

and the initial mass matrix is

$$M_0 = U_0^* M_0^{\rm diag} U_0^\dagger = \begin{pmatrix} m_1^0 c_{12}^2 + m_2^0 s_{12}^2 & \frac{(m_2^0 - m_1^0) s_{12} c_{12}}{\sqrt{2}} & \frac{(m_1^0 - m_2^0) s_{12} c_{12}}{\sqrt{2}} \\ \frac{(m_2^0 - m_1^0) s_{12} c_{12}}{\sqrt{2}} & \frac{1}{2}(m_3^0 + m_2^0 c_{12}^2 + m_1^0 s_{12}^2) & \frac{1}{2}(m_3^0 - m_2^0 c_{12}^2 - m_1^0 s_{12}^2) \\ \frac{(m_1^0 - m_2^0) s_{12} c_{12}}{\sqrt{2}} & \frac{1}{2}(m_3^0 - m_2^0 c_{12}^2 - m_1^0 s_{12}^2) & \frac{1}{2}(m_3^0 + m_2^0 c_{12}^2 + m_1^0 s_{12}^2) \end{pmatrix}, \tag{2.5}$$

where $M_0^{\rm diag} = {\rm diag}(m_1^0, m_2^0, m_3^0)$, and c_{jk}, s_{jk} denotes $\cos\theta_{jk}^0$ and $\sin\theta_{jk}^0$ respectively. Under a small perturbation the final (resultant) mass matrix can be written as

$$M = U_0^* M_0^{\rm diag} U_0^\dagger + E\,, \tag{2.6}$$

where the perturbation matrix E has the general form

$$E = M - M_0 = \begin{pmatrix} \epsilon_{11} & \epsilon_{12} & \epsilon_{13} \\ \epsilon_{12} & \epsilon_{22} & \epsilon_{23} \\ \epsilon_{13} & \epsilon_{23} & \epsilon_{33} \end{pmatrix}. \tag{2.7}$$

Treating the three masses as eigenvalues of the mass matrix with each column of the mixing matrix as the corresponding eigenvector, we can use traditional perturbation methods to find the corrections to the three angles and three masses. From experiment we know that m_1 and m_2 are nearly degenerate, so that degenerate perturbation theory with $|\delta m_{21}^0| \ll |\delta m_{31}^0|$ and $|\epsilon_{ij}| < |m_k^0|$ (where $\delta m_{ji}^0 = m_j^0 - m_i^0$, and the index k denotes the heaviest eigenstate), can be used. For simplicity, we assume E is real and employ the following notation:

$$\begin{aligned} &\epsilon_1 = \epsilon_{11}\,, \quad \epsilon_2 = \epsilon_{12} + \epsilon_{13}\,, \quad \epsilon_3 = \epsilon_{12} - \epsilon_{13}\,, \quad \epsilon_4 = \epsilon_{22} + \epsilon_{33} + 2\epsilon_{23}\,, \\ &\epsilon_5 = \epsilon_{22} - \epsilon_{33}\,, \quad \epsilon_6 = \epsilon_{22} + \epsilon_{33} - 2\epsilon_{23} - 2\epsilon_{11}\,. \end{aligned} \tag{2.8}$$

We find the first order corrections to the three masses to be

$$\delta m_i^{(1)} = \frac{1}{4}\left[4\epsilon_1 + \epsilon_6 \pm \left(2\delta m_{21}^0 - \sqrt{8\epsilon_3^2 + \epsilon_6^2 + 4(\delta m_{21}^0)^2 + 4\delta m_{21}^0(2\sqrt{2}\epsilon_3 \sin 2\theta_{12}^0 + \epsilon_6 \cos 2\theta_{12}^0)}\right)\right], \tag{2.9}$$

where the plus sign is for $i = 1$ and the minus sign is for $i = 2$, and

$$\delta m_3^{(1)} = \frac{1}{2}\epsilon_4\,. \tag{2.10}$$

Table 2.2 Best-fit values and 2σ ranges of the oscillation parameters [83], with $\delta m^2 \equiv |m_2|^2 - m_1^2$ and $\Delta m^2 \equiv |m_3|^2 - (m_1^2 + |m_2|^2)/2$.

Parameter	$\theta_{12}(^\circ)$	$\theta_{13}(^\circ)$	$\theta_{23}(^\circ)$	$\delta m^2(10^{-5}\mathrm{eV}^2)$	$\lvert\Delta m^2\rvert(10^{-3}\mathrm{eV}^2)$
NH	$33.6^{+2.1}_{-2.0}$	$8.9^{+0.9}_{-0.9}$	$38.4^{+3.6}_{-2.3}$	$7.54^{+0.46}_{-0.39}$	$2.43^{+0.12}_{-0.16}$
IH	$33.6^{+2.1}_{-2.0}$	$9.0^{+0.8}_{-1.0}$	$38.8^{+5.3}_{-2.3} \oplus 47.5 - 53.2$	$7.54^{+0.46}_{-0.39}$	$2.42^{+0.11}_{-0.16}$

The first order corrections to the mixing angles are

$$\delta\theta_{12}^{(1)} = \frac{1}{2}\arctan\frac{2\sqrt{2}\epsilon_3\cos 2\theta_{12}^0 - \epsilon_6\sin 2\theta_{12}^0}{2\sqrt{2}\epsilon_3\sin 2\theta_{12}^0 + \epsilon_6\cos 2\theta_{12}^0 + 2\delta m_{21}^0}\,, \tag{2.11}$$

$$\delta\theta_{23}^{(1)} = \frac{\epsilon_5 s_{12}^2 - \sqrt{2}\epsilon_2 s_{12}c_{12}}{2\delta m_{31}^0} + \frac{\epsilon_5 c_{12}^2 + \sqrt{2}\epsilon_2 s_{12}c_{12}}{2\delta m_{32}^0}\,, \tag{2.12}$$

$$\delta\theta_{13}^{(1)} = \frac{\sqrt{2}\epsilon_2 c_{12}^2 - \epsilon_5 s_{12}c_{12}}{2\delta m_{31}^0} + \frac{\sqrt{2}\epsilon_2 s_{12}^2 + \epsilon_5 s_{12}c_{12}}{2\delta m_{32}^0}\,, \tag{2.13}$$

and the second order correction to θ_{12} is

$$\delta\theta_{12}^{(2)} = -\frac{\sqrt{2}\epsilon_2\epsilon_5\cos 2(\theta_{12}^0 + \delta\theta_{12}^{(1)}) + (\epsilon_2^2 - \epsilon_5^2/2)\sin 2(\theta_{12}^0 + \delta\theta_{12}^{(1)})}{4\delta m_{21}^0\delta m_{32}^0}\,. \tag{2.14}$$

For $|\delta m_{21}^0| \ll |\delta m_{31}^0|$, the expressions for $\delta\theta_{23}^{(1)}$ and $\delta\theta_{13}^{(1)}$ simplify to

$$\delta\theta_{23}^{(1)} \simeq \frac{\epsilon_5}{2\delta m_{31}^0}\,, \quad \delta\theta_{13}^{(1)} \simeq \frac{\sqrt{2}\epsilon_2}{2\delta m_{31}^0}\,. \tag{2.15}$$

We note that while $\delta\theta_{23}^{(1)}$ and $\delta\theta_{13}^{(1)}$ are suppressed by a factor of order $\epsilon_j/\delta m_{31}^0$, to leading order $\delta\theta_{12}$ depends only on ratios of linear combinations of ϵ_3 and ϵ_6. Therefore large corrections to θ_{12} are possible even when the corrections to θ_{23} and θ_{13} are small.

A recent global three-neutrino fit [83] yields the parameter values in Table 2.2. We have done a numerical search to find perturbed mass matrices that give the oscillation parameters *and* which have small perturbations. In our search, we first fix $\theta_{23}^0 = 45^\circ$ and $\theta_{13}^0 = 0$, consistent with $\mu - \tau$ symmetry, and choose a particular value for θ_{12}^0 and the magnitude of m_1 for the normal hierarchy (or m_3 for the inverted hierarchy). The global fit in Ref. [83] then defines the magnitudes of the other two final masses and the three final mixing angles (since $\theta_{13}^0 = 0$, the initial Dirac phase does not matter).

We characterize the size of the perturbation as the root-mean-square (RMS) value of the perturbations, i.e.,

$$\epsilon_{RMS} = \sqrt{\frac{\sum_{i,j=1}^{3} |M_{ij} - M_{0ij}|^2}{9}}\,, \tag{2.16}$$

where i and j sum over neutrino flavors. Hence, ϵ_{RMS} is determined by the following quantities: three initial masses, two initial Majorana phases, two final Majorana phases and one final Dirac phase. We scan over these quantities with all phases taken to be either 0 or 180° to find the minimum value of ϵ_{RMS} for a given θ_{12}^0. We follow the same procedure for classes (b) and (c) below. For class (d), all values of the phases are allowed.

We show the perturbations that give the smallest ϵ_{RMS} for the normal hierarchy, $m_1 = 0$ and several values of θ_{12}^0 in Table 2.3. It is clear that the sizes of ϵ_{RMS} are approximately the same regardless of the value of θ_{12}^0; we find that the smallest ϵ_{RMS} for each θ_{12}^0 varies by at most 17% for the examples shown. This can be explained by the perturbation results derived above as follows. From Eq. (2.8) we have $\epsilon_{RMS} = \sqrt{\epsilon_1^2 + \epsilon_2^2 + \epsilon_3^2 + \frac{1}{2}\epsilon_5^2 + \frac{1}{4}\epsilon_4^2 + \frac{1}{4}(2\epsilon_1 + \epsilon_6)^2}/3$; since $m_3 \gg m_1, m_2$ for the normal hierarchy with $m_1 = 0$ eV and the first order perturbations of the three masses are much smaller than m_3, we can assume $\delta m_{31}^0 \approx m_3^0 \approx m_3 \approx \sqrt{\Delta m^2} = 0.0493$ eV. Then from Eq. (2.15) we know that in order to get the correction $\delta\theta_{23} = -6.6°$ and $\delta\theta_{13} = 8.9°$ for any value of θ_{12}^0, we need $\epsilon_5 = -0.0114$ eV and $\epsilon_2 = 0.0108$ eV, so that $\sqrt{\epsilon_2^2 + \epsilon_5^2/2}/3 = 0.00449$ eV, which is already close to the ϵ_{RMS} values found in Table 2.3. The small discrepancy can be explained by the first perturbation of the three masses and other ϵ's. Hence, we can say that the size of the perturbation mainly comes from the corrections to θ_{23} and θ_{13}. From Eq. (2.11) we know that the correction to θ_{12} is determined by the relative ratio of ϵ_3 to ϵ_6 and the actual size of the perturbation does not matter. This means that we can have large corrections for θ_{12}^0 with a (relatively) small perturbation.

We note that initial values of θ_{12} on the "dark side" ($\theta_{12}^0 > 45°$ and $m_1^0 < m_2^0$) can also fit the data with perturbations that are similar in magnitude to those needed for tri-bimaximal mixing (see the entry for $\theta_{12}^0 = 60°$ in Table 2.3).

In the top half of Table 2.3, ϵ_{11} and ϵ_{23} are much smaller than the other ϵ_{ij} for some values of θ_{12}^0. We have checked that if these values are set to zero, the experimental constraints can

Table 2.3 Top half: values of the perturbations (in 10^{-3} eV) that give the best-fit parameters in Table 2.2 *and* have the minimum ϵ_{RMS} for the given θ_{12}^0, for the normal hierarchy and $m_1 = 0$. Bottom half: representative values that fit the experimental data within 2σ and for which all ϵ_{ij} have similar magnitude (with $m_1^0 = 0$, $m_2^0 = 0.0054$ eV, $m_3^0 = 0.0595$ eV).

$\theta_{12}^0(^\circ)$	ϵ_{11}	ϵ_{12}	ϵ_{13}	ϵ_{22}	ϵ_{23}	ϵ_{33}	ϵ_{RMS}
60	-3.05	-3.50	-5.99	-2.72	-1.52	5.77	4.10
45 (BM)	-1.32	-4.74	-4.74	-3.58	-0.66	4.90	3.79
35.3 (TBM)	0.32	-4.66	-4.82	-4.40	0.16	4.08	3.74
30 (HM)	1.07	-4.31	-5.18	-4.78	0.54	3.71	3.79
0	0.00	-1.38	-8.11	-4.24	0.00	4.24	4.36
60	5.41	-4.17	-4.52	-5.00	-9.94	3.36	6.14
45 (BM)	6.76	-4.43	-4.26	-5.67	-9.27	2.69	6.08
35.3 (TBM)	7.66	-4.32	-4.37	-6.12	-8.82	2.24	6.08
30 (HM)	8.11	-4.17	-4.52	-6.35	-8.59	2.01	6.09
0	9.46	-2.52	-6.17	-7.02	-7.92	1.34	6.28

still be satisfied at the 2σ level without a large change in the nonzero parameters. Therefore if some perturbations are exactly zero due to symmetries, the resulting mass matrix can still fit the experimental data with small perturbations.

For the inverted hierarchy, some representative sets of ϵ_{ij} that give the minimum ϵ_{RMS} are shown in Table 2.4 for $m_3 = 0$. The minimum ϵ_{RMS} as a function of θ_{12}^0 varies only by about 1% in this case, i.e., the minimum ϵ_{RMS} varies with θ_{12}^0 even less for the inverted hierarchy than for the normal hierarchy.

Clearly, if perturbations are large enough that tri-bimaximal mixing can explain the experimental data, then other $\mu - \tau$ mixing scenarios, such as bimaximal, hexagonal mixing and golden ratio mixing, can also explain the experimental data with about the same size perturbation. Hence, tri-bimaximal mixing has no special position among the $\mu - \tau$ symmetry mixing scenarios when a perturbation is required to fit the experimental data. Also, it is possible for all the perturbations to have a similar magnitude and still give the oscillation parameters within their 2σ ranges; see the bottom half of Tables 2.3 and 2.4.

We also varied the size of the final masses by changing the value of m_1 in the normal

Table 2.4 Top half: same as Table 2.3, except for the inverted hierarchy and $m_3 = 0$. Bottom half: same as Table 2.3, except for the inverted hierarchy and $m_1^0 = 0.05$ eV, $m_2^0 = 0.052$ eV, $m_3^0 = 0$.

$\theta_{12}^0(^\circ)$	ϵ_{11}	ϵ_{12}	ϵ_{13}	ϵ_{22}	ϵ_{23}	ϵ_{33}	ϵ_{RMS}
60	-0.86	-4.94	-5.64	5.57	-0.43	-4.72	4.31
45 (BM)	-0.47	-5.29	-5.29	5.38	-0.23	-4.91	4.29
35.3 (TBM)	-0.05	-5.30	-5.28	5.17	0.03	-5.12	4.28
30 (HM)	0.16	-5.23	-5.36	5.07	0.08	-5.22	4.28
0	0.00	-4.47	-6.12	5.15	0.00	-5.15	4.32
60	-3.56	-4.89	-5.27	5.95	2.67	-3.92	4.49
45 (BM)	-3.06	-4.98	-5.18	5.70	2.92	-4.17	4.47
35.3 (TBM)	-2.73	-4.94	-5.22	5.54	3.08	-4.34	4.46
30 (HM)	-2.56	-4.89	-5.27	5.45	3.17	-4.42	4.46
0	-2.06	-4.28	-5.88	5.20	3.42	-4.67	4.50

hierarchy and m_3 in the inverted hierarchy. We find that the minimum ϵ_{RMS} decreases as the size of the final masses increases for both the normal and inverted hierarchies. For the quasi-degenerate case (in which the magnitude of the absolute masses is larger than $\sqrt{\Delta m^2}$) the size of the perturbation can be very small. This can be explained by the perturbation equations: since $\delta m_{31}^0 \approx m_3 - m_1 \approx \Delta m^2/(m_3 + m_1)$ for small perturbations, and Δm^2 is fixed by experimental data, then δm_{31}^0 will decrease if the masses increase, and similarly for δm_{32}^0. Then Eqs. (2.12) and (2.13) show that in order to get the same corrections for θ_{13}^0 and θ_{23}^0, the size of the perturbation should also decrease.

2.3 Perturbations to Other $\mu - \tau$ Symmetry

For class (b) ($\theta_{23}^0 = 45^\circ$, $\theta_{12}^0 = 0$), since the Dirac phase is irrelevant, the initial mixing matrix and mass matrix can be written as

$$U_0 = \begin{pmatrix} \cos\theta_{13}^0 & 0 & \sin\theta_{13}^0 \\ -\frac{\sin\theta_{13}^0}{\sqrt{2}} & \frac{1}{\sqrt{2}} & \frac{\cos\theta_{13}^0}{\sqrt{2}} \\ -\frac{\sin\theta_{13}^0}{\sqrt{2}} & -\frac{1}{\sqrt{2}} & \frac{\cos\theta_{13}^0}{\sqrt{2}} \end{pmatrix}, \tag{2.17}$$

and the initial mass matrix is

$$M_0 = U_0^* M_0^{\rm diag} U_0^\dagger =$$
$$\begin{pmatrix} m_1^0 c_{13}^2 + m_3^0 s_{13}^2 & \frac{(m_3^0 - m_1^0) s_{13} c_{13}}{\sqrt{2}} & \frac{(m_3^0 - m_1^0) s_{13} c_{13}}{\sqrt{2}} \\ \frac{(m_3^0 - m_1^0) s_{13} c_{13}}{\sqrt{2}} & \frac{1}{2}(m_2^0 + m_3^0 c_{13}^2 + m_1^0 s_{13}^2) & \frac{1}{2}(-m_2^0 + m_3^0 c_{13}^2 + m_1^0 s_{13}^2) \\ \frac{(m_3^0 - m_1^0) s_{13} c_{13}}{\sqrt{2}} & \frac{1}{2}(-m_2^0 + m_3^0 c_{13}^2 + m_1^0 s_{13}^2) & \frac{1}{2}(m_2^0 + m_3^0 c_{13}^2 + m_1^0 s_{13}^2) \end{pmatrix} . \qquad (2.18)$$

If we redefine the phase of the wavefunction ψ_3 to $-\psi_3$, or change the initial angle θ_{23}^0 from 45° to 135° and switch the indices 2 and 3, then the mass matrix in Eq. (2.18) is exactly the same as that in Eq. (2.5).

If we use the above matrix as the initial mass matrix, then corrections shift θ_{12} from 0° to 33.6°, and θ_{13} from the initial arbitrary angle to 8.9°. We used the same scan procedure as before and searched for the minimum ϵ_{RMS} for various values of θ_{13}^0 (see Table 2.5). We find that for $\theta_{13}^0 < 20^\circ$, we can still explain the data with about the same size perturbation as was found for class (a). For example, when $\theta_{13}^0 = 0^\circ$ for class (b), the initial mass matrix is the same as $\theta_{12}^0 = 0$ for class (a), and therefore the minimum ϵ_{RMS} is also the same. In particular, when θ_{13}^0 is close to 8.9° in class (b), the minimum ϵ_{RMS} is even smaller than the minimum value for class (a) because the correction to θ_{13} is smaller in this case. Although the correction to θ_{12} is large, it does not affect the size of the perturbation too much because its size is mainly due to the corrections to θ_{13} and θ_{23}, as noted before. However, for $\delta\theta_{13}$ greater than about 20°, the size of the perturbation required to fit the data becomes larger since θ_{13} must change by more than 10°.

For class (c) ($\theta_{23}^0 = 45^\circ$, $\theta_{12}^0 = 90^\circ$), we find that switching m_1^0 with m_2^0 makes the initial mass matrix the same as the initial mass matrix of class (b). Since we scan all possible values of m_1^0 and m_2^0, the minimum ϵ_{RMS} for a given θ_{13}^0 for class (c) is the same as for class (b).

For class (d), if we fix $\theta_{23}^0 = 45^\circ, \delta^0 = \pm 90^\circ$ and vary both θ_{12}^0 and θ_{13}^0, this category includes mixing scenarios such as the tetramaximal mixing pattern ($\mathrm{T}^4\mathrm{M}$) [82], and the correlative mixing pattern with $\delta = \pm 90^\circ$ [84]. For $\theta_{13}^0 < 20^\circ$ and $\theta_{12}^0 \leq 45^\circ$, the smallest ϵ_{RMS} for the normal hierarchy (with $m_1 = 0$) varies from 2.29×10^{-3} eV to 5.26×10^{-3} eV, where the minimum value occurs at $\theta_{13}^0 = 9^\circ$ and $\theta_{12}^0 = 32^\circ$, and the maximum value occurs at $\theta_{13}^0 = 20^\circ$

Table 2.5 Top half: same as Table 2.3, except for class (b) ($\theta_{12}^0 = 0$). Bottom half: same as Table 2.3, except for class (b) and $m_1^0 = 0$, $m_2^0 = 0.0054$ eV, $m_3^0 = 0.0595$ eV.

$\theta_{13}^0(^\circ)$	ϵ_{11}	ϵ_{12}	ϵ_{13}	ϵ_{22}	ϵ_{23}	ϵ_{33}	ϵ_{RMS}
0	0.00	-1.38	-8.11	-4.24	0.00	4.24	4.36
5	0.48	1.44	-5.28	-4.48	-0.24	4.00	3.27
10	-0.44	4.21	-2.52	-4.02	0.22	4.46	3.06
15	-2.64	6.59	-0.14	-2.92	1.32	5.56	3.90
20	-5.85	8.30	1.57	-1.32	2.93	7.17	5.24
0	9.46	-2.52	-6.17	-7.02	-7.92	1.34	6.28
5	9.01	1.13	-2.52	-6.80	-7.69	1.56	5.41
10	7.66	4.67	1.02	-6.12	-7.02	2.24	5.22
15	5.47	8.00	4.35	-5.03	-5.93	3.33	5.80
20	2.50	11.00	7.35	-3.54	-4.44	4.82	6.92

and $\theta_{12}^0 = 0$. Therefore small perturbations can fit the experimental data for a wide range of θ_{12}^0 and θ_{13}^0 for class (d).

In summary, we studied small perturbations to Majorana mass matrices with $\mu - \tau$ symmetry that yield experimentally preferred oscillation parameters. We find that the size of the perturbations (which decreases as the neutrino mass scale is increased), is mainly determined by the corrections to θ_{23} and θ_{13}, and that small perturbations can give a very large correction to θ_{12} because to first order, the θ_{12} correction depends only on the ratio of perturbation terms and not on their absolute size. Hence, most mixing scenarios with $\mu - \tau$ symmetry can explain the experimental data with perturbations of similar magnitude, and tri-bimaximal mixing has no special place among scenarios with $\mu - \tau$ symmetry. We also find that slightly perturbed $\mu - \tau$ symmetric models with $\theta_{12} = 0$ or 90° are viable for $\theta_{13} < 20^\circ$.

CHAPTER 3. SEESAW MECHANISM WITH FOUR TEXTURE ZEROS

3.1 Four Zeros in the Neutrino Yukawa Matrix

Low-energy neutrino phenomenology is described by nine parameters in the Majorana mass matrix of light neutrinos, which can be written as [80]

$$M = V^* \mathrm{diag}(m_1, m_2, m_3) V^\dagger, \tag{3.1}$$

with $V = U\mathrm{diag}(1, e^{i\phi_2/2}, e^{i\phi_3/2})$, and

$$U = \begin{bmatrix} c_{13}c_{12} & c_{13}s_{12} & s_{13}e^{-i\delta} \\ -s_{12}c_{23} - c_{12}s_{23}s_{13}e^{i\delta} & c_{12}c_{23} - s_{12}s_{23}s_{13}e^{i\delta} & s_{23}c_{13} \\ s_{12}s_{23} - c_{12}c_{23}s_{13}e^{i\delta} & -c_{12}s_{23} - s_{12}c_{23}s_{13}e^{i\delta} & c_{23}c_{13} \end{bmatrix}. \tag{3.2}$$

After the measurement of θ_{13} by the Daya Bay [48], RENO [49], and Double Chooz [85] experiments, five of them are known; the result of a recent global three-neutrino fit [83] is shown in Table 2.2. The tiny masses of light neutrinos can be elegantly explained by the seesaw mechanism [56], but, unfortunately, with the introduction of additional free parameters that cannot be measured in the forseeable future. The most popular seesaw model is the type I seesaw, which can be generated to include N right-handed neutrinos. According to Eq. (1.64), the mass matrix of the light neutrinos can be written as

$$M = -Y_\nu {M_R}^{-1} Y_\nu^T v^2/2 = Y^T Y\,, \tag{3.3}$$

where, for N heavy right-handed neutrinos, $M_R = \mathrm{diag}(M_1, M_2, \cdots, M_N)$, Y_ν is a $N \times 3$ Yukawa coupling matrix, and

$$Y = \frac{v}{\sqrt{2}} {M_R}^{-1/2} Y_\nu^T = \begin{bmatrix} y_{1e} & y_{1\mu} & y_{1\tau} \\ y_{2e} & y_{2\mu} & y_{2\tau} \\ \vdots & \vdots & \vdots \\ y_{Ne} & y_{N\mu} & y_{N\tau} \end{bmatrix}. \tag{3.4}$$

Note that on permuting the rows of the Y matrix (which is equivalent to reordering the right-handed neutrinos) or applying a rotation to the rows of the Y matrix (which is equivalent to a rotation in the space of the right-handed neutrinos), the mass matrix of the light neutrinos remains the same.

The standard seesaw model has $N = 3$ and permits any set of low-energy neutrino parameters in M_ν. A way to extract predictions from the seesaw model is to impose constraints on its parameters. The most economical seesaw model includes two right-handed neutrinos and two zeros in the Yukawa coupling matrix, or, equivalently, two zeros in Y [86]. The measurement of θ_{13} excludes the normal mass hierarchy (NH) and stringently constrains the allowed parameter space for the inverted mass hierarchy (IH); in particular, the phase δ must be such that Dirac CP violation is close to maximal [87]. Also, for two right-handed neutrinos, one of the light neutrinos must have vanishing mass, so the allowed values of the sum of all light neutrino masses (which affects structure formation in our universe) and $|M_{ee}|$ (which determines the rate for neutrinoless double-beta decay, a signal of lepton number violation) are limited.

Here we extend this most economical model to include a third right-handed neutrino. We use texture zeros in Y as extra constraints, which may arise in, e.g., extra dimensional models [87]. If there are 5 or more texture zeros in Y, the most economical model with two right-handed neutrinos or a block diagonal matrix is obtained; the latter is excluded by the current experimental data. So the simplest case for three right-handed neutrinos has four texture zeros in Y, which is equivalent to five nonzero elements; for previous work see Refs. [88, 89]. Here we derive analytic formulas that relate the free parameters to the dependent ones and determine the constraints on these models including the recent data on θ_{13}.

There are 3 basic ways to have 5 nonzero elements: (2, 2, 1), (3, 1, 1) or (3, 2, 0), where

the numbers indicate how many nonzero elements are in each row of the Y matrix. The (3, 2, 0) case is equivalent to two right-handed neutrinos with one texture zero element and one vanishing mass, and is equivalent to the most economical $N = 2$ model after a rotation in the right-handed neutrino space. So only the (2, 2, 1) and (3, 1, 1) cases need to be considered. There are 9 independent textures in the (2, 2, 1) case and 3 independent textures in the (3, 1, 1) case. We divide them into four classes:

Class 1

$$1A: \begin{bmatrix} \times & \times & 0 \\ \times & 0 & \times \\ \times & 0 & 0 \end{bmatrix} \quad 1B: \begin{bmatrix} \times & \times & 0 \\ \times & 0 & \times \\ 0 & \times & 0 \end{bmatrix} \quad 1C: \begin{bmatrix} \times & \times & 0 \\ \times & 0 & \times \\ 0 & 0 & \times \end{bmatrix}$$

Class 2

$$2A: \begin{bmatrix} \times & \times & 0 \\ 0 & \times & \times \\ \times & 0 & 0 \end{bmatrix} \quad 2B: \begin{bmatrix} \times & \times & 0 \\ 0 & \times & \times \\ 0 & \times & 0 \end{bmatrix} \quad 2C: \begin{bmatrix} \times & \times & 0 \\ 0 & \times & \times \\ 0 & 0 & \times \end{bmatrix}$$

Class 3

$$3A: \begin{bmatrix} \times & 0 & \times \\ 0 & \times & \times \\ \times & 0 & 0 \end{bmatrix} \quad 3B: \begin{bmatrix} \times & 0 & \times \\ 0 & \times & \times \\ 0 & \times & 0 \end{bmatrix} \quad 3C: \begin{bmatrix} \times & 0 & \times \\ 0 & \times & \times \\ 0 & 0 & \times \end{bmatrix}$$

Class 4

$$4A: \begin{bmatrix} \times & \times & \times \\ 0 & \times & 0 \\ 0 & 0 & \times \end{bmatrix} \quad 4B: \begin{bmatrix} \times & \times & \times \\ 0 & 0 & \times \\ \times & 0 & 0 \end{bmatrix} \quad 4C: \begin{bmatrix} \times & \times & \times \\ \times & 0 & 0 \\ 0 & \times & 0 \end{bmatrix}$$

For each class there are six possible permutations of the rows, so there are 72 individual cases in all [88].

With four zeros in Y, there are five nonzero elements left in Y, but only two phases are physical, so that there are seven free parameters in the four texture zero model. Hence, we can use the five observed oscillation parameters from the global fit to determine the allowed regions for the Dirac CP phase δ and m_1 (m_3) for the normal (inverted) hierarchy. Then we

can obtain the values of the Majorana phases ϕ_2 and ϕ_3, completing our knowledge of all the elements in the light neutrino mass matrix. The $\nu_e - \nu_e$ element of the light neutrino mass matrix will determine the rate for neutrinoless double-beta decay.

Furthermore, from Eq. (3.3) we can find Y and study leptogenesis. We find the baryon asymmetry in the minimal version of leptogenesis depend only on the elements of the Y matrix and the mass of the lightest RH neutrino. This can be seen from Eqs. (1.66), (1.69) and (1.70). Since $Y_{\nu\alpha i} = \frac{\sqrt{2}}{v} M_{Ri}^{1/2} y_{i\alpha}$, the lepton asymmetry becomes

$$\epsilon_1 = -\frac{3M_1}{8\pi v^2} \sum_{j\neq 1} \frac{\mathrm{Im}(y_{1e} y_{je}^* + y_{1\mu} y_{j\mu}^* + y_{1\tau} y_{j\tau}^*)^2}{|y_{1e}|^2 + |y_{1\mu}|^2 + |y_{1\tau}|^2}, \tag{3.5}$$

the effective neutrino mass becomes

$$\tilde{m}_1 = \sum_{\alpha=e,\mu,\tau} |y_{1\alpha}|^2, \tag{3.6}$$

and the baryon asymmetry is

$$\eta_{B0} = \frac{n_B}{n_\gamma} \simeq -3.4 \times 10^{-4} \times \epsilon_1 (\frac{0.01\mathrm{eV}}{\tilde{m}_1})^{1.16}. \tag{3.7}$$

We can see the baryon asymmetry is proportional to the lightest RH neutrino mass M_1 in this case. Since the elements of Y are determined by the light neutrino mass matrix, we can calculate the lightest right-handed neutrino mass M_1 from Eqs. (3.5), (3.6), and (3.7), ensuring that 10^{12} GeV $< M_1 \ll 10^{14}$ GeV.

3.2 Phenomenology

3.2.1 Class 1

The mass matrices of the three textures in Class 1 always have a zero in the (2, 3) entry. In fact, $M_{23} = 0$ is the only condition on Y for all the textures in Class 1, and the condition is the same for both mass hierarchies (normal and inverted). Take Class 1A for example; we can write

$$Y = \begin{bmatrix} a & b & 0 \\ c & 0 & d \\ e & 0 & 0 \end{bmatrix}, \tag{3.8}$$

where a, b, c, d, e are all nonzero complex numbers. Then the mass matrix of the light neutrinos becomes

$$M = Y^T Y = \begin{bmatrix} a^2 + c^2 + e^2 & ab & cd \\ ab & b^2 & 0 \\ cd & 0 & d^2 \end{bmatrix}. \tag{3.9}$$

Comparing Eq. (3.9) with the standard parametrization, if $M_{23} = 0$, we can find a solution for Y as follows:

$$b = \pm M_{22}^{1/2}, a = M_{12}/b, d = \pm M_{33}^{1/2}, c = M_{13}/d, e = \pm(M_{11} - a^2 - c^2)^{1/2}. \tag{3.10}$$

Since a, b, c, d, e are all nonzero complex numbers, a solution always exists. Solutions for Y for the other two textures in Class 1 may be derived in a similar fashion. Therefore, Class 1 is defined by the necessary and sufficient condition $M_{23} = 0$, which can be written as

$$m_1 = -\frac{m_3 e^{i\phi_3} U_{\tau 3} U_{\mu 3} + m_2 e^{i\phi_2} U_{\tau 2} U_{\mu 2}}{U_{\tau 1} U_{\mu 1}}. \tag{3.11}$$

Taking the absolute square gives

$$m_1^2 |U_{\mu 1}|^2 |U_{\tau 1}|^2 - m_2^2 |U_{\mu 2}|^2 |U_{\tau 2}|^2 - m_3^2 |U_{\mu 3}|^2 |U_{\tau 3}|^2 = 2\mathrm{Re}(m_3 e^{-i\phi_3} U_{\mu 3}^* U_{\tau 3}^* m_2 e^{i\phi_2} U_{\mu 2} U_{\tau 2}), \tag{3.12}$$

or, defining $\phi = \phi_3 - \phi_2$,

$$\begin{aligned} m_1^2 \quad & |U_{\mu 1}|^2 |U_{\tau 1}|^2 - m_2^2 |U_{\mu 2}|^2 |U_{\tau 2}|^2 - m_3^2 |U_{\mu 3}|^2 |U_{\tau 3}|^2 \\ = \quad & -2 m_2 m_3 c_{13}^2 s_{23} c_{23} \mathrm{Re}\left[e^{-i\phi} (c_{12} c_{23} - s_{12} s_{23} s_{13} e^{i\delta})(c_{12} s_{23} + s_{12} c_{23} s_{13} e^{i\delta}) \right] \\ = \quad & -2 m_2 m_3 c_{13}^2 s_{23} c_{23} \times \\ & \mathrm{Re}\left[c_{12}^2 s_{23} c_{23} \cos\phi + s_{12} c_{12} s_{13} (c_{23}^2 - s_{23}^2) \cos(\phi - \delta) - s_{12}^2 s_{23} c_{23} s_{13}^2 \cos(\phi - 2\delta) \right] \end{aligned} \tag{3.13}$$

Expanding the cosines yields the form

$$C = A \cos\phi + B \sin\phi, \tag{3.14}$$

with A, B and C as listed in Table 3.1.

Table 3.1 The coefficients A, B and C for each class.

$$C = A\cos\phi + B\sin\phi$$

Class	A	B	C
1	$-2m_2m_3c_{13}^2s_{23}c_{23}\times$ $\left[c_{12}^2s_{23}c_{23}+s_{12}c_{12}s_{13}(c_{23}^2-s_{23}^2)\cos\delta\right.$ $\left.-s_{12}^2s_{23}c_{23}s_{13}^2\cos(2\delta)\right]$	$-2m_2m_3c_{13}^2s_{23}c_{23}s_{12}s_{13}\times$ $\left[c_{12}(c_{23}^2-s_{23}^2)\sin\delta\right.$ $\left.-s_{12}s_{23}c_{23}s_{13}\sin(2\delta)\right]$	$m_1^2\lvert U_{\mu1}\rvert^2\lvert U_{\tau1}\rvert^2$ $-m_2^2\lvert U_{\mu2}\rvert^2\lvert U_{\tau2}\rvert^2$ $-m_3^2\lvert U_{\mu3}\rvert^2\lvert U_{\tau3}\rvert^2$
2	$-2m_2m_3c_{13}^2s_{12}c_{23}s_{13}\times$ $[c_{12}s_{23}\cos\delta+s_{12}c_{23}s_{13}\cos(2\delta)]$	$-2m_2m_3c_{13}^2s_{12}c_{23}s_{13}\times$ $[c_{12}s_{23}\sin\delta+s_{12}c_{23}s_{13}\sin(2\delta)]$	$m_1^2\lvert U_{e1}\rvert^2\lvert U_{\tau1}\rvert^2$ $-m_2^2\lvert U_{e2}\rvert^2\lvert U_{\tau2}\rvert^2$ $-m_3^2\lvert U_{e3}\rvert^2\lvert U_{\tau3}\rvert^2$
3	$2m_2m_3c_{13}^2s_{12}s_{23}s_{13}\times$ $[c_{12}c_{23}\cos\delta-s_{12}s_{23}s_{13}\cos(2\delta)]$	$2m_2m_3c_{13}^2s_{12}s_{23}s_{13}\times$ $[c_{12}c_{23}\sin\delta-s_{12}s_{23}s_{13}\sin(2\delta)]$	$m_1^2\lvert U_{e1}\rvert^2\lvert U_{\mu1}\rvert^2$ $-m_2^2\lvert U_{e2}\rvert^2\lvert U_{\mu2}\rvert^2$ $-m_3^2\lvert U_{e3}\rvert^2\lvert U_{\mu3}\rvert^2$
4A	$-2m_2^{-1}m_3^{-1}c_{13}^2s_{23}c_{23}\times$ $\left[c_{12}^2s_{23}c_{23}+s_{12}c_{12}s_{13}(c_{23}^2-s_{23}^2)\cos\delta\right.$ $\left.-s_{12}^2s_{23}c_{23}s_{13}^2\cos(2\delta)\right]$	$-2m_2^{-1}m_3^{-1}c_{13}^2s_{23}c_{23}s_{12}s_{13}\times$ $\left[c_{12}(c_{23}^2-s_{23}^2)\sin\delta\right.$ $\left.-s_{12}s_{23}c_{23}s_{13}\sin(2\delta)\right]$	$m_1^{-2}\lvert U_{\mu1}\rvert^2\lvert U_{\tau1}\rvert^2$ $-m_2^{-2}\lvert U_{\mu2}\rvert^2\lvert U_{\tau2}\rvert^2$ $-m_3^{-2}\lvert U_{\mu3}\rvert^2\lvert U_{\tau3}\rvert^2$
4B	$-2m_2^{-1}m_3^{-1}c_{13}^2s_{12}c_{23}s_{13}\times$ $[c_{12}s_{23}\cos\delta+s_{12}c_{23}s_{13}\cos(2\delta)]$	$-2m_2^{-1}m_3^{-1}c_{13}^2s_{12}c_{23}s_{13}\times$ $[c_{12}s_{23}\sin\delta+s_{12}c_{23}s_{13}\sin(2\delta)]$	$m_1^{-2}\lvert U_{e1}\rvert^2\lvert U_{\tau1}\rvert^2$ $-m_2^{-2}\lvert U_{e2}\rvert^2\lvert U_{\tau2}\rvert^2$ $-m_3^{-2}\lvert U_{e3}\rvert^2\lvert U_{\tau3}\rvert^2$
4C	$2m_2^{-1}m_3^{-1}c_{13}^2s_{12}c_{23}s_{13}\times$ $[c_{12}c_{23}\cos\delta-s_{12}s_{23}s_{13}\cos(2\delta)]$	$2m_2^{-1}m_3^{-1}c_{13}^2s_{12}c_{23}s_{13}\times$ $[c_{12}c_{23}\sin\delta-s_{12}s_{23}s_{13}\sin(2\delta)]$	$m_1^{-2}\lvert U_{e1}\rvert^2\lvert U_{\mu1}\rvert^2$ $-m_2^{-2}\lvert U_{e2}\rvert^2\lvert U_{\mu2}\rvert^2$ $-m_3^{-2}\lvert U_{e3}\rvert^2\lvert U_{\mu3}\rvert^2$

For Eq. (3.14), if $C^2 > A^2 + B^2$, there is no solution; if $C^2 < A^2 + B^2$, there are two solutions:

$$\phi = 2 \arctan \frac{B \pm \sqrt{A^2 + B^2 - C^2}}{A + C}. \tag{3.15}$$

We can write Eq. (3.11) in terms of ϕ as

$$m_1 = e^{i\phi_2} \frac{-m_3 e^{i\phi} U_{\tau 3} U_{\mu 3} - m_2 U_{\tau 2} U_{\mu 2}}{U_{\tau 1} U_{\mu 1}}. \tag{3.16}$$

Since m_1 is a non-negative real number, we get

$$\phi_2 = -\arg[\frac{-m_3 e^{i\phi} U_{\tau 3} U_{\mu 3} - m_2 U_{\tau 2} U_{\mu 2}}{U_{\tau 1} U_{\mu 1}}], \tag{3.17}$$

and

$$\phi_3 = \phi_2 + \phi. \tag{3.18}$$

Therefore, if m_1 (m_3) and δ in the normal (inverted) hierarchy are known, we can calculate A, B and C using the five measured oscillation parameters in Table 2.2. We scan the δ and m_1 (m_3) space to find the allowed regions, which are defined by the condition $C^2 < A^2 + B^2$ (see Fig. 3.1 for the normal hierarchy and the upper panel of Fig. 3.2 for the inverted hierarchy). We show allowed regions corresponding to the best-fit parameters, and those allowed at 2σ. We also plot iso-ϕ_2 and iso-$|M_{ee}|$ contours using the best-fit oscillation parameters. We only show the contours for the plus sign of ϕ in Eq. (3.15) because changing δ to $360^\circ - \delta$ yields the same contours for the minus solution.

The allowed regions can be further constrained using leptogenesis. We assume the lightest right-handed neutrino has mass between 10^{12} GeV and 10^{13} GeV and is much lighter than the others so that we can use Eq. (3.7). We also require $\tilde{m}_1 \geq 0.01$ eV. From Eqs. (3.6) and (3.5), we see that the baryon asymmetry depends on the sign choices of ϕ in Eq. (3.15) but not on the sign choices in Eq. (3.10), because different choices of signs in Eq. (3.10) change the signs of all parameters in one row of the Y matrix, which yield the same baryon asymmetry. The baryon asymmetry also depends on the row of Y that is associated with the lightest right-handed neutrino mass, but the order of the other two rows does not affect the baryon asymmetry.

Since Classes 1A, 1B and 1C have different textures, the allowed regions for successful leptogenesis are also different in these three cases. Here we only consider Class 1A as an

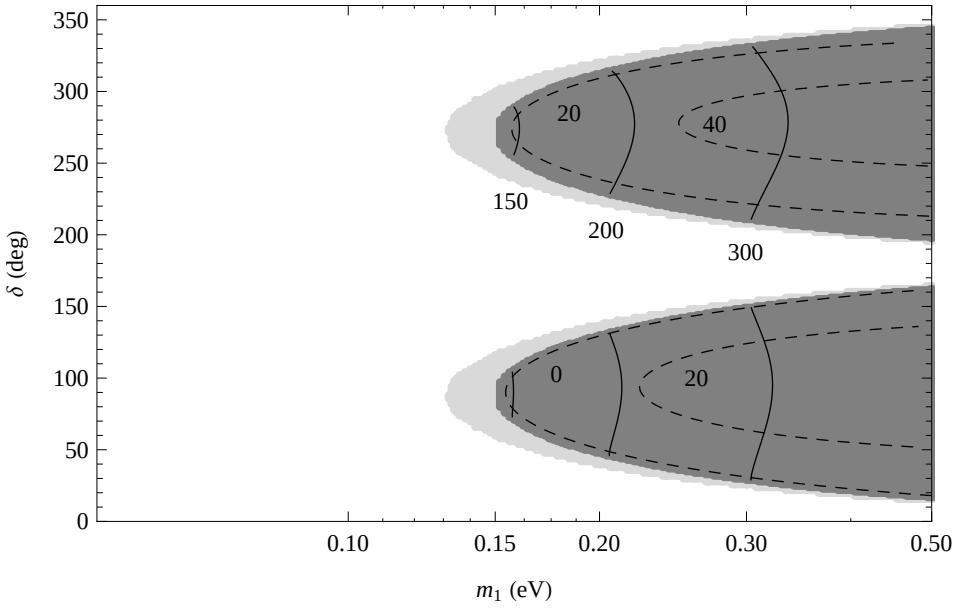

Figure 3.1 The allowed regions in the (m_1, δ) plane for Class 1 and the normal hierarchy. The dark shaded regions correspond to the best-fit parameters of the oscillation parameters, while the light shaded regions are allowed at 2σ. The solid lines are iso-$|M_{ee}|$ contours (in meV) and the dashed lines are iso-ϕ_2 contours (in degrees).

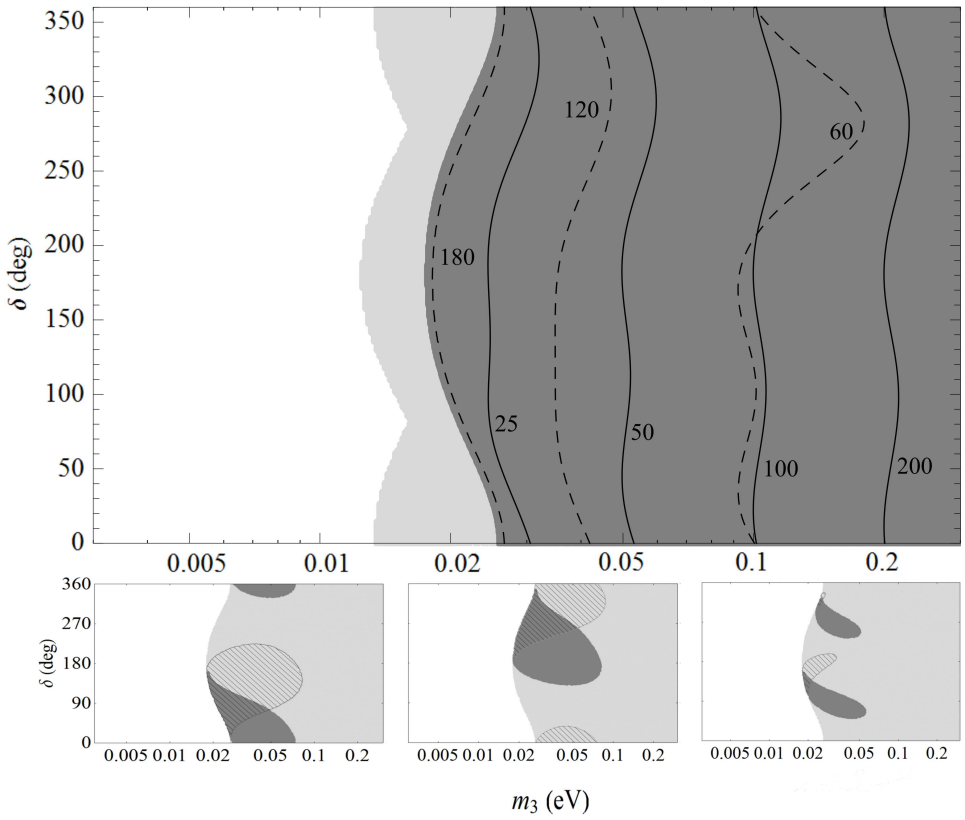

Figure 3.2 The upper panel shows the allowed regions in the (m_3, δ) plane for Class 1 and the inverted hierarchy. The shading and line types in the upper panel are as in Fig. 1. The lower panels show the allowed regions for Class 1A and the inverted hierarchy with the additional constraint of successful single-flavored leptogenesis. The hatched (dark shaded) regions use the plus (minus) solution of ϕ_2. From left to right the three graphs have the first, second and third row of Y associated with the lightest right-handed neutrino mass, respectively.

example. We find that successful leptogenesis is not possible for the normal hierarchy. For the inverted hierarchy, the allowed regions are shown in the three lower panels of Fig. 3.2. Although the constraints on δ vary according to which right-handed neutrino is lightest, in no case is the lightest left-handed neutrino allowed to be above 100 meV.

3.2.2 Class 2

Similar to Class 1, the only condition for Class 2 is $M_{13} = 0$, which is independent of hierarchy and can be written as

$$m_1 = -\frac{m_3 e^{i\phi_3} U_{\tau 3} U_{e3} + m_2 e^{i\phi_2} U_{\tau 2} U_{e2}}{U_{\tau 1} U_{e1}}. \tag{3.19}$$

After taking the absolute square, then as in Class 1 this may be put in the form of Eq. (3.14), with A, B and C as in Table 3.1.

The solutions for ϕ_2 and ϕ_3 then proceed as in Class 1. The allowed regions for the inverted hierarchy are shown in Fig. 3.3, along with iso-ϕ_2 and iso-$|M_{ee}|$ contours. We see that the solution found in Ref. [87] with $\lambda_{1e} = \lambda_{2\tau} = 0$ or $\lambda_{1\tau} = \lambda_{2e} = 0$ for the inverted hierarchy is a special case of our model with $m_3 = 0$. Leptogenesis predictions for Class 2A IH are also shown in Fig. 3.3, and give an upper bound on m_3 of about 200 meV. The allowed regions for the normal hierarchy are similar to Fig. 3.4.

3.2.3 Class 3

The only condition for Class 3 is $M_{12} = 0$, which can be written

$$m_1 = -\frac{m_3 e^{i\phi_3} U_{\mu 3} U_{e3} + m_2 e^{i\phi_2} U_{\mu 2} U_{e2}}{U_{\mu 1} U_{e1}}. \tag{3.20}$$

This condition is the same for both mass hierarchies and as before this may be put in the form of Eq. (3.14) with A, B and C as in Table 3.1.

Note that Class 3 is the same as Class 2 for any hierarchy with $U_{\tau j} \to U_{\mu j}$, or $s_{23} \to -c_{23}$ and $c_{23} \to s_{23}$, which is the same as $\delta \to \delta + 180^\circ$ when $\theta_{23} = 45^\circ$. Since $\theta_{23} \approx 45^\circ$, the phenomenology of Classes 2 and 3 will be similar. The allowed regions for the normal hierarchy are shown in Fig. 3.4; also shown are predictions for $|M_{ee}|$ and ϕ_2 and regions compatible with

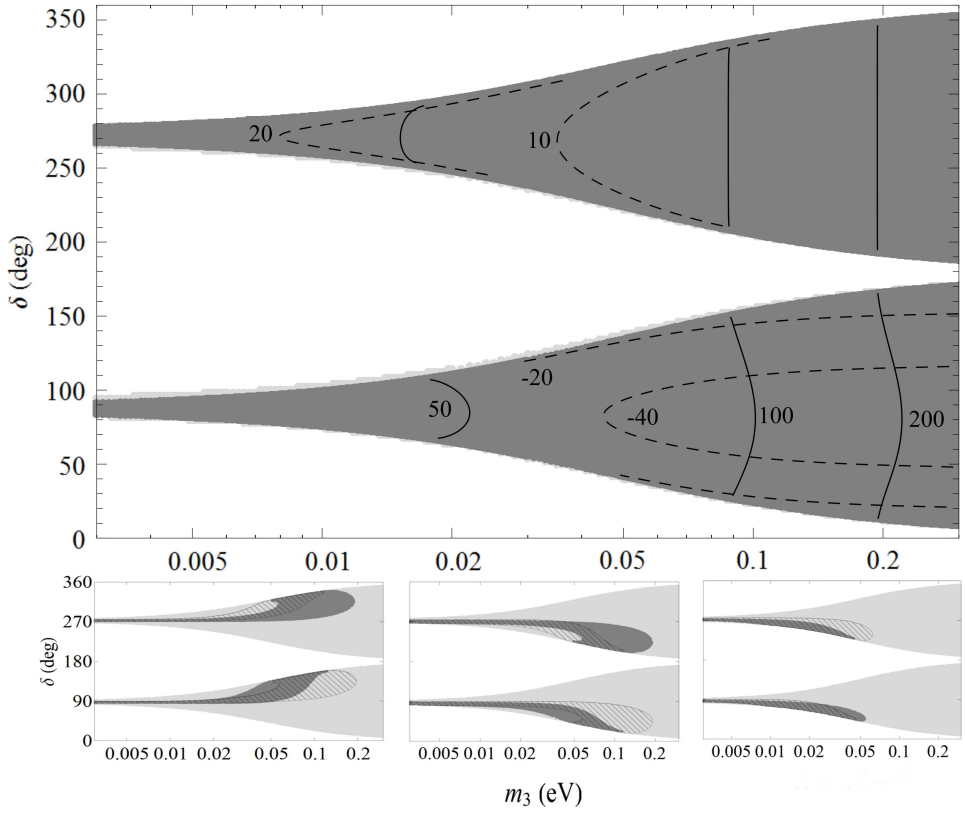

Figure 3.3 Same as Fig. 3.2, except for Class 2 and 2A and the inverted hierarchy.

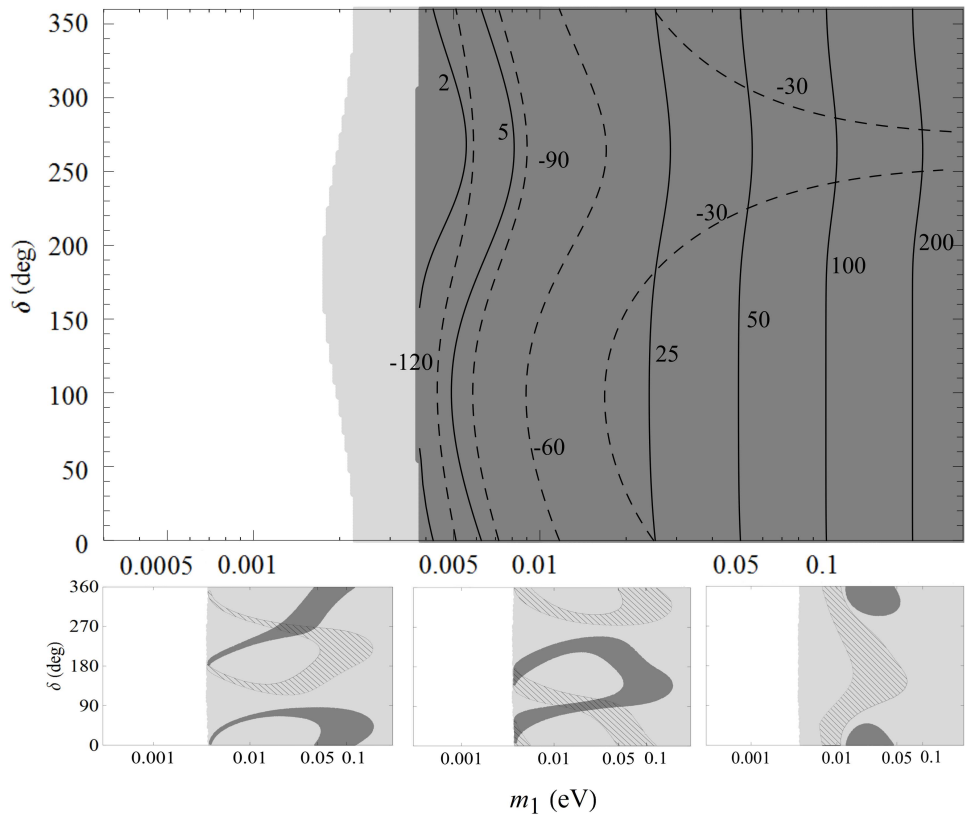

Figure 3.4 Same as Fig. 3.2, except for Class 3 and 3A and the normal hierarchy.

leptogenesis. The allowed regions for the inverted hierarchy are similar to those for Class 2 in Fig. 3.3 with $\delta \to \delta + 180°$. We note that the solution found in Ref. [87] with $\lambda_{1e} = \lambda_{2\mu} = 0$ or $\lambda_{1\mu} = \lambda_{2e} = 0$ for the inverted hierarchy is a special case in our model with $m_3 = 0$.

3.2.4 Class 4A

Class 4 has no texture zeros in the mass matrix. However, the existence of a solution for Y still depends on only one condition. Take Class 4A for example, in which case

$$Y = \begin{bmatrix} a & b & c \\ 0 & d & 0 \\ 0 & 0 & e \end{bmatrix} , \tag{3.21}$$

where a, b, c, d, e are all nonzero complex numbers. Then the mass matrix becomes

$$M = Y^T Y = \begin{bmatrix} a^2 & ab & ac \\ ab & b^2 + d^2 & bc \\ ac & bc & c^2 + e^2 \end{bmatrix}, \tag{3.22}$$

and we see that if $\frac{M_{11}}{M_{12}} = \frac{M_{13}}{M_{23}}$ is satisfied, the other variables can be directly determined. Hence the Class 4A condition is equivalent to $M_{11}M_{23} = M_{12}M_{13}$, which means the (2, 3) cofactor of M, $C_{23} = M_{12}M_{31} - M_{11}M_{32}$, vanishes. Since $(M^{-1})_{ij} = \frac{1}{\det M} C_{ji}$, the condition for Class 4A is equivalent to $(M^{-1})_{23} = 0$, i.e., a texture zero in the inverse mass matrix. Since $M^{-1} = V \mathrm{diag}(m_1^{-1}, m_2^{-1}, m_3^{-1}) V^T$, we can write the condition as

$$m_1^{-1} U_{\tau 1} U_{\mu 1} + m_2^{-1} e^{i\phi_2} U_{\tau 2} U_{\mu 2} + m_3^{-1} e^{i\phi_3} U_{\tau 3} U_{\mu 3} = 0\,, \tag{3.23}$$

or

$$m_1^{-1} = -\frac{m_2^{-1} e^{i\phi_2} U_{\tau 2} U_{\mu 2} + m_3^{-1} e^{i\phi_3} U_{\tau 3} U_{\mu 3}}{U_{\tau 1} U_{\mu 1}}. \tag{3.24}$$

The allowed regions for the normal hierarchy are shown in Fig. 3.5. The allowed regions for the inverted hierarchy are similar to Fig. 3.1 (Class 1 NH), and the iso-ϕ_2 and iso-$|M_{ee}|$ contours are similar with $\phi_2 \to -\phi_2$. The similarity of an IH scenario with an NH one may seem unusual, but can be understood by looking at the form of the A, B, and C coefficients in Table 2; multiplying the coefficients for Class 4A IH by $m_2 m_3$, and dividing the coefficients for Class 1 NH by $m_2 m_3$, we see that A and B are the same for the two cases. For the C coefficient, the dominant term in each case is the third one, proportional to $|U_{\mu 3}|^2 |U_{\tau 3}|^2$ times the ratio of a larger mass to a smaller one.

The comparison of Class 4A NH with Class 1 IH is more nuanced: when the lightest mass (m_1 for NH, m_3 for IH) is very small, the first two terms in the C coefficient have similar size for Class 1 IH, but only the first term is dominant for Class 4A NH. However, when the lightest mass is not so small, such that $m_1 \approx m_2$ in the NH, then the same terms in the C coefficient are dominant. Thus for higher values of the lightest mass, although not necessarily so large that all three masses are quasi-degenerate, Classes 4A NH and 1 IH give similar predictions. This can be seen by comparing Figs. 5 and 2: although the allowed regions and contours are quite

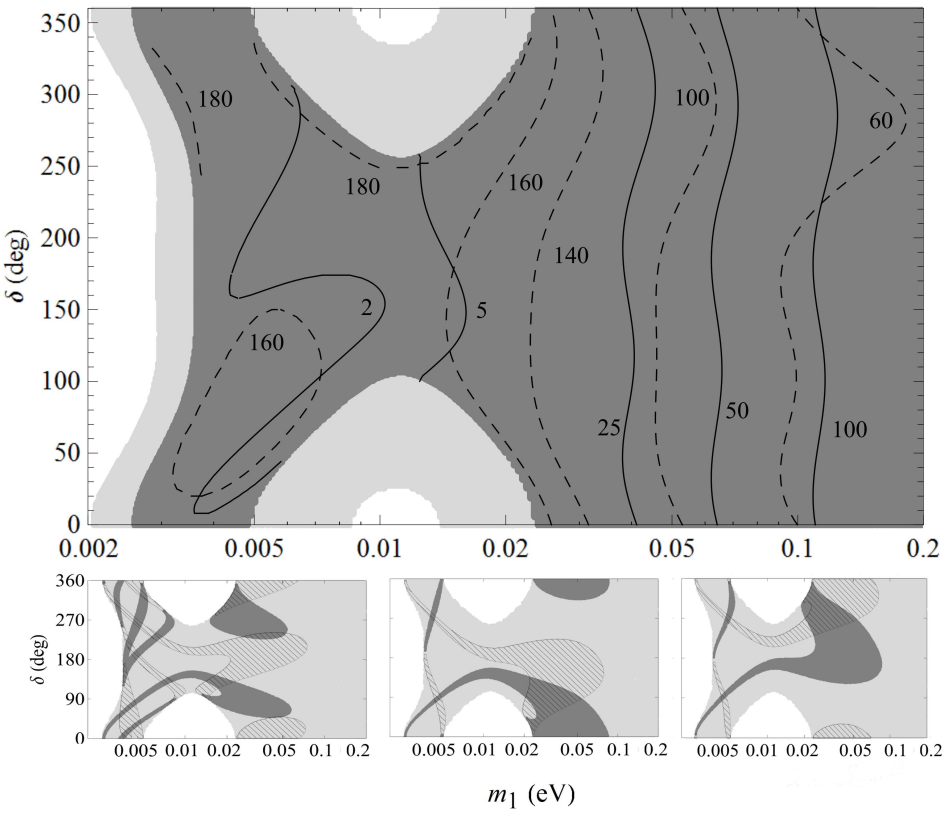

Figure 3.5 Same as Fig. 3.2, except for Class 4A and the normal hierarchy.

different when the lightest mass is below 20 meV, note the similarity of the $|M_{ee}| = 100$ meV and $\phi_2 = 60^\circ$ contours.

3.2.5 Class 4B

Similar to Class 4A, the condition for Class 4B is $(M^{-1})_{13} = 0$, which can be written as

$$m_1^{-1} = -\frac{m_2^{-1} e^{i\phi_2} U_{\tau 2} U_{e2} + m_3^{-1} e^{i\phi_3} U_{\tau 3} U_{e3}}{U_{\tau 1} U_{e1}}. \tag{3.25}$$

This condition is the same for both mass hierarchies, and the analysis follows as in previous classes, with A, B and C given in Table 3.1.

The allowed regions for the normal (inverted) hierarchy are shown in Fig. 3.6 (Fig. 3.7). The inverted hierarchy for this case is also similar to Class 2 NH: multiplying the A, B, and C coefficients by $m_2 m_3$ for Class 4B IH and dividing them by $m_2 m_3$ for Class 2 NH, A and B are identical for the two cases, and the dominant terms in C are also the same. As was true in

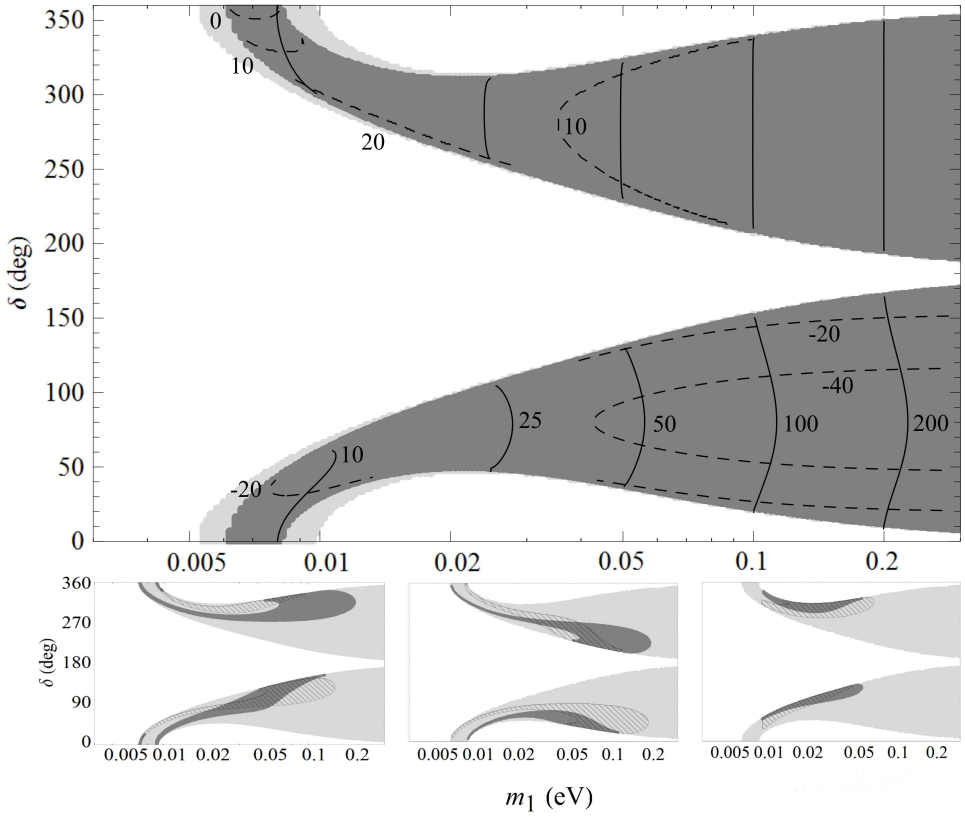

Figure 3.6 Same as Fig. 3.2, except for Class 4B and the normal hierarchy.

the previous section, the reverse correspondence between Class 4B NH and Class 2 IH exists only for larger values of the lightest mass (see Figs. 6 and 3 when the lightest mass is above 50 meV).

3.2.6 Class 4C

Similar to Class 4A, the condition for Class 4C is $(M^{-1})_{12} = 0$, which can be written as

$$m_1^{-1} = -\frac{m_2^{-1} e^{i\phi_2} U_{\mu 2} U_{e2} + m_3^{-1} e^{i\phi_3} U_{\mu 3} U_{e3}}{U_{\mu 1} U_{e1}}. \tag{3.26}$$

The corresponding values of A, B and C in Eq. (3.14) are given in Table 3.1.

Note that Class 4C is the same as Class 4B with $U_{\tau j} \to U_{\mu j}$, or $s_{23} \to -c_{23}$ and $c_{23} \to s_{23}$. As noted in Sec. 3.3, this transformation is equivalent to $\delta \to \delta + 180°$ when $\theta_{23} = 45°$. Therefore the allowed regions of Class 4C are similar to Class 4B in Fig. 3.6 for the normal hierarchy and in Fig. 3.7 for the inverted hierarchy with $\delta \to \delta + 180°$.

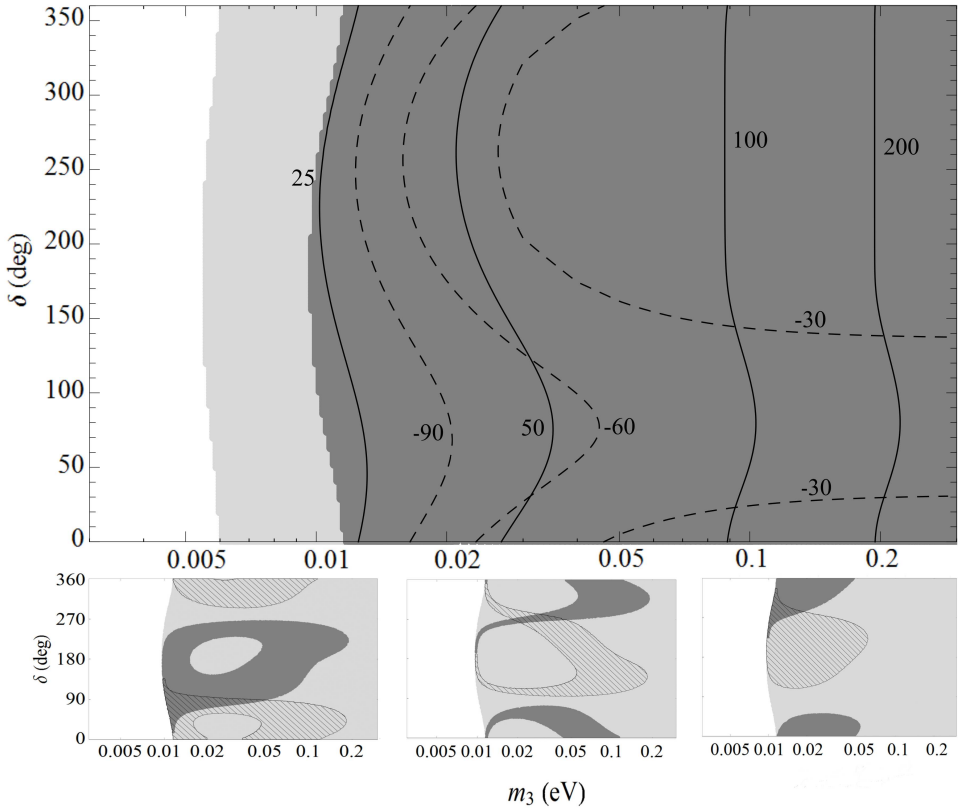

Figure 3.7 Same as Fig. 3.2, except for Class 4B and the inverted hierarchy.

The inverted hierarchy for this case is also similar to Class 3 NH, as can be seen by examining the A, B and C coefficients, and Class 4C NH and Class 3 IH give similar results for larger values of the lightest mass. Thus there is a general pattern that the texture zero NH and corresponding cofactor zero IH have similar predictions, and texture zero IH and corresponding cofactor zero NH have similar predictions when the lightest mass is not too small.

3.3 Discussion

We extended the most economical type I seesaw model to include three right-handed neutrinos. The simplest cases that fit the data have four texture zeros in the Yukawa couplings that connect the left-handed and right-handed neutrinos. These are equivalent to a single texture or cofactor zero for an off-diagonal element of the light neutrino mass matrix M. The cofactor zero condition is itself equivalent to a texture zero in M^{-1}. We used the latest experimental data to obtain the allowed regions for the lightest neutrino mass and Dirac CP phase δ, which can be measured in future neutrino experiments. We also used leptogenesis to further constrain the allowed regions; in general there is an upper bound on the lightest neutrino mass of about 100-200 meV for a single-flavored leptogenesis scenario. Figures 2 to 7 show that in any given model, not all values of δ are consistent with the leptogenesis predictions. Therefore a precise measurement of δ will reduce the number of viable models.

Once the lightest neutrino mass and Dirac CP phase are determined, these models make definite predictions for neutrinoless double beta decay. The minimum value of $|M_{ee}|$ for the best-fit oscillation parameters and the 2σ lower bounds are shown in Table 3.2. We find that the Class 1 NH and Class 4A IH have a minimum value for $|M_{ee}|$ of around 150 (130) meV for the best-fit (2σ-allowed) parameters, and could therefore be excluded by the $0\nu\beta\beta$ decay experiments that are currently running; Classes 2 IH and 3 IH have a minimum $|M_{ee}|$ of around 50 meV and can be definitively tested by experiments under construction. For Classes 3 NH and 4A NH the current lower bound on $|M_{ee}|$ is zero, and given the current measurements of the oscillation parameters, $0\nu\beta\beta$ decay will not constrain them. The remaining models have a minimum $|M_{ee}|$ in the range $1 - 20$ meV and can only be completely probed by significant improvements in the sensitivity of $0\nu\beta\beta$ experiments. The sum of light neutrino masses can also

Table 3.2 The minimum values of $|M_{ee}|$ (in 10^{-3} eV) in each class for the best-fit oscillation parameters, and the 2σ lower bounds.

Class	Best-fit		2σ lower bound	
	NH	IH	NH	IH
1	142.5	19.0	129.8	15.4
2	1.4	46.9	0.3	44.8
3	0.0	47.4	0.0	45.2
4A	0.0	150.3	0.0	138.3
4B	6.1	18.4	5.7	15.1
4C	8.4	18.2	7.5	14.9

be used to provide additional discrimination among these models. However, there is a general pattern that a texture zero NH and the corresponding cofactor zero IH have similar predictions, and a texture zero IH and the corresponding cofactor zero NH have similar predictions when the lightest mass is not too small. Therefore it may be difficult to uniquely specify the model from data, although experiments designed to determine the mass hierarchy could resolve this ambiguity.

Since the models studied in this chapter are equivalent to a single texture or cofactor zero for an off-diagonal element of M_ν, one might also consider examining models with a single texture or cofactor zero for a *diagonal* element of M_ν. Although not obtainable from texture zeros in the Yukawa couplings in a type I seesaw model, such models also have seven parameters in the light neutrino mass matrix and can be analyzed in a similar fashion. We will discuss the phenomenology of and possible motivation for these models in the next chapter.

CHAPTER 4. THE TEXTURE/COFACTOR ZERO MODELS

4.1 General Properties of the Texture/Cofactor Zero Models

The tiny masses of light neutrinos can be elegantly explained by the canonical seesaw mechanism [56], in which the mass matrix of the light neutrinos can be written as

$$M = -Y_\nu M_R^{-1} Y_\nu^T v^2/2, \tag{4.1}$$

where $v \approx 246$ GeV is the vacuum expectation value (VEV), Y_ν is 3×3 Yukawa coupling matrix and M_R is 3×3 heavy right-handed neutrino mass matrix. Here we assume all three light neutrinos are massive, so that the mass matrix of the light neutrinos is invertible (and therefore Y_ν must be invertible), and we can write the seesaw Eq. (4.1) as

$$M_R = -Y_\nu^T M^{-1} Y_\nu v^2/2\,, \tag{4.2}$$

Since $(M^{-1})_{ij} = \frac{1}{\det M} C_{ji}$, where C_{ji} is the (j,i) cofactor of M, and both the light and heavy neutrino mass matrices are symmetric, any texture zeros in the mass matrix are equivalent to cofactor zeros in the inverse of the mass matrix. Consequently, Eq. (4.2) implies that if the Yukawa coupling matrix is diagonal, then a cofactor zero in M implies a texture zero in M_R [90]. Similarly, a texture zero in M implies a cofactor zero in M_R when the Yukawa coupling matrix is diagonal.

An interesting feature about the structure of a texture or cofactor zero is that it is stable against radiative corrections. The one-loop renormalization group equation (RGE) describing the evolution of the light neutrino masses from the lightest right-handed neutrino mass scale M_1 to electroweak scale M_Z is [77]

$$16\pi^2 \frac{dM}{dt} = \alpha M + C[(Y_l Y_l^\dagger) M + M (Y_l Y_l^\dagger)^T], \tag{4.3}$$

where $t = \ln(\mu/M_1)$, μ is the renormalization scale and $Y_l = \mathrm{diag}(y_e, y_\mu, y_\tau)$ is the charged lepton Yukawa coupling matrix. In the SM, $C = -\frac{3}{2}$, $\alpha \approx -3g_2^2 + 6y_t^2 + \lambda$, and in the minimal supersymmetric standard model (MSSM), $C = 1$, $\alpha \approx -\frac{6}{5}g_1^2 - 6g_2^2 + 6y_t^2$, where g_1, g_2 are the gauge couplings, y_t is the top quark Yukawa coupling, and λ is the Higgs self-coupling. The solution to Eq. (4.3) can be written as [91]

$$M(M_Z) = I_\alpha \begin{bmatrix} I_e & 0 & 0 \\ 0 & I_\mu & 0 \\ 0 & 0 & I_\tau \end{bmatrix} M(M_1) \begin{bmatrix} I_e & 0 & 0 \\ 0 & I_\mu & 0 \\ 0 & 0 & I_\tau \end{bmatrix}. \tag{4.4}$$

where

$$I_\alpha = \exp\left[-\frac{1}{16\pi^2}\int_0^{\ln(M_1/M_Z)} \alpha(t)dt\right], \tag{4.5}$$

and

$$I_l = \exp\left[-\frac{C}{16\pi^2}\int_0^{\ln(M_1/M_Z)} y_l^2(t)dt\right], \tag{4.6}$$

for $l = e, \mu, \tau$. Since multiplying diagonal matrices will not change the structure of texture or cofactor zero, from Eq. (4.4), we can easily see that the texture or cofactor zero models will be stable against the RGE running from M_1 to M_Z.

4.2 Symmetry Realization

The texture zeros are due to an Abelian family symmetry that forbidden a specific entry in the Yukawa matrix and thus appears as a zero at high energies. All the texture and cofactor zero cases can be realized from discrete $\mathbb{Z}_N$ symmetries but it requires many scalar singlets [92]. Here we present a simple realization of the one cofactor zero models using a new $U(1)$ gauge symmetry that only requires two scalar singlets. We denote the charge of the new $U(1)$ gauge symmetry as Y', and make the charge assignments as follows: $Y'(q_L) = -Y'(u_R^c) = -Y'(d_R^c)$ for all families in the quark sector to avoid flavor changing neutral currents (FCNC); $Y'(l_{Li}) = -Y'(e_{Ri}^c) = -Y'(N_{Ri}^c)$ and $Y'(l_{Li}) \neq Y'(l_{Lj})$ for each family in the lepton sector; and $Y'(\phi) = 0$ for the SM Higgs. The anomaly-free requirement yields the condition [93]

$$9Y'(q_L) + Y'(l_{L1}) + Y'(l_{L2}) + Y'(l_{L3}) = 0. \tag{4.7}$$

If we consider the case with $Y'(q_L) \neq 0$, then the condition leads to a $B - \sum_\alpha x_\alpha L_\alpha$ gauge symmetry with the constraint $\sum_\alpha x_\alpha = 3$, where B and L are the baryon and lepton flavor numbers, respectively. One of the advantages of this model is that both the charged lepton and Dirac neutrino mass matrices are diagonal spontaneously because of the charge assignments of the $U(1)$ gauge symmetry. Hence a cofactor zero in M is equivalent to a cofactor zero in M_R^{-1}, which is equivalent to a texture zero in M_R. This can be achieved with a suitable $B - \sum_\alpha x_\alpha L_\alpha$ gauge symmetry and two SM gauge singlet scalars S_1 and S_2 with appropriate charges. Taking the $C_{11} = 0$ case for example, if we impose a $B - 3L_e - L_\mu + L_\tau$ symmetry on the model, then the $U(1)$ charge matrix for the right-handed neutrino mass term $Y'(\overline{N}_i^c N_j)$ is:

$$Y' = \begin{bmatrix} -6 & -4 & -2 \\ \cdot & -2 & 0 \\ \cdot & \cdot & 2 \end{bmatrix}. \tag{4.8}$$

Without any additional singlet scalars, the mass matrix of right-handed neutrinos will only have one non-vanishing entry with the scale $M_{B-3L_e-L_\mu+L\tau}$. By adding two additional singlet scalars S_1 and S_2 with $|Y'(S_1)| = 2$ and $|Y'(S_2)| = 4$ respectively, we can fill all the zero entries except the $(1,1)$ entry after S_1 and S_2 acquire VEVs:

$$\begin{aligned} M_R &= M_{B-3L_e-L_\mu+L\tau} \begin{bmatrix} 0 & 0 & 0 \\ \cdot & 0 & \times \\ \cdot & \cdot & 0 \end{bmatrix} + \langle S_1 \rangle \begin{bmatrix} 0 & 0 & \times \\ \cdot & \times & 0 \\ \cdot & \cdot & \times \end{bmatrix} + \langle S_2 \rangle \begin{bmatrix} 0 & \times & 0 \\ \cdot & 0 & 0 \\ \cdot & \cdot & 0 \end{bmatrix} \\ &\sim \begin{bmatrix} 0 & \times & \times \\ \cdot & \times & \times \\ \cdot & \cdot & \times \end{bmatrix}, \end{aligned} \tag{4.9}$$

where $\times$ denotes a non-vanishing entry. The other cases can be also realized similarly; a complete list is shown in Table 4.1.

Table 4.1 The anomaly-free $U(1)$ gauge symmetry realization for 6 classes with one cofactor zero in the light neutrino mass matrix. The Y' denotes the charge of the $U(1)$ gauge symmetry, and S_1, S_2 are two SM singlet scalars with non-vanishing VEVs.

Class	Symmetry generator	$\|Y'(S_1)\|$	$\|Y'(S_2)\|$
C_{11}=0	$B-3L_e-L_\mu+L_\tau$	2	4
C_{22}=0	$B+L_e-3L_\mu-L_\tau$	2	4
C_{33}=0	$B-L_e+L_\mu-3L_\tau$	2	4
C_{12}=0	$B-3L_e-L_\mu+L_\tau$	2	6
C_{23}=0	$B+L_e-3L_\mu-L_\tau$	2	6
C_{13}=0	$B-L_e+L_\mu-3L_\tau$	2	6

4.3 Phenomenology

4.3.1 One-zero Models

In this section, we study the phenomenological consequence of imposing one texture zero or one cofactor zero in the light neutrino mass matrix; for previous work see Refs. [94, 95, 96, 93]. Here we discuss the properties of one texture/cofactor zero in the diagonal entries of the mass matrix; the results for the off-diagonal cases can be found in the last chapter, which were obtained in models with four texture zeros in the Yukawa coupling matrix.

Our analysis proceeds as follows. For one texture/cofactor zero cases, there are 7 independent parameters in the light neutrino mass matrix; we take them to be θ_{12}, θ_{23}, θ_{13}, δm^2, Δm^2, the Dirac CP phase δ, and either m_1 (for normal hierarchy, NH, $m_1 < m_2 < m_3$) or m_3 (for inverted hierarchy, IH, $m_3 < m_1 < m_2$). Here we derive analytic formulas that relate the seven free parameters and determine the constraints on these models. For each case we find the allowed regions in m_1- (m_3-) δ plane given the best-fit values of θ_{12}, θ_{23}, θ_{13}, δm^2 and Δm^2, and also the 2σ allowed regions using the experimental uncertainties in the measured parameters. We also find iso-$|M_{ee}|$ contours relevant for neutrinoless double beta decay for the best-fit values.

4.3.1.1 $M_{ee} = 0$

The condition $M_{ee} = 0$ can be written as

$$m_1 = -\frac{m_3 e^{i\phi_3} U_{e3}^2 + m_2 e^{i\phi_2} U_{e2}^2}{U_{e1}^2}. \tag{4.10}$$

This condition is the same for all mass hierarchies. Taking the absolute square gives

$$m_1^2|U_{e1}|^4 - m_2^2|U_{e2}|^4 - m_3^2|U_{e3}|^4 = 2\mathrm{Re}(m_3 e^{-i\phi_3} U_{e3}^{*2} m_2 e^{i\phi_2} U_{e2}^2), \tag{4.11}$$

or, defining $\phi = \phi_3 - \phi_2$,

$$m_1^2|U_{e1}|^4 - m_2^2|U_{e2}|^4 - m_3^2|U_{e3}|^4 = 2m_2 m_3 c_{13}^2 s_{13}^2 s_{12}^2 \cos(-\phi + 2\delta). \tag{4.12}$$

Expanding the cosines yields the form of Eq. 3.14

$$C = A\cos\phi + B\sin\phi, \tag{4.13}$$

with A, B and C as listed in Table 4.2. Hence the only condition for $M_{11} = 0$ having a solution is $C^2 \leq A^2 + B^2$. Since C^2 and $A^2 + B^2$ do not depend on δ, it will only yield a constraint on m_1 for the normal hierarchy or m_3 for the inverted hierarchy. It can be easily seen that $C^2 \leq A^2 + B^2$ cannot be satisfied for the inverted hierarchy, which means that $M_{11} = 0$ for the inverted hierarchy is not possible. For the normal hierarchy and the best-fit oscillation parameters, the allowed range for m_1 is 0.0022 eV $\leq m_1 \leq$ 0.0066 eV, while the allowed range at 2σ is 0.0014 eV $\leq m_1 \leq$ 0.0085 eV.

4.3.1.2 $M_{\mu\mu} = 0$

From $M_{\mu\mu} = 0$, we get

$$m_1 = -\frac{m_3 e^{i\phi_3} U_{\mu 3}^2 + m_2 e^{i\phi_2} U_{\mu 2}^2}{U_{\mu 1}^2}\,, \tag{4.14}$$

which is independent of hierarchy. As before this may be put in the form of Eq. (3.14), with A, B and C given in Table 4.2. From Eq. (3.14), we can find the solution

$$\phi = 2\arctan\frac{B \pm \sqrt{A^2 + B^2 - C^2}}{A + C}, \tag{4.15}$$

Table 4.2 The expressions of A, B and C for one texture/cofactor zero in the diagonal entries of the mass matrix.

$$C = A\cos\phi + B\sin\phi$$

Class	A	B	C
$M_{11}=0$	$2m_2m_3c_{13}^2s_{13}^2s_{12}^2\cos(2\delta)$	$2m_2m_3c_{13}^2s_{13}^2s_{12}^2\sin(2\delta)$	$m_1^2\lvert U_{e1}\rvert^4 - m_2^2\lvert U_{e2}\rvert^4 - m_3^2\lvert U_{e3}\rvert^4$
$M_{22}=0$	$2m_2m_3s_{23}^2c_{13}^2\times$ $[c_{12}^2c_{23}^2 + s_{12}^2s_{23}^2s_{13}^2\cos(2\delta)$ $-2c_{12}s_{12}c_{23}s_{23}s_{13}\cos\delta]$	$2m_2m_3s_{23}^2c_{13}^2\times$ $[s_{12}^2s_{23}^2s_{13}^2\sin(2\delta)$ $-2c_{12}s_{12}c_{23}s_{23}s_{13}\sin\delta]$	$m_1^2\lvert U_{\mu1}\rvert^4 - m_2^2\lvert U_{\mu2}\rvert^4 - m_3^2\lvert U_{\mu3}\rvert^4$
$M_{33}=0$	$2m_2m_3c_{23}^2c_{13}^2\times$ $[c_{12}^2s_{23}^2 + s_{12}^2c_{23}^2s_{13}^2\cos(2\delta)$ $+2c_{12}s_{12}c_{23}s_{23}s_{13}\cos\delta]$	$2m_2m_3c_{23}^2c_{13}^2\times$ $[s_{12}^2c_{23}^2s_{13}^2\sin(2\delta)$ $+2c_{12}s_{12}c_{23}s_{23}s_{13}\sin\delta]$	$m_1^2\lvert U_{\tau1}\rvert^4 - m_2^2\lvert U_{\tau2}\rvert^4 - m_3^2\lvert U_{\tau3}\rvert^4$
$C_{11}=0$	$2m_2^{-1}m_3^{-1}c_{13}^2s_{13}^2s_{12}^2\cos(2\delta)$	$2m_2^{-1}m_3^{-1}c_{13}^2s_{13}^2s_{12}^2\sin(2\delta)$	$m_1^{-2}\lvert U_{e1}\rvert^4 - m_2^{-2}\lvert U_{e2}\rvert^4 - m_3^{-2}\lvert U_{e3}\rvert^4$
$C_{22}=0$	$2m_2^{-1}m_3^{-1}s_{23}^2c_{13}^2\times$ $[c_{12}^2c_{23}^2 + s_{12}^2s_{23}^2s_{13}^2\cos(2\delta)$ $-2c_{12}s_{12}c_{23}s_{23}s_{13}\cos\delta]$	$2m_2^{-1}m_3^{-1}s_{23}^2c_{13}^2\times$ $[s_{12}^2s_{23}^2s_{13}^2\sin(2\delta)$ $-2c_{12}s_{12}c_{23}s_{23}s_{13}\sin\delta]$	$m_1^{-2}\lvert U_{\mu1}\rvert^4 - m_2^{-2}\lvert U_{\mu2}\rvert^4 - m_3^{-2}\lvert U_{\mu3}\rvert^4$
$C_{33}=0$	$2m_2^{-1}m_3^{-1}c_{23}^2c_{13}^2\times$ $[c_{12}^2s_{23}^2 + s_{12}^2c_{23}^2s_{13}^2\cos(2\delta)$ $+2c_{12}s_{12}c_{23}s_{23}s_{13}\cos\delta]$	$2m_2^{-1}m_3^{-1}c_{23}^2c_{13}^2\times$ $[s_{12}^2c_{23}^2s_{13}^2\sin(2\delta)$ $+2c_{12}s_{12}c_{23}s_{23}s_{13}\sin\delta]$	$m_1^{-2}\lvert U_{\tau1}\rvert^4 - m_2^{-2}\lvert U_{\tau2}\rvert^4 - m_3^{-2}\lvert U_{\tau3}\rvert^4$

Then we can write Eq. (4.14) as

$$m_1 = e^{i\phi_2} \frac{-m_3 e^{i\phi} U_{\mu 3}^2 - m_2 U_{\mu 2}^2}{U_{\mu 1}^2}. \tag{4.16}$$

Since m_1 is a non-negative real number in the standard parametrization, we get

$$\phi_2 = -\arg[\frac{-m_3 e^{i\phi} U_{\mu 3}^2 - m_2 U_{\mu 2}^2}{U_{\mu 1}^2}], \tag{4.17}$$

and

$$\phi_3 = \phi_2 + \phi. \tag{4.18}$$

It is then possible to calculate the magnitude of the $\nu_e - \nu_e$ element of the neutrino mass matrix

$$|M_{ee}| = |m_1 c_{12}^2 c_{13}^2 + m_2 e^{-i\phi_2} s_{12}^2 c_{13}^2 + m_3 e^{-i\phi_3} s_{13}^2 e^{2i\delta}|, \tag{4.19}$$

which determines the rate for neutrinoless double-beta decay, a signal of lepton number violation. The allowed regions of the Dirac CP phase δ and the lightest mass m_1 (m_3) are defined by the set of them that satisfy the condition $C^2 \leq A^2 + B^2$. We scan over δ and m_1 (m_3) space to find the allowed regions; see Fig. 4.1 for the normal hierarchy and Fig. 4.2 for the inverted hierarchy, where regions corresponding to the best-fit parameters and those allowed at 2σ are shown. The lightest mass for the normal hierarchy is always larger than 0.027 eV at 2σ, while for the inverted hierarchy, it is strongly dependent on δ. We also plot iso-$|M_{ee}|$ contours using the best-fit oscillation parameters. Here only the contours for the plus sign of ϕ in Eq. (4.15) are shown because changing δ to $360^\circ - \delta$ yields the same contours for the minus solution.

4.3.1.3 $M_{\tau\tau} = 0$

From $M_{\tau\tau} = 0$, we get

$$m_1 = -\frac{m_3 e^{i\phi_3} U_{\tau 3}^2 + m_2 e^{i\phi_2} U_{\tau 2}^2}{U_{\tau 1}^2}\,, \tag{4.20}$$

which is independent of hierarchy. This may be put in the form of Eq. (3.14), with A, B and C as in Table 4.2. We find that the normal hierarchy is excluded at 2σ. The allowed region of δ versus m_3 for the inverted hierarchy is shown in Fig. 4.3, along with iso-$|M_{ee}|$ contours. We notice that for the best-fit oscillation parameters, the lightest mass m_3 has an upper bound of 0.047 eV, but there is no upper bound at 2σ.

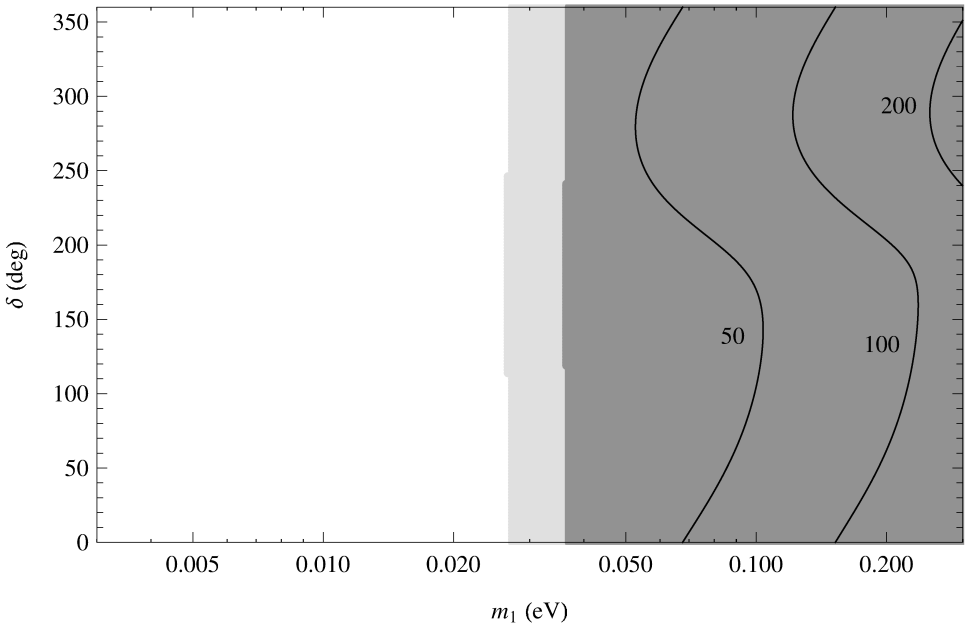

Figure 4.1 The allowed regions in the (m_1, δ) plane for $M_{\mu\mu} = 0$ and the normal hierarchy. The dark shaded regions correspond to the best-fit parameters of the oscillation parameters, while the light shaded regions are allowed at 2σ. The solid lines are iso-$|M_{ee}|$ contours (in meV).

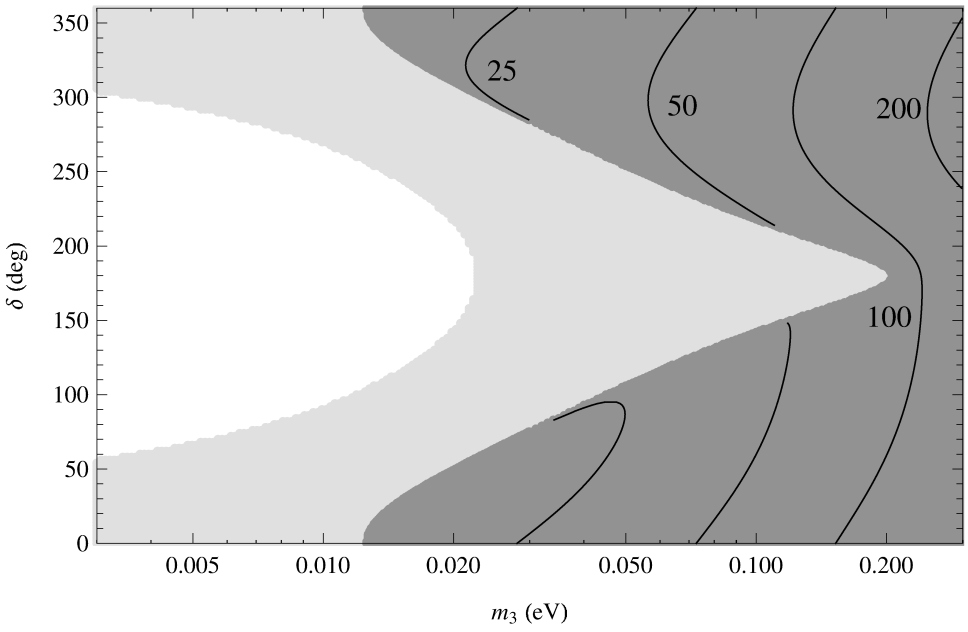

Figure 4.2 Same as Fig. 4.1, except for $M_{\mu\mu} = 0$ and the inverted hierarchy.

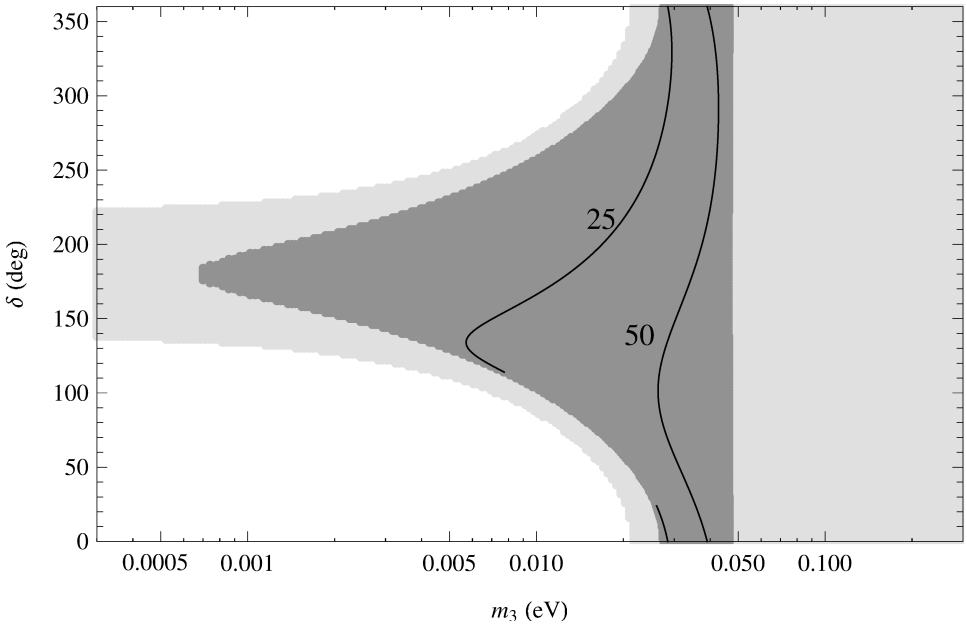

Figure 4.3 Same as Fig. 4.1, except for $M_{\tau\tau} = 0$ and the inverted hierarchy.

4.3.1.4 $C_{ee} = 0$

If $C_{ee} = 0$, then also $(M^{-1})_{ee} = 0$. Since $M^{-1} = V\,\mathrm{diag}(m_1^{-1}, m_2^{-1}, m_3^{-1})V^T$, we can write the condition as

$$m_1^{-1} = -\frac{m_3^{-1} e^{i\phi_3} U_{e3}^2 + m_2^{-1} e^{i\phi_2} U_{e2}^2}{U_{e1}^2}\,, \tag{4.21}$$

which is the same for either mass hierarchy. Taking the absolute square, we write this in the form of Eq. (3.14), with A, B and C as in Table 4.2. Since C^2 and $A^2 + B^2$ do not depend on δ, it will only yield a constraint on m_1 (m_3) for the normal (inverted) hierarchy. We find that the normal hierarchy is excluded at 2σ. For the inverted hierarchy and best-fit oscillation parameters, the allowed range for m_3 is 0.0013 eV $\leq m_3 \leq$ 0.0031 eV, while the allowed range at 2σ is 0.0010 eV $\leq m_3 \leq$ 0.0042 eV.

4.3.1.5 $C_{\mu\mu} = 0$

From $C_{\mu\mu} = 0$, which is equivalent to $(M^{-1})_{\mu\mu} = 0$, we get

$$m_1^{-1} = -\frac{m_3^{-1} e^{i\phi_3} U_{\mu 3}^2 + m_2^{-1} e^{i\phi_2} U_{\mu 2}^2}{U_{\mu 1}^2}\,, \tag{4.22}$$

which is the same for either mass hierarchy, and may be put in the form of Eq. (3.14), with A, B and C as in Table 4.2. The allowed region of δ versus m_1 for the normal ordering is shown in Fig. 4.4 and the allowed region of δ versus m_3 for the inverted ordering is shown in Fig. 4.5.

The allowed regions for Class $C_{\mu\mu} = 0$ IH (Fig. 4.5) are similar to those for Class $M_{\mu\mu} = 0$ NH (Fig. 4.1). The similarity of a cofactor-zero IH scenario with a texture-zero NO can be understood by looking at the form of the A, B, and C coefficients in Table 4.2. If we multiply the coefficients for Class $C_{\mu\mu} = 0$ IH by $m_2 m_3$, and divide the coefficients for Class $M_{\mu\mu} = 0$ NH by $m_2 m_3$, we see that A and B become the same for the two cases. For the C coefficient, the dominant term in each case is the third one, proportional to $|U_{\mu 3}|^4$ times the ratio of a larger mass to a smaller one. Therefore the allowed regions for these two cases are similar.

One can also see a similarity between cofactor-zero models with NH and texture-zero models with IH, although the correspondence occurs only for larger values of the lightest mass. For example, for Class $C_{\mu\mu} = 0$ NH and Class $M_{\mu\mu} = 0$ IH, after multiplying the A, B, and C coefficients for the NH by m2m3 and dividing the coefficients for the IH by $m_2 m_3$, the A and B coefficients are the same. When the lightest mass is not so small, such that $m_1 \approx m_2$ in the NH, then the same terms in the C coefficient are dominant and proportional to a large mass divided by a small mass. Thus for higher values of the lightest mass, the allowed regions of Classes $C_{\mu\mu} = 0$ NH and $M_{\mu\mu} = 0$ IH must be similar. This can be seen by comparing Figs. 4.4 and 4.2. However, for small values of the lightest mass, the first two terms in the C coefficient have similar size for Class $M_{\mu\mu} = 0$ IH, but only the first term is dominant for Class $C_{\mu\mu} = 0$ NH. Thus the allowed regions are quite different when the lightest mass is below 20 meV.

4.3.1.6 $C_{\tau\tau} = 0$

From $C_{\tau\tau} = 0$, which is equivalent to $(M^{-1})_{\tau\tau} = 0$, we get

$$m_1^{-1} = -\frac{m_3^{-1} e^{i\phi_3} U_{\tau 3}^2 + m_2^{-1} e^{i\phi_2} U_{\tau 2}^2}{U_{\tau 1}^2}. \tag{4.23}$$

This condition is the same for either mass hierarchy. After taking the absolute square, then as before this may be put in the form of Eq. (3.14), with A, B and C as in Table 4.2. We find that for the inverted hierarchy, this case is not allowed for the best-fit parameters, but is

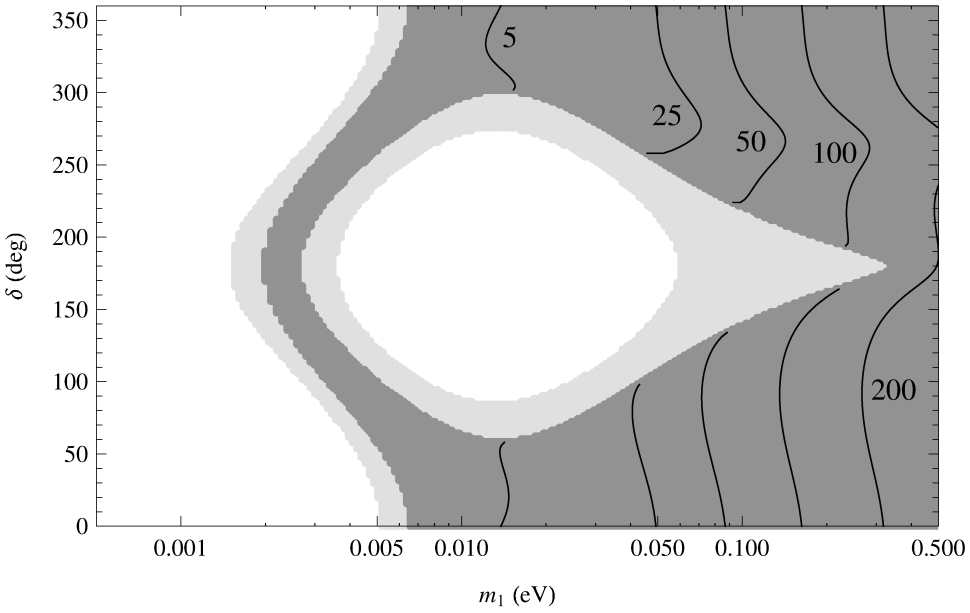

Figure 4.4 Same as Fig. 4.1, except for $C_{\mu\mu} = 0$ and the normal hierarchy.

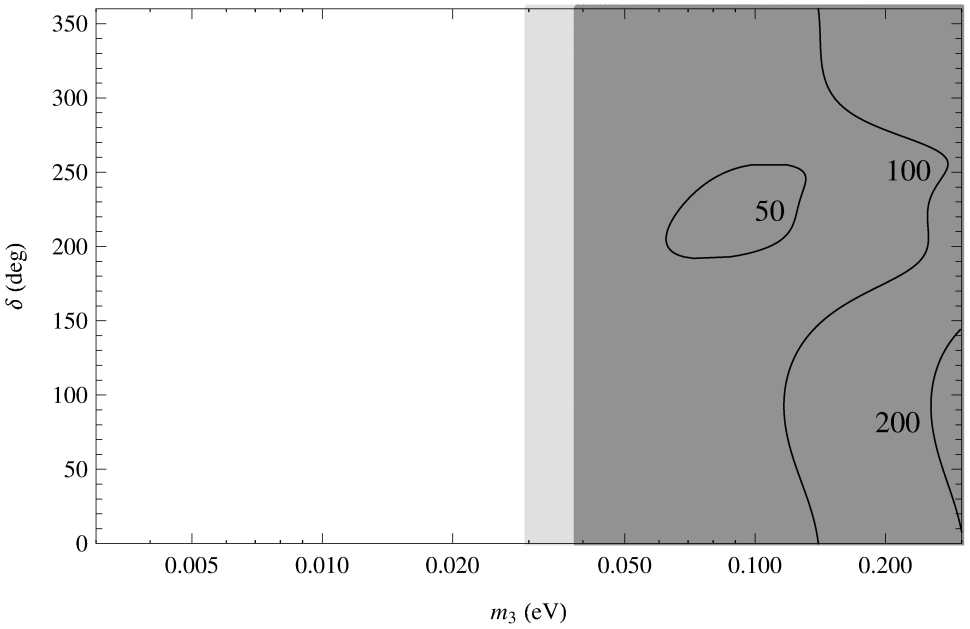

Figure 4.5 Same as Fig. 4.1, except for $C_{\mu\mu} = 0$ and the inverted hierarchy.

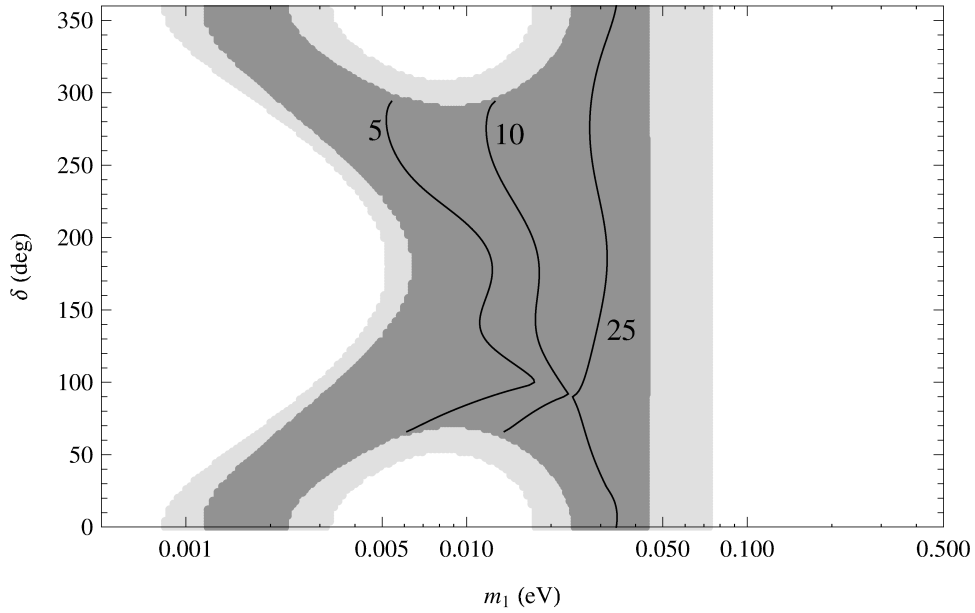

Figure 4.6 Same as Fig. 4.1, except for $C_{\tau\tau} = 0$ and the normal hierarchy.

allowed at 2σ, with a lower bound on m_3 of 0.033 eV. The allowed region of δ versus m_3 for the normal hierarchy is shown in Fig. 4.6, along with iso-$|M_{ee}|$ contours. We see that the lightest mass m_1 has an upper bound of 0.044 eV for the best-fit oscillation parameters, and 0.071 eV at 2σ. Noticed the allowed regions for Class $M_{\tau\tau} = 0$ IH and Class $C_{\tau\tau} = 0$ NH also have a similar correspondence in the A, B, and C coefficients, and they have similar allowed regions for higher values of the lightest mass; see Figs. 4.6 and 4.3.

4.3.2 Two-zero Models

In this section, we study the consequences of imposing two texture/cofactor zeros in the neutrino mass matrix. There are three classes of such ansatzes: two texture zeros (TT) [97, 98], two cofactor zeros (CC) [99, 100], and one texture zero and one cofactor zero (TC) [101]. Of the nine real parameters of M, five are fixed by measurements of the three mixing angles and two mass-squared differences; for a recent global three-neutrino fit see Ref. [53]. The remaining four parameters, which we take to be the lightest mass, the Dirac phase, and the two Majorana phases, can then be determined from the four constraints that define the two texture/cofactor zeros. Consequently, the rate for neutrinoless double beta decay ($0\nu\beta\beta$) which is given by the

magnitude of the $\nu_e - \nu_e$ element of the neutrino mass matrix,

$$|M_{ee}| = |m_1 c_{12}^2 c_{13}^2 + m_2 e^{-i\phi_2} s_{12}^2 c_{13}^2 + m_3 e^{-i\phi_3} s_{13}^2 e^{2i\delta}|\,, \tag{4.24}$$

is also determined.

4.3.2.1 Two texture zeros

The condition for a vanishing element $M_{\alpha\beta} = M_{\alpha\beta}^* = 0$ is

$$m_1 U_{\alpha 1} U_{\beta 1} + m_2 e^{i\phi_2} U_{\alpha 2} U_{\beta 2} + m_3 e^{i\phi_3} U_{\alpha 3} U_{\beta 3} = 0\,. \tag{4.25}$$

Since there are two such constraints that depend linearly on the masses, the masses are related by

$$\frac{m_1}{c_1} = \frac{m_2 e^{i\phi_2}}{c_2} = \frac{m_3 e^{i\phi_3}}{c_3}\,, \tag{4.26}$$

where c_j are complex numbers that are quartic in the matrix elements of U. Then, with $\delta m^2 = m_2^2 - m_1^2$ and $\Delta m^2 = |m_3^2 - \frac{1}{2}(m_1^2 + m_2^2)|$, we get two equations that relate m_1 to the oscillation parameters and the Dirac phase δ,

$$m_1 = \sqrt{\frac{\delta m^2}{|c_2/c_1|^2 - 1}}\,, \tag{4.27}$$

$$m_1 = \sqrt{\frac{\frac{1}{2}\delta m^2 \pm \Delta m^2}{|c_3/c_1|^2 - 1}}\,, \tag{4.28}$$

where the plus and minus signs correspond to the normal hierarchy (NH) and the inverted hierarchy (IH), respectively. (For the NH the lightest mass is m_1, and for the IH the lightest mass is $m_3 = \sqrt{m_1^2 + \frac{1}{2}\delta m^2 - \Delta m^2}$.) For a fixed set of oscillation parameters each of these two equations give m_1 as a function of δ, and the intersections of the curves give the allowed values of m_1 and δ. We use the data from the latest global fit of Ref. [53] to find the 2σ allowed regions for the lightest mass and δ that satisfy Eqs. (4.27) and (4.28). Note that if we replace δ by $-\delta$, the two constraints from the Eqs. (4.27) and (4.28) will be the same since the magnitude of c_i does not depend on the sign of δ, but because the latest global fit has a preference for negative values of δ [53], the allowed regions for $0 \leq \delta \leq 180^\circ$ are a little larger than for $180^\circ \leq \delta \leq 360^\circ$.

For two texture zeros in the mass matrix, there are $\frac{6!}{2!4!} = 15$ different cases to consider. If two off-diagonal entries vanish, the mass matrices are block diagonal and have one neutrino

Table 4.3 The expressions for c_1, c_2 and c_3 for Class X. The symbol $\times$ denotes a nonzero matrix element.

Case	Structure	c_1	c_2	c_3
X_1	$\begin{pmatrix} 0 & 0 & \times \\ 0 & \times & \times \\ \times & \times & \times \end{pmatrix}$	$U^*_{\tau 1}U_{e2}U_{e3}$	$U^*_{\tau 2}U_{e3}U_{e1}$	$U^*_{\tau 3}U_{e1}U_{e2}$
X_2	$\begin{pmatrix} 0 & \times & 0 \\ \times & \times & \times \\ 0 & \times & \times \end{pmatrix}$	$U^*_{\mu 1}U_{e2}U_{e3}$	$U^*_{\mu 2}U_{e3}U_{e1}$	$U^*_{\mu 3}U_{e1}U_{e2}$
X_3	$\begin{pmatrix} \times & \times & \times \\ \times & \times & 0 \\ \times & 0 & 0 \end{pmatrix}$	$U^*_{e1}U_{\tau 2}U_{\tau 3}$	$U^*_{e2}U_{\tau 3}U_{\tau 1}$	$U^*_{e3}U_{\tau 1}U_{\tau 2}$
X_4	$\begin{pmatrix} \times & \times & \times \\ \times & 0 & 0 \\ \times & 0 & \times \end{pmatrix}$	$U^*_{e1}U_{\mu 2}U_{\mu 3}$	$U^*_{e2}U_{\mu 3}U_{\mu 1}$	$U^*_{e3}U_{\mu 1}U_{\mu 2}$
X_5	$\begin{pmatrix} \times & 0 & \times \\ 0 & 0 & \times \\ \times & \times & \times \end{pmatrix}$	$U^*_{\tau 1}U_{\mu 2}U_{\mu 3}$	$U^*_{\tau 2}U_{\mu 3}U_{\mu 1}$	$U^*_{\tau 3}U_{\mu 1}U_{\mu 2}$
X_6	$\begin{pmatrix} \times & \times & 0 \\ \times & \times & \times \\ 0 & \times & 0 \end{pmatrix}$	$U^*_{\mu 1}U_{\tau 2}U_{\tau 3}$	$U^*_{\mu 2}U_{\tau 3}U_{\tau 1}$	$U^*_{\mu 3}U_{\tau 1}U_{\tau 2}$

decoupled from the others, which is inconsistent with the data. Therefore, we only need to consider 12 cases that can be divided into three categories:

1. **One zero on diagonal, off-diagonal zero sharing column and row.** The six possibilities of this type, X_1, X_2, X_3, X_4, X_5, and X_6, are displayed in Table 4.3. Using the unitarity of U and the fact that the cofactors of U_{ij} are equal to U^*_{ij}, e.g., $U_{e1}U_{\mu 2} - U_{e2}U_{\mu 1} = U^*_{\tau 3}$, we obtain the simplified expressions for c_1, c_2, and c_3 provided in Table 4.3. From a numerical analysis, we find that at the 2σ level, only X_1, X_2 and X_5 are allowed for the normal hierarchy and X_5 and X_6 are allowed for the inverted hierarchy. The allowed regions for X_1 and X_2 for the normal hierarchy are shown in Figs. 4.7 and 4.8. The allowed regions for X_5 for the normal and inverted hierarchy are shown in Figs. 4.9 and 4.10, respectively. For the best-fit values of the measured oscillation parameters, X_2 NH and X_5 IH are not allowed, and the best-fit points for X_1 NH and X_5 NH are shown in Figs. 4.7 and 4.9 respectively. Both hierarchies for X_5 have nearly maximal CP

Table 4.4 The expressions for c_1, c_2 and c_3 for Class Y. The symbol $\times$ denotes a nonzero matrix element.

Case	Structure	c_1	c_2	c_3
Y_1	$\begin{pmatrix} \times & \times & 0 \\ \times & 0 & \times \\ 0 & \times & \times \end{pmatrix}$	$U^*_{e1}U_{e2}U_{\mu 3} - U^*_{\tau 1}U_{\mu 2}U_{\tau 3}$	$U_{e1}U^*_{e2}U_{\mu 3} - U_{\mu 1}U^*_{\tau 2}U_{\tau 3}$	$U_{\mu 1}U_{e2}U^*_{e3} - U_{\tau 1}U_{\mu 2}U^*_{\tau 3}$
Y_2	$\begin{pmatrix} \times & 0 & \times \\ 0 & \times & \times \\ \times & \times & 0 \end{pmatrix}$	$U^*_{\mu 1}U_{\tau 2}U_{\mu 3} - U^*_{e1}U_{e2}U_{\tau 3}$	$U_{\tau 1}U^*_{\mu 2}U_{\mu 3} - U_{e1}U^*_{e2}U_{\tau 3}$	$U_{\mu 1}U_{\tau 2}U^*_{\mu 3} - U_{\tau 1}U_{e2}U^*_{e3}$
Y_3	$\begin{pmatrix} 0 & \times & \times \\ \times & \times & 0 \\ \times & 0 & \times \end{pmatrix}$	$U^*_{\tau 1}U_{e2}U_{\tau 3} - U^*_{\mu 1}U_{\mu 2}U_{e3}$	$U_{e1}U^*_{\tau 2}U_{\tau 3} - U_{\mu 1}U^*_{\mu 2}U_{e3}$	$U_{\tau 1}U_{e2}U^*_{\tau 3} - U_{e1}U_{\mu 2}U^*_{\mu 3}$

Table 4.5 The expressions for c_1, c_2 and c_3 for Class Z. The symbol $\times$ denotes a nonzero matrix element.

Case	Structure	c_1	c_2	c_3
Z_1	$\begin{pmatrix} \times & \times & \times \\ \times & 0 & \times \\ \times & \times & 0 \end{pmatrix}$	$(U_{\mu 2}U_{\tau 3} + U_{\mu 3}U_{\tau 2})U^*_{e1}$	$(U_{\mu 3}U_{\tau 1} + U_{\mu 1}U_{\tau 3})U^*_{e2}$	$(U_{\mu 1}U_{\tau 2} + U_{\mu 2}U_{\tau 1})U^*_{e3}$
Z_2	$\begin{pmatrix} 0 & \times & \times \\ \times & \times & \times \\ \times & \times & 0 \end{pmatrix}$	$(U_{e2}U_{\tau 3} + U_{e3}U_{\tau 2})U^*_{\mu 1}$	$(U_{e3}U_{\tau 1} + U_{e1}U_{\tau 3})U^*_{\mu 2}$	$(U_{e1}U_{\tau 2} + U_{e2}U_{\tau 1})U^*_{\mu 3}$
Z_3	$\begin{pmatrix} 0 & \times & \times \\ \times & 0 & \times \\ \times & \times & \times \end{pmatrix}$	$(U_{e2}U_{\mu 3} + U_{e3}U_{\mu 2})U^*_{\tau 1}$	$(U_{e3}U_{\mu 1} + U_{e1}U_{\mu 3})U^*_{\tau 2}$	$(U_{e1}U_{\mu 2} + U_{e2}U_{\mu 1})U^*_{\tau 3}$

violation, i.e., δ close to 90° or 270°, and a lower bound on the lightest mass of about 30 meV. For X_5 NH and X_5 IH, the upper bound on the lightest mass is about 290 meV and 250 meV, respectively. For comparison, the 95% C.L. limit from cosmology is $\sum m_i < 660$ meV [102]. The allowed region for X_6 IH is very similar to that for X_5 IH.

2. **One zero on diagonal, off-diagonal zero not sharing column and row.** The three possibilities of this type, Y_1, Y_2 and Y_3, and the corresponding c_i's are displayed in Table 4.4. At the 2σ level, Y_1 and Y_2 are allowed for the inverted hierarchy, and their allowed regions are very similar to that for X_5 IH; Y_1 is also allowed for the normal hierarchy and the allowed region is very similar to that for X_5 NH; Y_3 is excluded at 2σ. All the allowed cases have nearly maximal CP violation, and a lower bound on the lightest mass of about 30 meV, similar to X_5 NH and X_5 IH; see Figs. 4.9 and 4.10.

3. **Two zeros on diagonal.** The three possibilities of this type, Z_1, Z_2 and Z_3, and the corresponding c_i's are listed in Table 4.5. The numerical results show that only Z_1 for the inverted hierarchy is allowed at the 2σ level, and the allowed regions are shown in Fig. 4.11. Z_1 for the normal hierarchy is excluded at 2σ for $m_1 < 0.3$ eV, which is consistent with the result of Ref. [103].

Although the allowed regions for the seven acceptable textures of Ref. [94] have been further restricted by the determination of θ_{13}, all seven textures remain allowed. Further restrictions on the Dirac CP phase δ [98] can also be placed by the latest global fit [53] for each case.

4.3.2.2 Two cofactor zeros

In Ref. [100] it was shown that for matrices with two zero cofactors, the lightest mass can vanish only if $\theta_{13} = 0$. Since θ_{13} is nonzero at the 7.7σ level [104], we assume there are no vanishing neutrino masses and the mass matrix is invertible. Since $(M^{-1})_{\alpha\beta} = \frac{1}{\det M} C_{\beta\alpha}$ (where $C_{\alpha\beta}$ is the (α, β) cofactor of M), and the Majorana neutrino mass matrix is symmetric, $C_{\alpha\beta} = 0$ is equivalent to $(M^{-1})_{\alpha\beta} = 0$. Because $M^{-1} = V \mathrm{diag}(m_1^{-1}, m_2^{-1}, m_3^{-1}) V^T$, the constraint is

$$m_1^{-1} U_{\alpha 1} U_{\beta 1} + m_2^{-1} e^{i\phi_2} U_{\alpha 2} U_{\beta 2} + m_3^{-1} e^{i\phi_3} U_{\alpha 3} U_{\beta 3} = 0 \,. \tag{4.29}$$

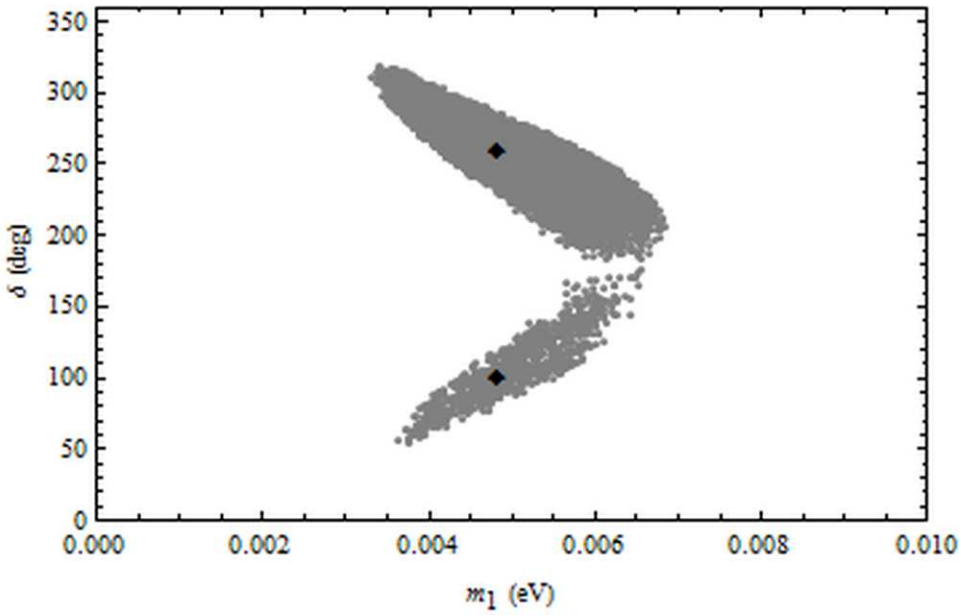

Figure 4.7 The 2σ allowed regions in the (m_1, δ) plane for the TT X_1 case and the normal hierarchy. The black diamonds indicate m_1 and δ for the best-fit values of the five oscillation parameters.

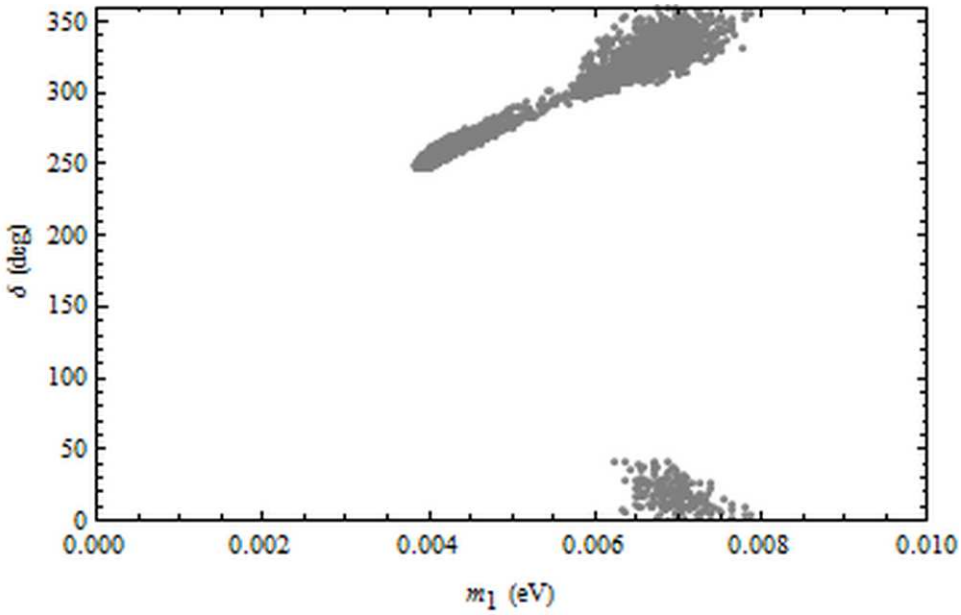

Figure 4.8 Same as Fig. 4.7, except for TT X_2 and the normal hierarchy. This case is not allowed for the best-fit oscillation parameters.

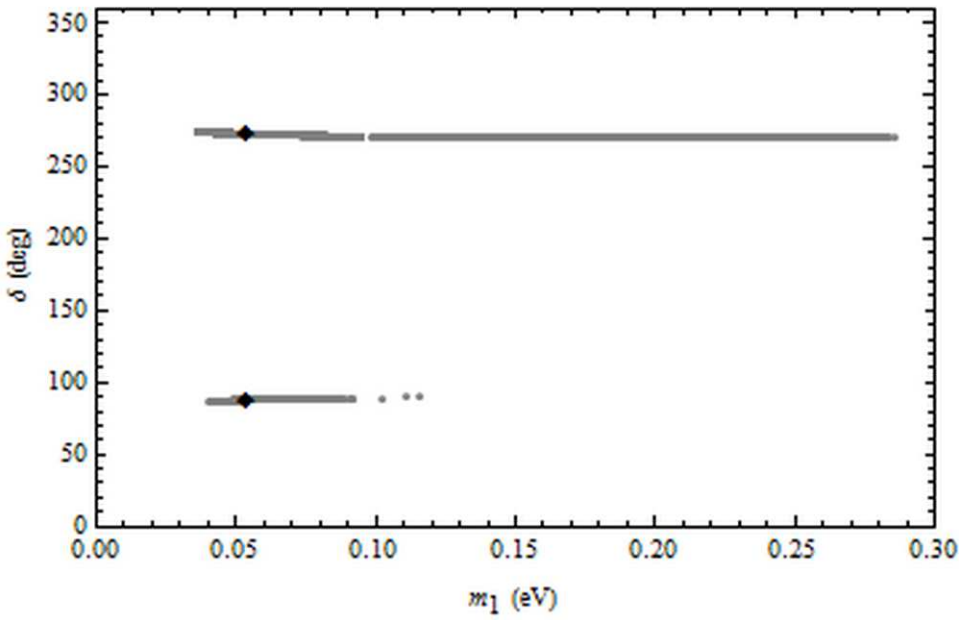

Figure 4.9 Same as Fig. 4.7, except for TT X_5 and the normal hierarchy.

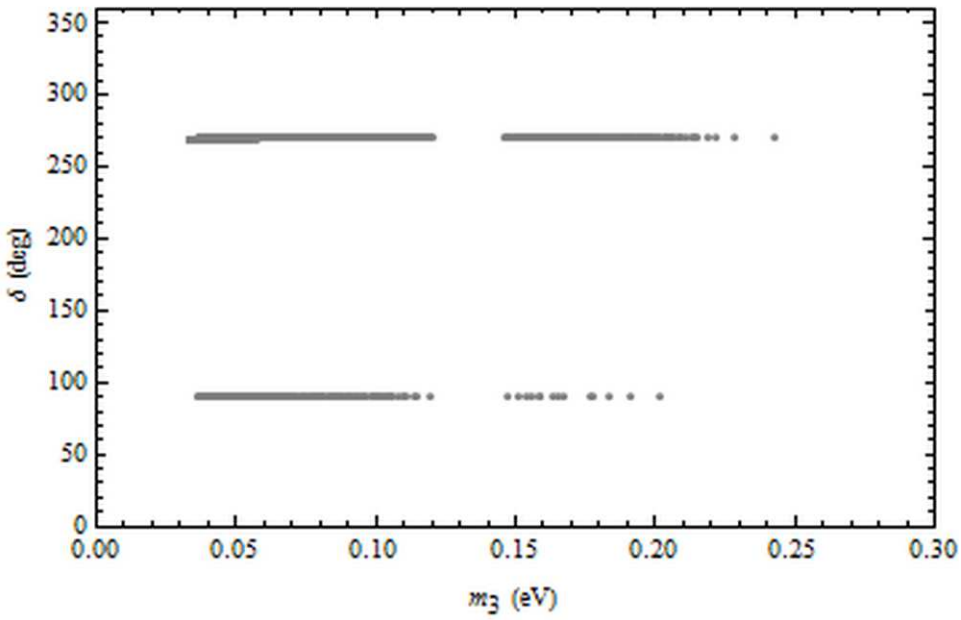

Figure 4.10 Same as Fig. 4.7, except for TT X_5 and the inverted hierarchy. This case is not allowed for the best-fit oscillation parameters.

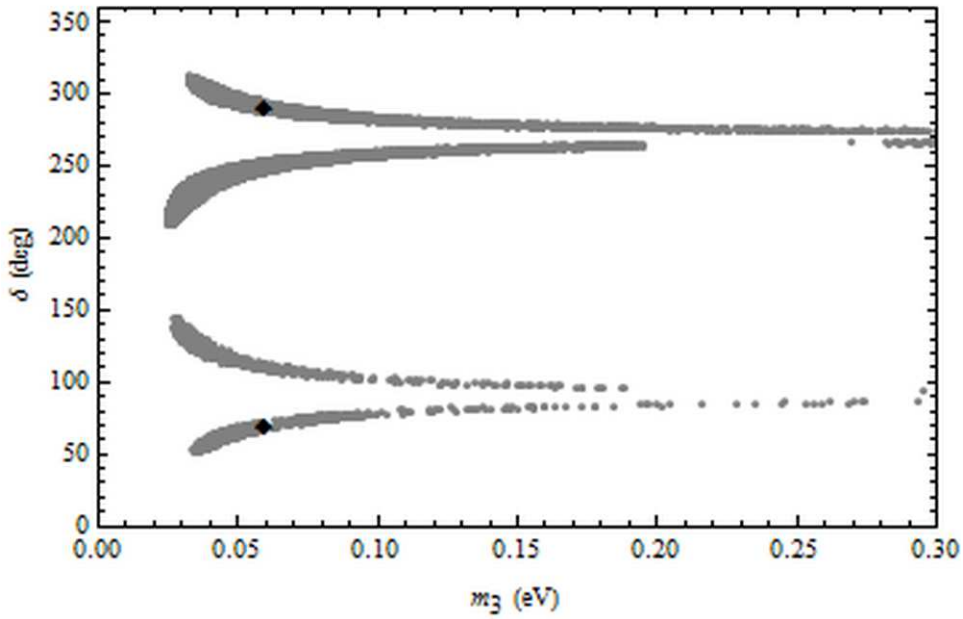

Figure 4.11 Same as Fig. 4.7, except for TT Z_1 and the inverted hierarchy.

The above equation is the same as Eq. (4.25), except that the m_i's are replaced by their inverses. Hence, we can follow a procedure similar to that for the TT case to find the favored values of the lightest mass and δ. Since the cofactor matrix is also diagonalized by the mixing matrix V, it cannot be block diagonal, and only 12 different patterns need to be considered. It is possible to employ the notation for the TT case if the locations of the two zeros are the same in the cofactor matrix as in the mass matrix. Then all the c_i's are identical, and the only difference from the TT case is that Eqs. (4.27) and (4.28) are replaced by

$$m_1 = \sqrt{\frac{\delta m^2}{|c_1/c_2|^2 - 1}}\,, \tag{4.30}$$

$$m_1 = \sqrt{\frac{\frac{1}{2}\delta m^2 \pm \Delta m^2}{|c_1/c_3|^2 - 1}}\,. \tag{4.31}$$

As for the TT case, there are three categories:

1. **One zero on diagonal, off-diagonal zero sharing column and row.** An interesting fact is that the two cofactor zero cases in this class yield the same allowed regions as for the two texture zero cases in the same class [99, 100]; the correspondence is listed in Table 4.6. The reason for this is that the two cofactor zero conditions in this category

Table 4.6 The correspondence between the two cofactor zero cases and two texture zero cases for Class X.

Two cofactor zeros	X_1	X_2	X_3	X_4	X_5	X_6
Two texture zeros	X_3	X_4	X_1	X_2	X_6	X_5

imply either two texture zeros, or three cofactor zeros in a row or column. The latter possibility which gives a vanishing mass is excluded since $\theta_{13} \neq 0$. From Table 4.6, we readily find the cases that are allowed at 2σ: X_3, X_4 and X_6 for the normal hierarchy, and X_5 and X_6 for the inverted hierarchy. The allowed regions in the $m_1(m_3)$-δ plane are the same as those for the corresponding cases in the TT ansatz.

2. **One zero on diagonal, off-diagonal zero not sharing column and row.** There are three possibilities of this type: Y_1, Y_2 and Y_3; see Table 4.4. At the 2σ level, Y_1 and Y_2 are allowed for the inverted hierarchy, and their allowed regions are very similar to that for TT X_5 IH; Y_2 is also allowed for the normal hierarchy and the allowed region is very similar to that for TT X_5 NH; Y_3 is excluded at 2σ. All the allowed cases have nearly maximal CP violation, and a lower bound on the lightest mass of about 30 meV, similar to TT X_5 NH and and TT X_5 IH.

3. **Two zeros on diagonal.** There are three possibilities of this type: Z_1, Z_2 and Z_3; see Table 4.5. We find numerically that Z_1 is allowed at 2σ for the normal hierarchy only. The other cases are excluded at 2σ. The allowed regions for Z_1 for the normal hierarchy are shown in Fig. 4.12.

4.3.2.3 One texture zero and one cofactor zero

There are 36 possibilities with one texture zero and one cofactor zero, of which 21 are equivalent to a TT case [101]. So we only need to study the remaining 15 cases listed in Table 4.7. The two constraints $M_{\alpha\beta} = 0$ and $C_{\alpha'\beta'} = 0$ can be written as

$$m_1 A_1 + m_2 e^{-i\phi_2} A_2 + m_3 e^{-i\phi_3} A_3 = 0\,, \tag{4.32}$$

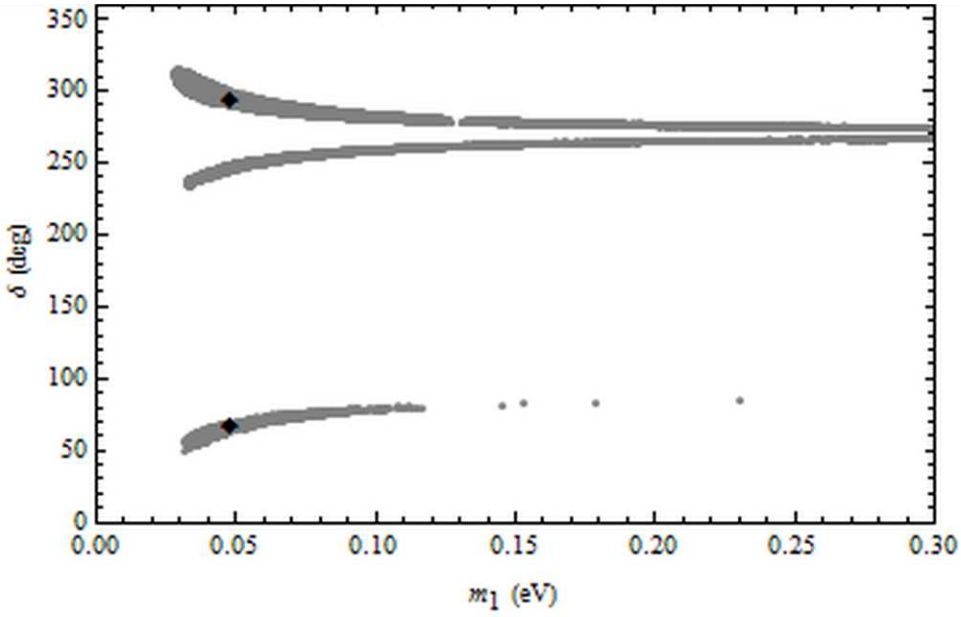

Figure 4.12 Same as Fig. 4.7, except for CC Z_1 and the normal hierarchy.

Table 4.7 The 15 cases with one texture zero and one cofactor zero that are not reducible to a TT case.

Case	Conditions
$1A$	$M_{ee}=0, C_{ee}=0$
$1B$	$M_{ee}=0, C_{e\mu}=0$
$1C$	$M_{ee}=0, C_{e\tau}=0$
$2A$	$M_{e\mu}=0, C_{ee}=0$
$2D$	$M_{e\mu}=0, C_{\mu\mu}=0$
$3A$	$M_{e\tau}=0, C_{ee}=0$
$3F$	$M_{e\tau}=0, C_{\tau\tau}=0$
$4B$	$M_{\mu\mu}=0, C_{e\mu}=0$
$4D$	$M_{\mu\mu}=0, C_{\mu\mu}=0$
$4E$	$M_{\mu\mu}=0, C_{\mu\tau}=0$
$5D$	$M_{\mu\tau}=0, C_{\mu\mu}=0$
$5F$	$M_{\mu\tau}=0, C_{\tau\tau}=0$
$6C$	$M_{\tau\tau}=0, C_{e\tau}=0$
$6E$	$M_{\tau\tau}=0, C_{\mu\tau}=0$
$6F$	$M_{\tau\tau}=0, C_{\tau\tau}=0$

and

$$m_1^{-1}B_1 + m_2^{-1}e^{i\phi_2}B_2 + m_3^{-1}e^{i\phi_3}B_3 = 0\,, \tag{4.33}$$

where $A_i = U^*_{\alpha i}U^*_{\beta i}$, and $B_i = U_{\alpha' i}U_{\beta' i}$ for $i = 1, 2, 3$. Solving these two equations, we get

$$\frac{m_3}{m_1}e^{-i\phi_3} = \frac{1}{2A_3B_1}(A_2B_2 - A_1B_1 - A_3B_3 \pm \sqrt{\Lambda})\,, \tag{4.34}$$

$$\frac{m_2}{m_1}e^{-i\phi_2} = \frac{1}{2A_2B_1}(A_3B_3 - A_1B_1 - A_2B_2 \mp \sqrt{\Lambda})\,, \tag{4.35}$$

where $\Lambda = A_1^2B_1^2 + A_2^2B_2^2 + A_3^2B_3^2 - 2(A_1A_2B_1B_2 + A_1A_3B_1B_3 + A_2A_3B_2B_3)$. Taking the absolute values of the above equations, we can find the two mass ratios, $\sigma = m_2/m_1$ and $\rho = m_3/m_1$. Then,

$$\begin{aligned} m_1 &= \sqrt{\frac{\delta m^2}{\sigma^2 - 1}}, \\ m_1 &= \sqrt{\frac{\frac{1}{2}\delta m^2 \pm \Delta m^2}{\rho^2 - 1}}\,, \end{aligned} \tag{4.36}$$

A numerical study shows that at 2σ, only $2D$, $3F$ and $4B$ are allowed for the normal hierarchy, and only $2A$, $2D$, $3A$, $3F$, $4B$ and $6C$ are allowed for the inverted hierarchy. The allowed regions for $2D$ and $3F$ for the normal hierarchy are shown in Figs. 4.13 and 4.14, and the allowed regions for $2A$, $4B$ and $6C$ for the inverted hierarchy are shown in Figs. 4.15, 4.16 and 4.17, respectively. The allowed region for $3A$ IH is very similar to that for $2A$ IH. The allowed region for $4B$ NH is very similar to that for TT X_5 NH, and the allowed regions for $2D$ IH and $3F$ IH are very similar to that for TT X_5 IH. They have nearly maximal CP violation, and a lower bound on the lightest mass of about 30 meV. For $3F$ NH and $6C$ IH there are four best-fit points since there are four solutions to the one texture zero and one cofactor zero conditions.

4.3.2.4 Discussion of the two-zero models

There are 7 cases that are allowed at the 2σ level for the two texture zero ansatz, 7 cases that are allowed for the two cofactor zero ansatz, and 6 cases that are allowed for the one texture and one cofactor zero ansatz. Seven cases allow both hierarchies, so there are a total of 27 possible two-zero cases allowed at 2σ. However, there are many similarities among the allowed

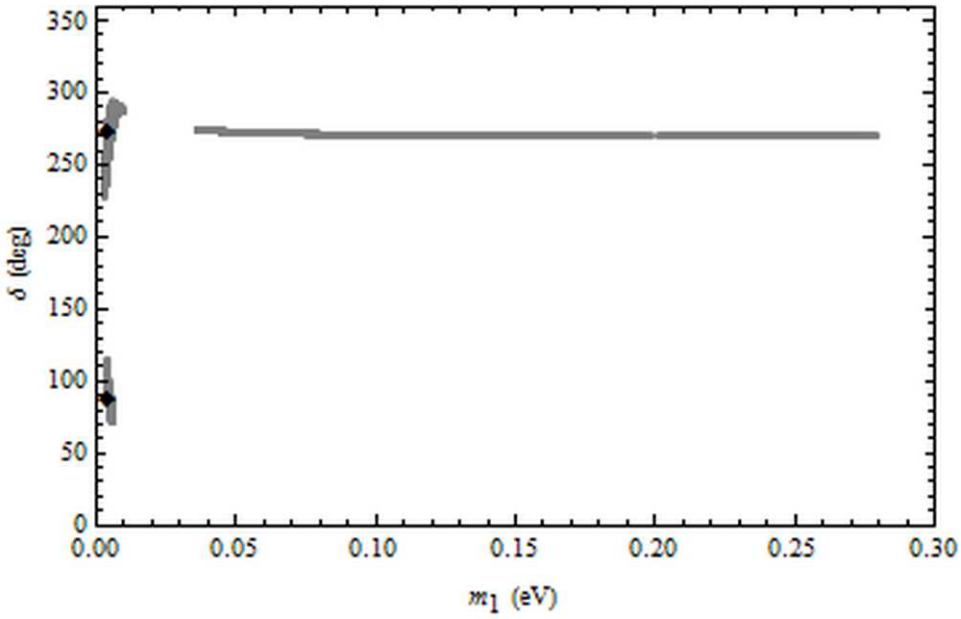

Figure 4.13 Same as Fig. 4.7, except for TC $2D$ and the normal hierarchy.

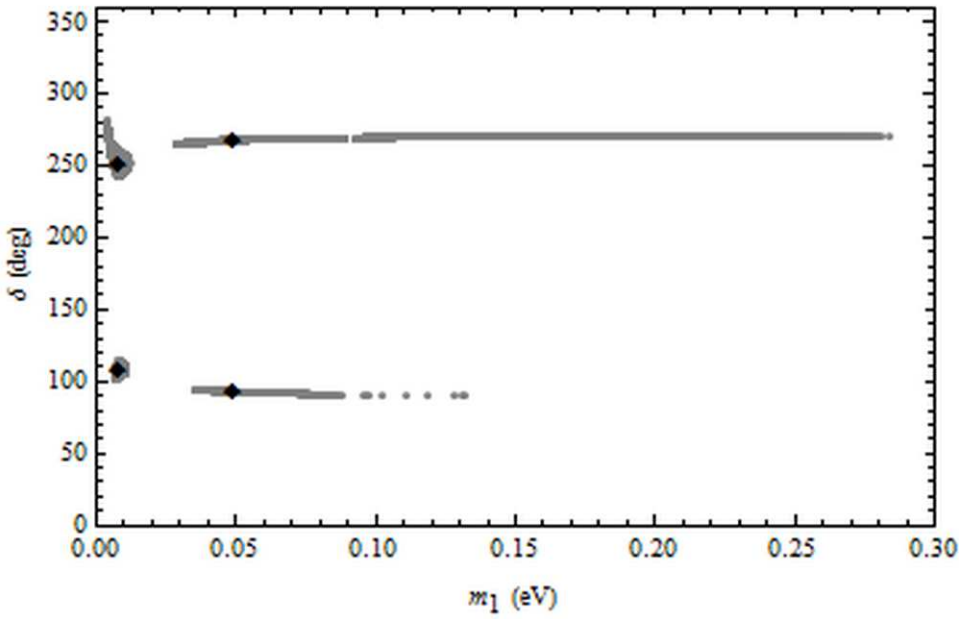

Figure 4.14 Same as Fig. 4.7, except for TC $3F$ and the normal hierarchy.

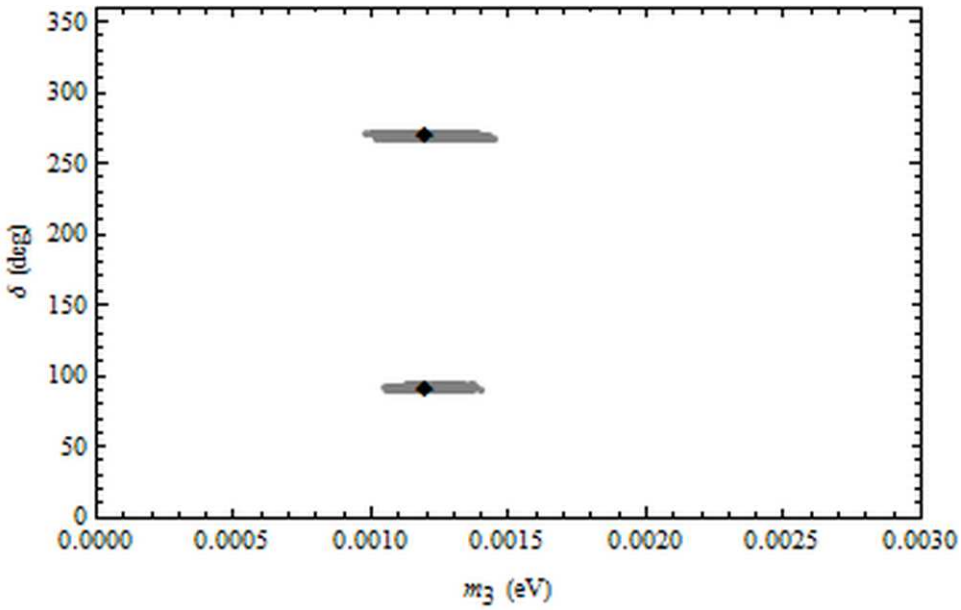

Figure 4.15 Same as Fig. 4.7, except for TC 2A and the inverted hierarchy.

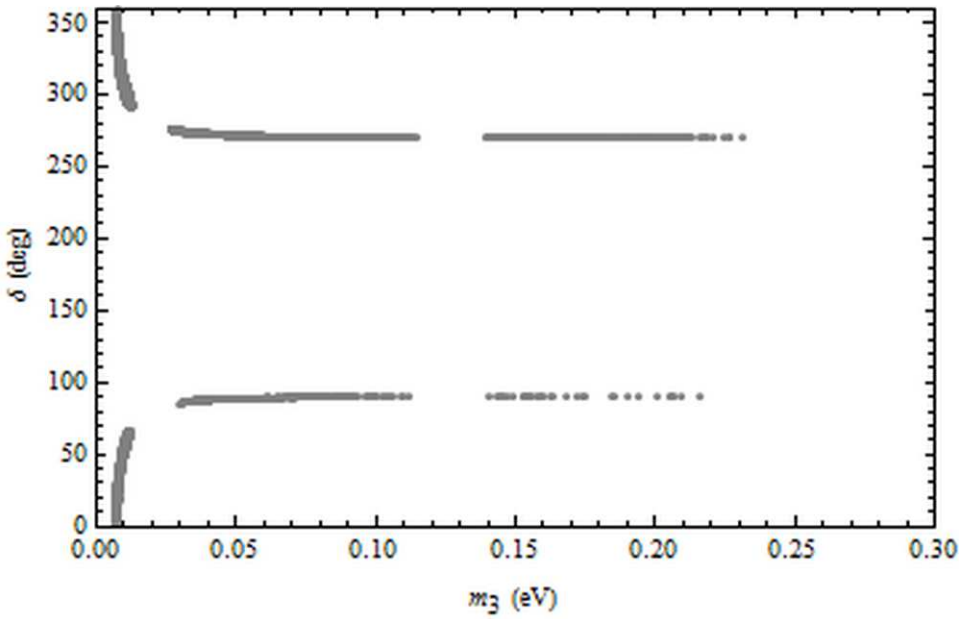

Figure 4.16 Same as Fig. 4.7, except for TC 4B and the inverted hierarchy. This case is not allowed for the best-fit oscillation parameters.

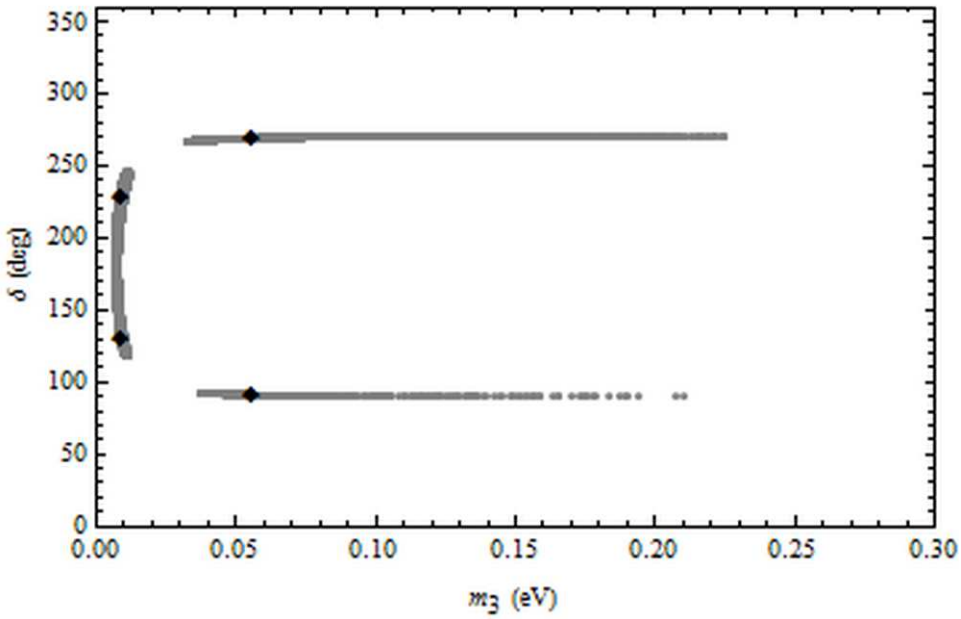

Figure 4.17 Same as Fig. 4.7, except for TC 6C and the inverted hierarchy. There are four best-fit points since there are four solutions to the TC conditions.

regions for these cases. In the next section we will discuss that any case with a homogeneous relationship among elements of M with one mass hierarchy yields predictions for the oscillation parameters and phases similar to those given by a case with the same homogeneous relationship among cofactors of M with the opposite mass hierarchy. The only exceptions are when the lightest mass is small, of order 20 meV or less, or when the allowed ranges of the oscillation parameters differ significantly for the two mass hierarchies. The latter situation occurs for θ_{23}, which is constrained at the 2σ level to be less than about 45.3° for the NH but can have larger values for the IH.

A texture or cofactor zero is the simplest homogeneous relationship; therefore, CC cases can be dual to TT cases (and, of course, vice versa), and some TC cases can be dual to other such cases.[1] We can identify 8 cases where allowed regions are similar due to the dual-case argument, 6 cases where a case is allowed at 2σ but its dual case is not because the lightest mass is small, 5 cases where an IH case is allowed but its dual case is disfavored because θ_{23} must be larger than 45.3°. A complete listing of dual case relationships is given in Table 4.8.

[1]In principle, the TC cases 1A, 2D, and 6F could be self-dual, which means they would have similar allowed regions for the NH and IH, but these are not allowed at 2σ.

We note that the allowed regions for the CC Z_1 NH case (Fig. 4.12) are similar to the allowed regions for its dual case, TT Z_1 IH (Fig. 4.11). The region for $90^\circ \leq \delta \leq 180^\circ$ in Fig. 4.11 does not appear in Fig. 4.12 because θ_{23} has values that are larger than 45.3° for the inverted hierarchy for $90^\circ \leq \delta \leq 180^\circ$, while such values of θ_{23} are disfavored for the normal hierarchy.

We can also use the effective Majorana mass for the neutrinoless double beta decay to differentiate two-zero cases. In Table 4.9, we list the minimum and maximum values of $|M_{ee}|$ at the 2σ level for each case. Note that for TT X_1 and X_2, and CC X_3 and X_4, $|M_{ee}|$ is identically zero, and therefore they are not listed in the table. We also omit the cases of CC X_5 IH, X_6 NH and X_6 IH because they give the same phenomenology as the corresponding cases in the TT class, as given in Table 4.6.

We find that there are four different types of cases phenomenologically:

1. **Cases that allow only a small value for the lightest mass, less than 10 meV.** This includes 6 cases: TT X_1 NH, TT X_2 NH, CC X_3 NH, CC X_4 NH, TC $2A$ IH and TC $3A$ IH (Figs. 4.7, 4.8 and 4.15, respectively). The value of $|M_{ee}|$ is either zero (for the TT cases) or close to 50 meV (for the TC cases).

2. **Cases that restrict δ to be very close to 90° or 270°.** This group consists of 5 cases with NH (TT X_5, CC X_6, TT Y_1, CC Y_2, and TC $4B$) and 10 cases with IH (TT X_5, TT X_6, CC X_5, CC X_6, TT Y_1, CC Y_1, TT Y_2, CC Y_2, TC $2D$, and TC $3F$), all of which have a minimum value for the lightest mass of about 30 meV. In all NH cases of this type, the maximum value for m_1 is about 290 meV and 35 meV $\lesssim |M_{ee}| \lesssim$ 290 meV; in all IH cases, the maximum value for m_3 is about 250 meV and 55 meV $\lesssim |M_{ee}| \lesssim$ 250 meV. Therefore it will be very difficult to distinguish these cases from each other.

3. **Cases in which maximal CP violation is approached for larger values of the lightest mass.** This group includes TT Z_1 IH and CC Z_1 NH (Figs. 4.11 and 4.12). In these cases a wide range of δ is possible, although maximal CP violation is not allowed.

4. **Cases that are a mixture of types 1 and 2.** The TC cases $2D$ NH, $3F$ NH, $4B$ IH, and $6C$ IH allow values of the lightest mass less than 10 meV, and also have nearly

Table 4.8 A listing of which allowed cases have dual cases that are also allowed, and which do not. The "Maybe" designation is for situations in which the dual case has a NH and $\theta_{23} > 45.3°$; the global analysis of Ref. [53] suggests that for a NH, $\theta_{23} < 45.3°$ at 2σ. "Maybe" indicates that the exclusion of the dual case on this basis is not robust.

Case	Hierarchy	Dual case allowed?
TT X_1	NH	No, m_1 small
TT X_2	NH	No, m_1 small
TT X_5	NH	Yes, CC X_5 IH
TT X_5	IH	Maybe, CC X_5 NH, if the θ_{23} restriction were absent
TT X_6	IH	Yes, CC X_6 NH
TT Y_1	NH	Yes, CC Y_1 IH
TT Y_1	IH	Maybe, CC Y_1 NH, if the θ_{23} restriction were absent
TT Y_2	IH	Yes, CC Y_2 NH
TT Z_1	IH	Yes, CC Z_1 NH (for $\delta \in [0, 90°] \cup [180°, 360°]$)
CC X_3	NH	No, m_1 small
CC X_4	NH	No, m_1 small
CC X_6	IH	Maybe, TT X_6 NH, if the θ_{23} restriction were absent
CC Y_2	IH	Maybe, TT Y_2 NH, if the θ_{23} restriction were absent
TC $2A$	IH	No, m_3 small
TC $2D$	NH	Yes, TC $4B$ IH (except for low m_1 and m_3 and if the θ_{23} restriction were absent)
TC $2D$	IH	Yes, TC $4B$ NH
TC $3A$	IH	No, m_3 small
TC $3F$	NH	Yes, TC $6C$ IH (except for low m_1 and m_3)
TC $3F$	IH	Maybe, TC $6C$ NH, if the θ_{23} restriction were absent

maximal CP violation when the lightest mass is above about 30 meV (Figs. 4.13, 4.14, 4.16, and 4.17).

Due to the large number of cases and their overlapping predictions, it is currently not possible to uniquely determine any given case. The latest experimental result from EXO-200 [60] sets an upper limit on the effective mass $|M_{ee}|$ of less than $140 - 380$ meV at 90% C.L. However, with future sensitivities to $|M_{ee}|$ of about 20 meV [61], and a precision measurement of δ in future long baseline oscillation experiments, we might be able to distinguish between these cases. Here we run a test on the survivability of two-zero cases by applying an upper limit on $|M_{ee}|$ and assuming specific values for δ with the 3σ resolution attainable with a 350 kt-yr exposure at the Long-Baseline Neutrino Experiment [105]. The results in Table 4.10 are

Table 4.9 The minimum and maximum values of $|M_{ee}|$ (in meV) at 2σ. CC X_5 and CC X_6 are not shown since they are equivalent to TT X_6 and TT X_5, respectively. $|M_{ee}|$ is identically zero for TT X_1, TT X_2, CC X_3 and CC X_4.

Case	Hierarchy	Minimum	Maximum
TT X_5	NH	37	286
TT X_5	IH	58	247
TT X_6	IH	62	215
TT Y_1	NH	34	276
TT Y_1	IH	57	230
TT Y_2	IH	60	226
TT Z_1	IH	24	>1000
CC Y_1	IH	59	231
CC Y_2	NH	34	275
CC Y_2	IH	56	227
CC Z_1	NH	15	>1000
TC $2A$	IH	45	49
TC $2D$	NH	3	279
TC $2D$	IH	60	227
TC $3A$	IH	45	49
TC $3F$	NH	3	281
TC $3F$	IH	57	217
TC $4B$	NH	35	281
TC $4B$	IH	16	232
TC $6C$	IH	15	229

qualitative without specific confidence levels ascribable.

4.4 Dual Models of the Neutrino Mass Spectrum

Many neutrino models have been built to explain the experimental results and provide guidance for the next generation of experiments. Some of the models predict a relationship among the elements of the light neutrino mass matrix, while other models predict the same relationship among the cofactors of the light neutrino mass matrix. In the last chapter and previous sections, we found that there are strong similarities between single texture zero models with one mass hierarchy and single cofactor zero models with the opposite mass hierarchy if the lightest mass in each case is not too small. This curious feature was also discussed in Ref. [106]. The phenomenon is not unique – models with two equalities between mass matrix elements are similar to models with two equalities between cofactors with the opposite mass hierarchy, as noted in Ref. [107]. This similarity to also exist between models with two texture zeros in the light neutrino mass matrix [97] and models with two cofactor zeros in the light neutrino mass matrix [99].

In this section we generalize this correspondence by showing that any model with a homogeneous relationship among elements of the light neutrino mass matrix with one mass hierarchy predicts oscillation parameters and Majorana phases similar to those of models with the same homogeneous relationship among cofactors of the mass matrix with the opposite mass hierarchy. Since the neutrino mass hierarchy remains undetermined, two such models are indistinguishable using current data. The allowed oscillation parameters are nearly identical when the masses are quasi-degenerate, but can differ in some cases when the lightest neutrino mass is very small, of order of 20 meV or less.

4.4.1 Comparison Between Element and Cofactor Models

The light neutrino mass matrix can be written in the form of Eq. (3.1), i.e.,

$$M = V^* \mathrm{diag}(m_1, m_2, m_3) V^\dagger \,, \tag{4.37}$$

Table 4.10 The two-zero cases that survive (indicated by a tick mark) an upper limit on $|M_{ee}|$ and a measurement of δ (as in the second row) with the 3σ resolution attainable by the Long-Baseline Neutrino Experiment with 350 kt-yr of data [105]. The CC Class X is not shown since it is equivalent to the TT Class X.

Case	$\lvert M_{ee}\rvert < 20$ meV				$\lvert M_{ee}\rvert < 50$ meV				$\lvert M_{ee}\rvert < 100$ meV			
	0	90°	180°	270°	0	90°	180°	270°	0	90°	180°	270°
TT X_1 NH	×	√	√	√	×	√	√	√	×	√	√	√
TT X_2 NH	√	√	×	√	√	√	×	√	√	√	×	√
TT X_5 NH	×	×	×	×	×	√	×	√	×	√	×	√
TT X_5 IH	×	×	×	×	×	×	×	×	×	√	×	√
TT X_6 IH	×	×	×	×	×	×	×	×	×	√	×	√
TT Y_1 NH	×	×	×	×	×	√	×	√	×	√	×	√
TT Y_1 IH	×	×	×	×	×	×	×	×	×	√	×	√
TT Y_2 IH	×	×	×	×	×	×	×	×	×	√	×	√
TT Z_1 IH	×	×	×	×	×	√	√	√	×	√	√	√
CC Y_1 IH	×	×	×	×	×	×	×	×	×	√	×	√
CC Y_2 NH	×	×	×	×	×	√	×	√	×	√	×	√
CC Y_2 IH	×	×	×	×	×	×	×	×	×	√	×	√
CC Z_1 NH	×	√	×	√	×	√	×	√	×	√	×	√
TC 2A IH	×	×	×	×	×	√	×	√	×	√	×	√
TC 2D NH	×	√	×	√	×	√	×	√	×	√	×	√
TC 2D IH	×	×	×	×	×	×	×	×	×	√	×	√
TC 3A IH	×	×	×	×	×	√	×	√	×	√	×	√
TC 3F NH	×	√	×	√	×	√	×	√	×	√	×	√
TC 3F IH	×	×	×	×	×	×	×	×	×	√	×	√
TC 4B NH	×	×	×	×	×	√	×	√	×	√	×	√
TC 4B IH	√	√	×	√	√	√	×	√	√	√	×	√
TC 6C IH	×	√	√	√	×	√	√	√	×	√	√	√

where V is a unitary matrix. Either a normal mass hierarchy (NH, $m_1 < m_2 < m_3$) or an inverted mass hierarchy (IH, $m_3 < m_1 < m_2$) are allowed, following the convention that the mass-squared difference $m_2^2 - m_1^2$ is responsible for the oscillation of solar neutrinos.

Suppose a model imposes a relationship among *elements* of the mass matrix M given by

$$f\left(M_{\alpha\beta}\right) = 0\,, \tag{4.38}$$

where $\alpha, \beta = e, \mu, \tau$ and f is a homogeneous function of the $M_{\alpha\beta}$. We take the coefficients in the homogeneous function to be real, as in most models. Then from Eq. (4.37), $M_{\alpha\beta} = m_1 V_{\alpha1}^* V_{\beta1}^* + m_2 V_{\alpha2}^* V_{\beta2}^* + m_3 V_{\alpha3}^* V_{\beta3}^*$ and Eq. (4.38) becomes

$$f\left(m_1 V_{\alpha1}^* V_{\beta1}^* + m_2 V_{\alpha2}^* V_{\beta2}^* + m_3 V_{\alpha3}^* V_{\beta3}^*\right) = 0\,. \tag{4.39}$$

Since the coefficients in the homogeneous function are real, the complex conjugate of the above equation is

$$f\left(m_1 V_{\alpha1} V_{\beta1} + m_2 V_{\alpha2} V_{\beta2} + m_3 V_{\alpha3} V_{\beta3}\right) = 0 \qquad \text{(element condition)}. \tag{4.40}$$

Now consider a model that imposes the same homogeneous relationship among *cofactors* of the light neutrino mass matrix, i.e.,

$$f\left(C_{\alpha\beta}\right) = 0\,, \tag{4.41}$$

where $C_{\alpha\beta}$ is the (α, β) cofactor of M, given by $(M^{-1})_{\alpha\beta} = \frac{1}{\det M} C_{\beta\alpha}$. Since the mass matrix is symmetric and f is a homogeneous function, we have $f\left((M^{-1})_{\alpha\beta}\right) = 0$. Then since $M^{-1} = V \mathrm{diag}(m_1^{-1}, m_2^{-1}, m_3^{-1}) V^T$, we can write the condition as

$$f\left(m_1^{-1} V_{\alpha1} V_{\beta1} + m_2^{-1} V_{\alpha2} V_{\beta2} + m_3^{-1} V_{\alpha3} V_{\beta3}\right) = 0 \qquad \text{(cofactor condition)}. \tag{4.42}$$

To compare the element NH case with the cofactor IH case, we divide the argument in Eq. (4.40) by m_3, multiply the argument in Eq. (4.42) by m_3, and use the properties of homogeneous functions to write the condition for the element NH case as

$$f\left(\frac{m_1}{m_3} V_{\alpha1} V_{\beta1} + \frac{m_2}{m_3} V_{\alpha2} V_{\beta2} + V_{\alpha3} V_{\beta3}\right) = 0\,, \tag{4.43}$$

and the condition for the cofactor IH case as

$$f\left(\frac{m_3}{m_1} V_{\alpha1} V_{\beta1} + \frac{m_3}{m_2} V_{\alpha2} V_{\beta2} + V_{\alpha3} V_{\beta3}\right) = 0\,. \tag{4.44}$$

In the quasi-degenerate regime ($m_1 \simeq m_2 \simeq m_3$), all the mass ratios are approximately unity so that the three mixing angles and three phases allowed by the constraints are nearly identical for the two hierarchies.

For masses lighter than about 100 meV, the leading term in each argument is the third term, and they are identical. The only differences in the sub-leading terms are the two mass ratios. In Fig. 4.18 we plot the fractional difference between the two mass ratios with opposite hierarchies versus the lightest mass using the recent best-fit values [83], $\delta m^2 \equiv m_2^2 - m_1^2 = 7.54 \times 10^{-5}$ eV^2 and $\Delta m^2 \equiv |m_3^2 - (m_1^2 + m_2^2)/2| = 2.43 \times 10^{-3}$ eV^2 for the normal hierarchy and 2.42×10^{-3} eV^2 for the inverted hierarchy. The percentage difference between $(\frac{m_1}{m_3})_{\rm NH}$ and $(\frac{m_3}{m_1})_{\rm IH}$ is very small and always less than 1.7% for any value of the lightest mass. The percentage difference between $(\frac{m_2}{m_3})_{\rm NH}$ and $(\frac{m_3}{m_2})_{\rm IH}$ becomes less than 10% (5%) {2%} if the lightest mass is larger than 19 (27) {42} meV. Hence except for conditions with α and β such that $V_{\alpha 3} V_{\beta 3}$ is small compared to $V_{\alpha 1} V_{\beta 1}$ and $V_{\alpha 2} V_{\beta 2}$, the two conditions are almost the same for masses that are not nearly degenerate. Even in some extreme cases, such as $\alpha = \beta = e$, for which the θ_{13}-dependent leading term is relatively small, the two conditions are almost identical if the lightest mass is larger than about 20 meV, with the percentage difference between the two mass ratios less than 10%.

To compare the element IH case with the cofactor NH case, we divide the argument in Eq. (4.40) by m_1 and multiply the argument in Eq. (4.42) by m_1 to obtain

$$f\left(V_{\alpha 1} V_{\beta 1} + \frac{m_2}{m_1} V_{\alpha 2} V_{\beta 2} + \frac{m_3}{m_1} V_{\alpha 3} V_{\beta 3}\right) = 0\,, \tag{4.45}$$

for the element IH case and

$$f\left(V_{\alpha 1} V_{\beta 1} + \frac{m_1}{m_2} V_{\alpha 2} V_{\beta 2} + \frac{m_1}{m_3} V_{\alpha 3} V_{\beta 3}\right) = 0\,, \tag{4.46}$$

for the cofactor NH case. Again, in the quasi-degenerate regime the two conditions are nearly identical, and the allowed values of the mixing angles and phases are almost equal in the two models.

For masses lighter than about 100 meV, the leading terms in each argument are the first two terms if the lightest mass is not very small. The percentage difference between $(\frac{m_2}{m_1})_{\rm IH}$ and

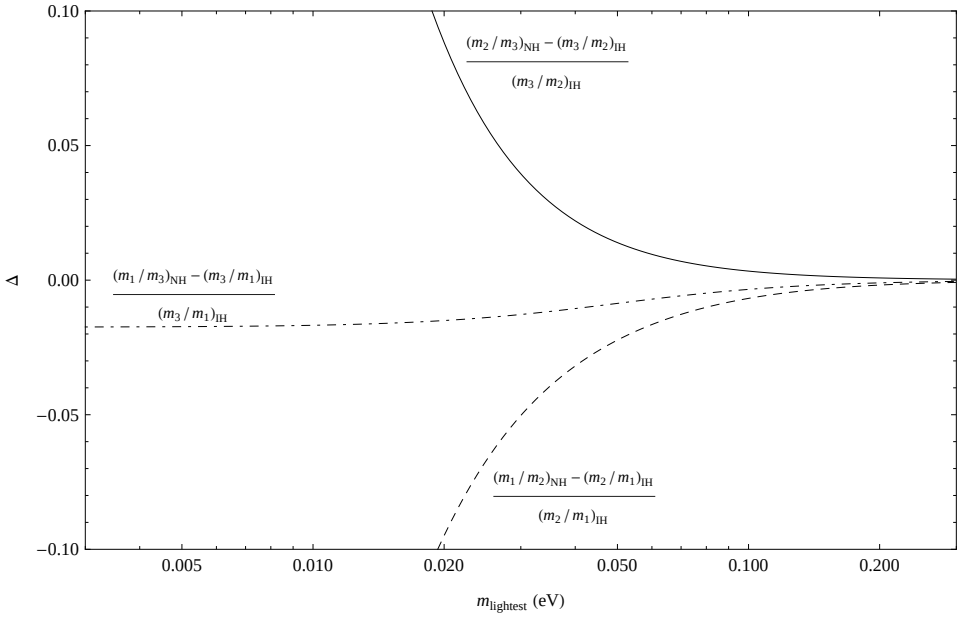

Figure 4.18 Fractional differences in mass ratios Δ for the two mass hierarchies as a function of the lightest neutrino mass. We set $\delta m^2 \equiv m_2^2 - m_1^2 = 7.54 \times 10^{-5}$ eV^2 and $\Delta m^2 \equiv m_3^2 - (m_1^2 + m_2^2)/2 = 2.43 \times 10^{-3}$ eV^2 for the normal hierarchy and 2.42×10^{-3} eV^2 for the inverted hierarchy.

$(\frac{m_1}{m_2})_{\rm NH}$ is less than 10% (5%) {2%} if the lightest mass is larger than 19 (30) {53} meV. Hence, if the lightest mass is not very small, the two conditions are almost identical. The sub-leading terms are always close to each other because the percentage difference between $(\frac{m_1}{m_3})_{\rm NH}$ and $(\frac{m_3}{m_1})_{\rm IH}$ is always less than 1.7% for any value of the lightest mass.

In the above analysis we only considered real coefficients in the homogeneous functions. For complex coefficients, the complex conjugate of Eq. (4.39) does not give Eq. (4.40). However, if the cofactor-based model has coefficients that are the complex conjugate of the coefficients in the element-based model, then the cofactor-based model is dual to the corresponding element-based model.

Although our proof used only one condition, the same arguments can easily be applied to multiple conditions. The only requirement is that there be two models with the same homogeneous conditions for the elements and cofactors, respectively. A consequence is that a model with two texture zeros yields predictions for the oscillation parameters and Majorana phases similar to those of the corresponding model with two cofactor zeros. Likewise, as noted

in Ref. [107], models with two equalities between mass matrix elements are similar to models with two equalities between cofactors.

4.4.2 Application to Neutrino Model Building

The homogeneous relationships in Eqs. (4.38) and (4.41) are quite common in neutrino mass models, such as texture zero models [94], cofactor zero models [95], scaling models [108], and models in which two mass matrix elements or cofactors are equal [107]. The latter includes the $\mu - \tau$ symmetric models that impose $|M_{e\mu}| = |M_{e\tau}|$ and $|M_{\mu\mu}| = |M_{\tau\tau}|$. However, the existence of an element/cofactor duality requires models that have the same homogeneous relationship among elements in one model and cofactors in a second model. While models with conditions on the elements are common, models with conditions on cofactors are not so common. However, models with the same homogeneous relationships among cofactors can be defined. In particular, the existence of the inverse of the right-handed neutrino mass matrix in the conventional seesaw mechanism [56], with $M = M_D^T M_R^{-1} M_D$, provides a good motivation for the corresponding cofactor models, as we discuss below.

M_D is proportional to the unit matrix. A simple example arises when $M_D = m_D I$, so that inverting the seesaw formula gives $M^{-1} = M_R/m_D^2$. Since $M^{-1} = C^T/\mathrm{Det}(M)$, it follows that $M_R \propto C^T$. Now since M_R is symmetric, any homogeneous relationship among the elements of the right-handed neutrino mass matrix M_R will be equivalent to the same homogeneous relationship among the cofactors of the light neutrino mass matrix. Thus a dual cofactor model can be obtained by having the same homogeneous conditions on M_R in one model as there are on M in the dual element model; the cofactor conditions on M are inherited from M_R.

This leads to an even more ambitious conclusion: any model consistent with the observed mixing angles (and phases) for the light neutrinos will have a dual model with the opposite mass hierarchy. We can build the dual model by choosing M_R to be proportional to M, and according to our argument above (with M_D proportional to the unit matrix), the model generated by M_R would have a light neutrino cofactor matrix that is proportional to M. Thus the cofactors are related to each other in the same way the elements of M are related to each other, so the model

generated by M_R with the opposite mass hierarchy will be dual to the model represented by M, and we cannot distinguish these two models without knowing the mass hierarchy.

M_D is diagonal. Next we relax the condition that the Dirac mass matrix is proportional to the unit matrix and consider the case where it is diagonal. If we assume that the same homogeneous relationship holds for both the light neutrino mass matrix and the right-handed neutrino mass matrix, under what conditions will the cofactor matrix of M have the same homogeneous relationship as the elements of M?

Defining $M_D = \mathrm{diag}(c_1, c_2, c_3)$ and $(M_R)_{ij} = R_{ij}$, since M_R is symmetric, the cofactor matrix for M becomes

$$C = (\mathrm{Det}M)M_D^{-1}M_R^T(M_D^T)^{-1} = (\mathrm{Det}M)\begin{bmatrix} R_{11}/c_1^2 & R_{12}/c_1c_2 & R_{13}/c_1c_3 \\ R_{12}/c_1c_2 & R_{22}/c_2^2 & R_{23}/c_2c_3 \\ R_{13}/c_1c_3 & R_{23}/c_2c_3 & R_{33}/c_3^2 \end{bmatrix}. \tag{4.47}$$

We see that a texture zero in M_R still translates to a cofactor zero for M [90]. However, in general a more complicated homogeneous relationship among elements in M_R, such as those involving more than one element, will not be inherited by the corresponding cofactor matrix unless there is a special relationship among the c_i. For example, $R_{\mu\mu} = R_{\tau\tau}$ does not imply $C_{\mu\mu} = C_{\tau\tau}$ unless $c_2 = c_3$.

4.4.3 Resolving the Dual Model Ambiguity

We have shown that if a model has a homogeneous relationship among *elements* of the light neutrino mass matrix, it will yield predictions for the oscillation parameters and Majorana phases similar to those of another model with the opposite mass hierarchy that has the same homogeneous relationship among *cofactors* of the mass matrix, except when the lightest neutrino mass is very small, of order 20 meV or less. Many existing models have one or more homogeneous relationships among mass matrix elements, but there are fewer models that are constructed by imposing homogeneous relationships among cofactors. However, any model that fits current neutrino data will have a dual model with the opposite mass hierarchy. We have shown that if the Dirac mass matrix is proportional to the identity matrix, a dual cofactor-based model can be generated via the seesaw mechanism if the right-handed neutrino

mass matrix has the same homogeneous relationships as the light mass matrix elements in an element-based model. Since the mass hierarchy has not been experimentally determined, we cannot currently distinguish these dual models from each other.

Current global fits to oscillation data have almost identical best-fit values for the neutrino mixing angles and mass-squared differences for the two hierarchies. However, different allowed regions for the oscillation parameters for different mass hierarchies can lead to a breakdown of duality. In fact, the 2σ allowed regions are somewhat different, especially for the value of θ_{23}, where second octant values ($\theta_{23} > \pi/4$) are allowed only for the inverted hierarchy [83]. Due to this difference, the 2σ allowed regions for dual models differ even in the quasi-degenerate regime in a few cases we have studied.

The dual model ambiguity can be resolved by experiments that distinguish between the normal and inverted hierarchies, such as long baseline neutrino experiments (T2K [109], NOνA [110], and LBNE [111]), atmospheric neutrino experiments (PINGU [112], and INO [113]) and medium baseline reactor experiments (JUNO [114]), or a combination of these [115]. Also, tritium beta decay, neutrinoless double beta decay ($0\nu\beta\beta$), and structure formation in our universe depend on the nature of the neutrino mass pectrum, and in principle can be used to distinguish between dual models. The 95% C.L. sensitivity of the KATRIN experiment [116] to the effective neutrino mass $m_\beta = (\sum_i |V_{ei}|^2 m_i^2)^{1/2}$ is 0.35 eV with an uncertainty of 0.08 eV^2 on m_β^2, which is insufficient to break the duality. The effective Majorana mass measured by $0\nu\beta\beta$ experiments is constrained to be smaller than 140-380 meV at the 90% C.L. [60], which cannot break the duality. The future sensitivity of $0\nu\beta\beta$ experiments is expected to be 50 meV or lower [61], which would provide a partial but strongly model-dependent resolution of the dual model ambiguity. The current 95% C.L. upper bound on Σm_i from cosmology is 0.66 eV [102], which permits a quasi-degenerate spectrum, so that the duality is unbroken. In the future, lensing measurements will probe Σm_i as low as 0.05 eV [117], which will distinguish between dual models.

CHAPTER 5. SUMMARY AND OUTLOOK

5.1 Summation

In this thesis, we have studied the phenomenological results of several classes of neutrino models: the $\mu-\tau$ symmetrical models, the seesaw models with four zeros in the Yukawa matrix, and the texture/cofactor zero models. Most of the results have been published in collaborations with Danny Marfatia and Kerry Whisnant in several papers [118, 96, 119, 120, 121].

After the discovery of non-zero mixing angle θ_{13}, many popular $\mu-\tau$ symmetrical models are in disagreement with the experimental data. We investigated the effect of small perturbations on the $\mu-\tau$ symmetrical models that yield experimentally preferred oscillation parameters. We found that with small perturbations, the deviations of θ_{13} and θ_{23} can be fulfilled, but the θ_{12} correction can be very large, which means the underlying unperturbed mixing need not have θ_{12} close to the experimentally preferred value. Due to our observation, the class of possible neutrino mass models that can lead to acceptable phenomenology can be expanded to include most mixing scenarios with $\mu-\tau$ symmetry, and tri-bimaximal mixing has no special place among scenarios with $\mu-\tau$ symmetry. Based on this result, we proposed a new class of $\mu-\tau$ symmetric models with unperturbed θ_{12} equal to zero or 90°, and found they can be viable for $\theta_{13}^0 < 20^\circ$ under small perturbation.

We extended the most economical type I seesaw model to include three right-handed neutrinos and studied the simplest cases that have four texture zeros in the Yukawa couplings matrix. In the context of low energy phenomenology, these models are equivalent to a single texture or cofactor zero for an off-diagonal element of the light neutrino mass matrix M. The cofactor zero condition is itself equivalent to a texture zero in M^{-1}. We derived analytic formulas that relate the Dirac CP phase, the lightest mass and the two Majorana phases to the five

observed oscillation parameters and determine the constraints on these models. We used the latest experimental data to obtain the allowed regions for the lightest neutrino mass and Dirac CP phase δ, which can be measured in future neutrino experiments. Once the lightest neutrino mass and Dirac CP phase are determined, we can make definite predictions for neutrinoless double beta decay, which will be probed in future experiments. We also used leptogenesis to further constrain the allowed regions, and found there is an upper bound on the lightest neutrino mass of about 100-200 meV for a single-flavored leptogenesis scenario.

We also studied a variety of neutrino models that have one or two texture and/or cofactor zeros. The one-zero models have two remaining free neutrino parameters, and we determined the constraints in the space of the CP phase and lightest mass using a global fit to neutrino parameters, including recent data on θ_{13}. The two-zero models have no remaining independent parameters and therefore have tighter constraints. We also made predictions for neutrinoless double beta decay for these models. For the one cofactor zero models, we proposed a simple realization based on a new U(1) gauge symmetry. During our study of the texture and/or cofactor zero models, we found there are strong similarities between a texture zero model and cofactor zero model with the opposite mass hierarchy. We generalized this correspondence by showing that any neutrino model with a homogeneous relationship among elements of the light neutrino mass matrix with one mass hierarchy predicts oscillation parameters and Majorana phases similar to those of models with the same homogeneous relationship among cofactors of the mass matrix with the opposite mass hierarchy if the lightest mass is not too small, e.g., less than about 20 meV. This general result applies to texture and/or cofactor zero models, scaling models, and models that have two equal mass matrix elements or cofactors, e.g. $\mu-\tau$ symmetric models. We showed that determining the mass hierarchy would be crucial to distinguish these dual models. The measurement of tritium beta decay, neutrinoless double beta decay, and structure formation in our universe can also be used to distinguish between dual models.

5.2 Outlook

The research progress of neutrino physics in the past few decades seems to be driven by experimental results. Hence, in this section we will first briefly discuss some key experiments

that may yield promising results in the next decade. After that, we will mention some research directions that we can explore in the next stage.

5.2.1 Future Neutrino Experiments

The next main goals of neutrino experiments are to determine the neutrino mass hierarchy and measure the Dirac CP phase δ. The current and proposed long baseline neutrino experiments (T2K [109], NOνA [110], and LBNE [111]) can achieve both goals by using neutrino and antineutrino beams. This can be seen as follows. From Eqs. (1.33) and (1.34), we know the matter effect for neutrinos and antineutrinos travelling through the Earth are different. To the second order of the small parameters θ_{13} and $|\delta m^2_{21}/\delta m^2_{31}|$, the probabilities for the NH are [122]

$$\begin{aligned} P(\nu_\mu \to \nu_e) &= x^2 f^2 + 2xyfg\cos(\delta+\Delta) + y^2 g^2, \\ P(\bar{\nu}_\mu \to \bar{\nu}_e) &= x^2 \bar{f}^2 + 2xy\bar{f}g\cos(\delta-\Delta) + y^2 g^2, \end{aligned} \tag{5.1}$$

and for the IH,

$$\begin{aligned} P(\nu_\mu \to \nu_e) &= x^2 \bar{f}^2 - 2xy\bar{f}g\cos(\delta-\Delta) + y^2 g^2, \\ P(\bar{\nu}_\mu \to \bar{\nu}_e) &= x^2 f^2 - 2xyfg\cos(\delta+\Delta) + y^2 g^2, \end{aligned} \tag{5.2}$$

where

$$\begin{aligned} x = \sin\theta_{23}\sin 2\theta_{13},\ \ y = \alpha\cos\theta_{23}\sin 2\theta_{12}, \\ f, \bar{f} = \sin\Big[(1\mp\hat{A})\Delta\Big]/(1\mp\hat{A}),\ \ g = \sin(\hat{A}\Delta)/\hat{A}, \end{aligned} \tag{5.3}$$

and $\Delta = |\Delta_{31}|$, $\hat{A} = |A/\delta m^2_{31}|$, $\alpha = |\delta m^2_{21}/\delta m^2_{31}|$. Hence, by studying the transitions of $\nu_\mu \to \nu_e$ and $\bar{\nu}_\mu \to \bar{\nu}_e$, one can determine both the mass hierarchy and measure the Dirac CP phase.

In addition to the long baseline neutrino experiments, a medium-baseline reactor neutrino experiments such as JUNO [114] can also provide a unique way to determine the mass hierarchy. This can be seen in the following equation,

$$P(\bar{\nu}_e \to \bar{\nu}_e) = 1 - \sin^2 2\theta_{13}(\cos^2\theta_{12}\sin^2\Delta_{31} + \sin^2\theta_{12}\sin^2\Delta_{32}) - \cos^4\theta_{13}\sin^2 2\theta_{12}\sin^2\Delta_{21}. \tag{5.4}$$

Hence, an excellent detector with energy resolution of 3% and absolute energy scale calibration at <1% can measure the large mass-squared splitting between Δ_{31} and Δ_{21}. The medium-baseline reactor neutrino experiments are free of any effects due to the unknown Dirac CP phase, thus provide a complementary measurement of the mass hierarchy to the long baseline neutrino experiments.

5.2.2 Future Research Directions

In our study of the perturbation to $\mu-\tau$ symmetrical models, we mainly focused on the real case. One direction we can pursue is to generalize the perturbation results to the complex case, therefore we can make predictions on the Dirac CP phase and the Majorana phases. Also, in the previous work, we used the basis where the charged leptons are diagonal, thus the mixing symmetry mainly comes from the neutrino sector. In the future, we would like to study models with mixing in both the charged lepton and neutrino sectors, and thus explore the effects due to the charged lepton corrections.

Also we know the lepton sector has large mixing angles, which is quite different from the quark sector. In the lepton sector, the seesaw mechanism is introduced as an elegant way to generate the small masses for the light neutrinos. However, the different mass generation mechanisms could be the reason for the difference between the structure of the lepton sector and the quark sector. We would like to explore the texture of both the Dirac mass matrix and heavy right-handed neutrino mass matrix in the seesaw mechanism, and look for a simple and natural explanation of the large mixing angles in the lepton sector. Also, we would like to see if we can find a connection between the mixing angles in the lepton sector and the quark sector. A preliminary work has been shown in Ref. [123].

From an experimental point of view, the next main goal is to determine the mass hierarchy and Dirac CP phase. In order to use the matter effect to separate the two mass hierarchies, a baseline at least as long as the distance between Fermilab and Homestake is needed [122], e.g. LBNE experiment, but that requires a new beam line. The current experiments (MINOS and NOνA) have a shorter baseline and therefore do not uniquely determine the parameters in the whole parameter space. Multiple detectors can help [124], but one current proposal

(CHIPS [125]) still does not completely remove all the ambiguities. We are planning to look at two detectors at different off-axis angles and also we would like to look at a variety of on-axis beam energies.

Another important question in neutrino physics is related to the nature of neutrinos: whether they are Dirac or Majorana particles is still unknown at the current stage. The neutrinoless double beta decay experiments are the most promising way to answer this question, but it is still possible that the effective mass $|M_{ee}|$ is equal to zero or it is too small to be detected in the foreseeable future. Another way of resolving this problem is to search for the lepton number violation processes in collider experiments. We would like to investigate these possible lepton number violation processes and look for a preferred channel that could lead to the discovery or constraint to the Majorana neutrinos.

BIBLIOGRAPHY

[1] S. L. Glashow, Nucl. Phys. **22**, 579 (1961).

[2] F. Englert and R. Brout, Phys. Rev. Lett. **13**, 321 (1964).

[3] P. W. Higgs, Phys. Rev. Lett. **13**, 508 (1964).

[4] G. S. Guralnik, C. R. Hagen and T. W. B. Kibble, Phys. Rev. Lett. **13**, 585 (1964).

[5] S. Weinberg, Phys. Rev. Lett. **19**, 1264 (1967).

[6] A. Salam, Conf. Proc. C **680519**, 367 (1968).

[7] S. L. Glashow, J. Iliopoulos and L. Maiani, Phys. Rev. D **2**, 1285 (1970).

[8] G. 't Hooft and M. J. G. Veltman, Nucl. Phys. B **44**, 189 (1972).

[9] D. J. Gross and F. Wilczek, Phys. Rev. Lett. **30**, 1343 (1973).

[10] H. D. Politzer, Phys. Rev. Lett. **30**, 1346 (1973).

[11] C. Berger *et al.* [PLUTO Collaboration], Phys. Lett. B **82**, 449 (1979); Phys. Lett. B **86**, 418 (1979); D. P. Barber, U. Becker, H. Benda, A. Boehm, J. G. Branson, J. Bron, D. Buikman and J. Burger *et al.*, Phys. Rev. Lett. **43**, 830 (1979); R. Brandelik *et al.* [TASSO Collaboration], Phys. Lett. B **86**, 243 (1979).

[12] G. Arnison *et al.* [UA1 Collaboration], Phys. Lett. B **122**, 103 (1983); M. Banner *et al.* [UA2 Collaboration], Phys. Lett. B **122**, 476 (1983).

[13] P. Bagnaia *et al.* [UA2 Collaboration], Phys. Lett. B **129**, 130 (1983).

[14] J. J. Aubert *et al.* [E598 Collaboration], Phys. Rev. Lett. **33**, 1404 (1974); J. E. Augustin *et al.* [SLAC-SP-017 Collaboration], Phys. Rev. Lett. **33**, 1406 (1974).

[15] S. W. Herb, D. C. Hom, L. M. Lederman, J. C. Sens, H. D. Snyder, J. K. Yoh, J. A. Appel and B. C. Brown *et al.*, Phys. Rev. Lett. **39**, 252 (1977).

[16] F. Abe *et al.* [CDF Collaboration], Phys. Rev. Lett. **74**, 2626 (1995) [hep-ex/9503002]; S. Abachi *et al.* [D0 Collaboration], Phys. Rev. Lett. **74**, 2632 (1995) [hep-ex/9503003].

[17] G. Aad *et al.* [ATLAS Collaboration], Phys. Lett. B **716**, 1 (2012) [arXiv:1207.7214 [hep-ex]]; S. Chatrchyan *et al.* [CMS Collaboration], Phys. Lett. B **716**, 30 (2012) [arXiv:1207.7235 [hep-ex]].

[18] B. Pontecorvo, Sov. Phys. JETP **6**, 429 (1957) [Zh. Eksp. Teor. Fiz. **33**, 549 (1957)]; Z. Maki, M. Nakagawa and S. Sakata, Prog. Theor. Phys. **28**, 870 (1962).

[19] S. Schael *et al.* [ALEPH and DELPHI and L3 and OPAL and SLD and LEP Electroweak Working Group and SLD Electroweak Group and SLD Heavy Flavour Group Collaborations], Phys. Rept. **427**, 257 (2006) [hep-ex/0509008].

[20] V. Barger, D. Marfatia and K. Whisnant, "The physics of neutrinos", Princeton University Press (2012).

[21] L. Wolfenstein, Phys. Rev. D **17**, 2369 (1978).

[22] V. D. Barger, K. Whisnant, S. Pakvasa and R. J. N. Phillips, Phys. Rev. D **22**, 2718 (1980).

[23] S. P. Mikheev and A. Y. .Smirnov, Sov. J. Nucl. Phys. **42**, 913 (1985) [Yad. Fiz. **42**, 1441 (1985)]; Nuovo Cim. C **9**, 17 (1986).

[24] Z. -z. Xing and S. Zhou, Springer-Verlag, Berlin Heidelberg (2011)

[25] R. N. Mohapatra and P. B. Pal, World Sci. Lect. Notes Phys. **60**, 1 (1998) [World Sci. Lect. Notes Phys. **72**, 1 (2004)].

[26] J. N. Bahcall, A. M. Serenelli and S. Basu, Astrophys. J. **621**, L85 (2005) [astro-ph/0412440]; J. N. Bahcall, M. H. Pinsonneault and S. Basu, Astrophys. J. **555**, 990 (2001) [astro-ph/0010346].

[27] R. Davis, Phys. Rev. Lett. **12**, 303 (1964).

[28] R. Davis, Jr., D. S. Harmer and K. C. Hoffman, Phys. Rev. Lett. **20**, 1205 (1968).

[29] B. T. Cleveland, T. Daily, R. Davis, Jr., J. R. Distel, K. Lande, C. K. Lee, P. S. Wildenhain and J. Ullman, Astrophys. J. **496**, 505 (1998).

[30] Y. Fukuda *et al.* [Super-Kamiokande Collaboration], Phys. Rev. Lett. **81**, 1158 (1998) [Erratum-ibid. **81**, 4279 (1998)] [hep-ex/9805021];Phys. Rev. Lett. **82**, 2430 (1999) [hep-ex/9812011];Phys. Rev. Lett. **86**, 5651 (2001) [hep-ex/0103032];Phys. Lett. B **539**, 179 (2002) [hep-ex/0205075];Phys. Rev. D **69**, 011104 (2004) [hep-ex/0309011].

[31] Q. R. Ahmad *et al.* [SNO Collaboration], Phys. Rev. Lett. **87**, 071301 (2001) [nucl-ex/0106015]; Phys. Rev. C **75**, 045502 (2007) [nucl-ex/0610020].

[32] C. Arpesella *et al.* [Borexino Collaboration], Phys. Rev. Lett. **101**, 091302 (2008) [arXiv:0805.3843 [astro-ph]].

[33] J. N. Abdurashitov *et al.* [SAGE Collaboration], J. Exp. Theor. Phys. **95**, 181 (2002) [Zh. Eksp. Teor. Fiz. **122**, 211 (2002)] [astro-ph/0204245].

[34] W. Hampel *et al.* [GALLEX Collaboration], Phys. Lett. B **447**, 127 (1999).

[35] M. Altmann *et al.* [GNO Collaboration], Phys. Lett. B **490**, 16 (2000) [hep-ex/0006034].

[36] Q. R. Ahmad *et al.* [SNO Collaboration], Phys. Rev. Lett. **89**, 011301 (2002) [nucl-ex/0204008]; Phys. Rev. Lett. **89**, 011302 (2002) [nucl-ex/0204009]; Phys. Rev. Lett. **101** (2008) 111301 [arXiv:0806.0989 [nucl-ex]].

[37] Y. Ashie *et al.* [Super-Kamiokande Collaboration], Phys. Rev. Lett. **93**, 101801 (2004) [hep-ex/0404034].

[38] S. H. Ahn *et al.* [K2K Collaboration], Phys. Lett. B **511**, 178 (2001) [hep-ex/0103001];Phys. Rev. Lett. **90**, 041801 (2003) [hep-ex/0212007]; Phys. Rev. Lett. **93**, 051801 (2004) [hep-ex/0402017]; E. Aliu *et al.* [K2K Collaboration], Phys. Rev. Lett. **94**, 081802 (2005) [hep-ex/0411038].

[39] K. Abe *et al.* [T2K Collaboration], Phys. Rev. Lett. **107**, 041801 (2011) [arXiv:1106.2822 [hep-ex]]; Phys. Rev. D **85**, 031103 (2012) [arXiv:1201.1386 [hep-ex]]; Phys. Rev. Lett. **112**, 061802 (2014) [arXiv:1311.4750 [hep-ex]].

[40] P. Adamson *et al.* [MINOS Collaboration], Phys. Rev. Lett. **101**, 131802 (2008) [arXiv:0806.2237 [hep-ex]]; Phys. Rev. Lett. **103**, 261802 (2009) [arXiv:0909.4996 [hep-ex]]; Phys. Rev. Lett. **106**, 181801 (2011) [arXiv:1103.0340 [hep-ex]]; Phys. Rev. Lett. **107**, 021801 (2011) [arXiv:1104.0344 [hep-ex]];

[41] P. Adamson *et al.* [MINOS Collaboration], Phys. Rev. Lett. **110**, no. 25, 251801 (2013) [arXiv:1304.6335 [hep-ex]].

[42] Y. Declais, J. Favier, A. Metref, H. Pessard, B. Achkar, M. Avenier, G. Bagieu and R. Brissot *et al.*, Nucl. Phys. B **434**, 503 (1995); F. Boehm, J. Busenitz, B. Cook, G. Gratta, H. Henrikson, J. Kornis, D. Lawrence and K. B. Lee *et al.*, Phys. Rev. D **64**, 112001 (2001) [hep-ex/0107009]; M. Apollonio *et al.* [CHOOZ Collaboration], Phys. Lett. B **466**, 415 (1999) [hep-ex/9907037].

[43] M. Apollonio *et al.* [CHOOZ Collaboration], Phys. Lett. B **420**, 397 (1998) [hep-ex/9711002]; Phys. Lett. B **466**, 415 (1999) [hep-ex/9907037]; Eur. Phys. J. C **27**, 331 (2003) [hep-ex/0301017].

[44] S. Abe *et al.* [KamLAND Collaboration], Phys. Rev. Lett. **100**, 221803 (2008) [arXiv:0801.4589 [hep-ex]].

[45] B. Aharmim *et al.* [SNO Collaboration], Phys. Rev. C **81**, 055504 (2010) [arXiv:0910.2984 [nucl-ex]].

[46] P. Adamson *et al.* [MINOS Collaboration], Phys. Rev. Lett. **107**, 181802 (2011) [arXiv:1108.0015 [hep-ex]].

[47] Y. Abe *et al.* [DOUBLE-CHOOZ Collaboration], Phys. Rev. Lett. **108**, 131801 (2012) [arXiv:1112.6353 [hep-ex]].

[48] F. P. An *et al.* [DAYA-BAY Collaboration], Phys. Rev. Lett. **108**, 171803 (2012) [arXiv:1203.1669 [hep-ex]].

[49] J. K. Ahn *et al.* [RENO Collaboration], Phys. Rev. Lett. **108**, 191802 (2012) [arXiv:1204.0626 [hep-ex]].

[50] F. P. An *et al.* [Daya Bay Collaboration], Phys. Rev. Lett. **112**, 061801 (2014) [arXiv:1310.6732 [hep-ex]].

[51] P. Adamson *et al.* [MINOS Collaboration], Phys. Rev. Lett. **106**, 181801 (2011) [arXiv:1103.0340 [hep-ex]].

[52] G. L. Fogli, E. Lisi, A. Marrone, A. Palazzo and A. M. Rotunno, Phys. Rev. Lett. **101**, 141801 (2008) [arXiv:0806.2649 [hep-ph]]; Phys. Rev. D **84**, 053007 (2011) [arXiv:1106.6028 [hep-ph]].

[53] F. Capozzi, G. L. Fogli, E. Lisi, A. Marrone, D. Montanino and A. Palazzo, Phys. Rev. D **89**, 093018 (2014) [arXiv:1312.2878 [hep-ph]].

[54] P. A. R. Ade *et al.* [Planck Collaboration], arXiv:1303.5076 [astro-ph.CO].

[55] B. Kayser, F. Gibrat-Debu and F. Perrier, World Sci. Lect. Notes Phys. **25**, 1 (1989).

[56] P. Minkowski, Phys. Lett. B **67** (1977) 421; T. Yanagida, in *Proceedings of the Workshop on the Unified Theory and the Baryon Number in the Universe*, eds. O. Sawada et al., (KEK Report 79-18, Tsukuba, 1979), p. 95; M. Gell-Mann, P. Ramond and R. Slansky, in *Supergravity*, eds. P. van Nieuwenhuizen et al., (North-Holland, 1979), p. 315; S.L. Glashow, in *Quarks and Leptons*, Cargèse, eds. M. L évy et al., (Plenum, 1980), p. 707; R. N. Mohapatra and G. Senjanović, Phys. Rev. Lett. **44** (1980) 912.

[57] W. Konetschny and W. Kummer, Phys. Lett. B **70**, 433 (1977); J. Schechter and J. W. F. Valle, Phys. Rev. D **22**, 2227 (1980); T. P. Cheng and L. -F. Li, Phys. Rev. D **22**, 2860 (1980); G. Lazarides, Q. Shafi and C. Wetterich, Nucl. Phys. B **181**, 287 (1981); R. N. Mohapatra and G. Senjanovic, Phys. Rev. D **23**, 165 (1981).

[58] R. Foot, H. Lew, X. G. He and G. C. Joshi, Z. Phys. C **44**, 441 (1989).

[59] L. Wolfenstein, Phys. Lett. B **107**, 77 (1981).

[60] M. Auger *et al.* [EXO Collaboration], Phys. Rev. Lett. **109**, 032505 (2012) [arXiv:1205.5608 [hep-ex]].

[61] W. Rodejohann, J. Phys. G **39**, 124008 (2012) [arXiv:1206.2560 [hep-ph]].

[62] Z. -z. Xing, Phys. Rev. D **68**, 053002 (2003) [hep-ph/0305195].

[63] E. Komatsu *et al.* [WMAP Collaboration], Astrophys. J. Suppl. **192**, 18 (2011) [arXiv:1001.4538 [astro-ph.CO]].

[64] A. D. Sakharov, Pisma Zh. Eksp. Teor. Fiz. **5**, 32 (1967) [JETP Lett. **5**, 24 (1967)] [Sov. Phys. Usp. **34**, 392 (1991)] [Usp. Fiz. Nauk **161**, 61 (1991)].

[65] M. Dine and A. Kusenko, Rev. Mod. Phys. **76**, 1 (2003) [hep-ph/0303065]; J. M. Cline, hep-ph/0609145; S. Davidson, E. Nardi and Y. Nir, Phys. Rept. **466**, 105 (2008) [arXiv:0802.2962 [hep-ph]].

[66] M. Fukugita and T. Yanagida, Phys. Lett. B **174**, 45 (1986).

[67] J. A. Harvey and M. S. Turner, Phys. Rev. D **42**, 3344 (1990).

[68] G. F. Giudice, A. Notari, M. Raidal, A. Riotto and A. Strumia, Nucl. Phys. B **685**, 89 (2004) [hep-ph/0310123].

[69] S. Blanchet and P. Di Bari, New J. Phys. **14**, 125012 (2012) [arXiv:1211.0512 [hep-ph]].

[70] See e.g., M. Hirsch, D. Meloni, S. Morisi, S. Pastor, E. Peinado, J. W. F. Valle, A. Adulpravitchai and D. Aristizabal Sierra *et al.*, arXiv:1201.5525 [hep-ph].

[71] P. F. Harrison, D. H. Perkins and W. G. Scott, Phys. Lett. B **530**, 167 (2002) [hep-ph/0202074].

[72] F. Vissani, hep-ph/9708483; V. D. Barger, S. Pakvasa, T. J. Weiler and K. Whisnant, Phys. Lett. B **437**, 107 (1998) [hep-ph/9806387]; A. J. Baltz, A. S. Goldhaber and M. Goldhaber, Phys. Rev. Lett. **81**, 5730 (1998) [hep-ph/9806540].

[73] C. H. Albright, A. Dueck and W. Rodejohann, Eur. Phys. J. C **70**, 1099 (2010) [arXiv:1004.2798 [hep-ph]].

[74] A. Datta, F. S. Ling and P. Ramond, Nucl. Phys. B **671**, 383 (2003) [hep-ph/0306002]; Y. Kajiyama, M. Raidal and A. Strumia, Phys. Rev. D **76**, 117301 (2007) [arXiv:0705.4559 [hep-ph]]; L. L. Everett and A. J. Stuart, Phys. Rev. D **79**, 085005 (2009) [arXiv:0812.1057 [hep-ph]].

[75] W. Rodejohann, Phys. Lett. B **671**, 267 (2009) [arXiv:0810.5239 [hep-ph]]; A. Adulpravitchai, A. Blum and W. Rodejohann, New J. Phys. **11**, 063026 (2009) [arXiv:0903.0531 [hep-ph]].

[76] J. Barry and W. Rodejohann, Phys. Rev. D **81**, 093002 (2010) [Erratum-ibid. D **81**, 119901 (2010)] [arXiv:1003.2385 [hep-ph]]; S. F. King, JHEP **1101**, 115 (2011) [arXiv:1011.6167 [hep-ph]].

[77] S. Antusch, J. Kersten, M. Lindner, M. Ratz and M. A. Schmidt, JHEP **0503**, 024 (2005) [hep-ph/0501272].

[78] S. Antusch, S. F. King and M. Malinsky, Phys. Lett. B **671**, 263 (2009) [arXiv:0711.4727 [hep-ph]]; JHEP **0805**, 066 (2008) [arXiv:0712.3759 [hep-ph]].

[79] S. Antusch and S. F. King, Phys. Lett. B **631**, 42 (2005) [hep-ph/0508044]; S. Boudjemaa and S. F. King, Phys. Rev. D **79**, 033001 (2009) [arXiv:0808.2782 [hep-ph]].

[80] J. Beringer *et al.* [Particle Data Group Collaboration], Phys. Rev. D **86**, 010001 (2012).

[81] P. F. Harrison and W. G. Scott, Phys. Lett. B **547**, 219 (2002) [hep-ph/0210197].

[82] Z.-Z. Xing, Phys. Rev. D **78**, 011301 (2008) [arXiv:0805.0416 [hep-ph]].

[83] G. L. Fogli, E. Lisi, A. Marrone, D. Montanino, A. Palazzo and A. M. Rotunno, Phys. Rev. D **86**, 013012 (2012) [arXiv:1205.5254 [hep-ph]].

[84] Z.-Z. Xing, Phys. Lett. B **696**, 232 (2011) [arXiv:1011.2954 [hep-ph]].

[85] Y. Abe *et al.* [Double Chooz Collaboration], Phys. Lett. B **723**, 66 (2013) [arXiv:1301.2948 [hep-ex]].

[86] P. H. Frampton, S. L. Glashow and T. Yanagida, Phys. Lett. B **548**, 119 (2002) [hep-ph/0208157].

[87] K. Harigaya, M. Ibe and T. T. Yanagida, Phys. Rev. D **86**, 013002 (2012) [arXiv:1205.2198 [hep-ph]].

[88] G. C. Branco, D. Emmanuel-Costa, M. N. Rebelo and P. Roy, Phys. Rev. D **77**, 053011 (2008) [arXiv:0712.0774 [hep-ph]].

[89] M. Randhawa, G. Ahuja and M. Gupta, Phys. Rev. D **65**, 093016 (2002) [hep-ph/0203109]; Z. -z. Xing and H. Zhang, Phys. Lett. B **569**, 30 (2003) [hep-ph/0304234]; K. Matsuda and H. Nishiura, Phys. Rev. D **74**, 033014 (2006) [hep-ph/0606142]; G. Ahuja, S. Kumar, M. Randhawa, M. Gupta and S. Dev, Phys. Rev. D **76**, 013006 (2007) [hep-ph/0703005 [HEP-PH]]; S. Dev, S. Kumar, S. Verma, S. Gupta and R. R. Gautam, Eur. Phys. J. C **72**, 1940 (2012) [arXiv:1203.1403 [hep-ph]]; J. Barranco, D. Delepine and L. Lopez-Lozano, Phys. Rev. D **86**, 053012 (2012) [arXiv:1205.0859 [hep-ph]]; M. Gupta and G. Ahuja, Int. J. Mod. Phys. A **26**, 2973 (2011) [arXiv:1206.3844 [hep-ph]]; B. Adhikary and P. Roy, Adv. High Energy Phys. **2013**, 324756 (2013) [arXiv:1211.0371 [hep-ph]]; S. Choubey, W. Rodejohann and P. Roy, Nucl. Phys. B **808**, 272 (2009) [Erratum-ibid. **818**, 136 (2009)] [arXiv:0807.4289 [hep-ph]]; B. Adhikary, A. Ghosal and P. Roy, JHEP **0910**, 040 (2009) [arXiv:0908.2686 [hep-ph]]; B. Adhikary, M. Chakraborty and A. Ghosal, Phys. Rev. D **86**, 013015 (2012) [arXiv:1205.1355 [hep-ph]].

[90] E. Ma, Phys. Rev. D **71**, 111301 (2005) [hep-ph/0501056].

[91] J. R. Ellis and S. Lola, Phys. Lett. B **458**, 310 (1999) [hep-ph/9904279]; P. H. Chankowski and S. Pokorski, Int. J. Mod. Phys. A **17**, 575 (2002) [hep-ph/0110249]; J. w. Mei and Z. z. Xing, Phys. Rev. D **69**, 073003 (2004) [hep-ph/0312167].

[92] W. Grimus, A. S. Joshipura, L. Lavoura and M. Tanimoto, Eur. Phys. J. C **36**, 227 (2004) [hep-ph/0405016].

[93] T. Araki, J. Heeck and J. Kubo, JHEP **1207**, 083 (2012) [arXiv:1203.4951 [hep-ph]].

[94] For texture zeros in the light neutrino mass matrix, see
P. H. Frampton, S. L. Glashow and D. Marfatia, Phys. Lett. B **536**, 79 (2002) [hep-ph/0201008]; Z. -z. Xing, Phys. Lett. B **530**, 159 (2002) [hep-ph/0201151]; H. Fritzsch, Z. -z. Xing and S. Zhou, JHEP **1109**, 083 (2011) [arXiv:1108.4534 [hep-ph]]; Z. -z. Xing, Phys. Rev. D **69**, 013006 (2004) [hep-ph/0307007]; A. Merle and W. Rodejohann, Phys. Rev. D **73**, 073012 (2006) [hep-ph/0603111]; E. I. Lashin and N. Chamoun, Phys. Rev. D **85**, 113011 (2012) [arXiv:1108.4010 [hep-ph]]. P. O. Ludl, S. Morisi and E. Peinado, Nucl. Phys. B **857**, 411 (2012) [arXiv:1109.3393 [hep-ph]].

[95] For cofactor zeros in the light neutrino mass matrix, see
L. Lavoura, Phys. Lett. B **609**, 317 (2005) [hep-ph/0411232]; E. I. Lashin and N. Chamoun, Phys. Rev. D **78**, 073002 (2008) [arXiv:0708.2423 [hep-ph]]; E. I. Lashin and N. Chamoun, Phys. Rev. D **80**, 093004 (2009) [arXiv:0909.2669 [hep-ph]]; S. Dev, S. Verma, S. Gupta and R. R. Gautam, Phys. Rev. D **81**, 053010 (2010) [arXiv:1003.1006 [hep-ph]]; S. Dev, S. Gupta, R. R. Gautam and L. Singh, Phys. Lett. B **706**, 168 (2011) [arXiv:1111.1300 [hep-ph]].

[96] J. Liao, D. Marfatia and K. Whisnant, Phys. Rev. D **87**, 073013 (2013) [arXiv:1302.2372 [hep-ph]].

[97] P. H. Frampton, S. L. Glashow and D. Marfatia, Phys. Lett. B **536**, 79 (2002) [hep-ph/0201008]; Z.-z. Xing, Phys. Lett. B **530**, 159 (2002) [hep-ph/0201151]; Phys. Lett. B **539**, 85 (2002) [hep-ph/0205032];

[98] H. Fritzsch, Z. -z. Xing and S. Zhou, JHEP **1109**, 083 (2011) [arXiv:1108.4534 [hep-ph]]; P. O. Ludl, S. Morisi and E. Peinado, Nucl. Phys. B **857**, 411 (2012) [arXiv:1109.3393 [hep-ph]].

[99] L. Lavoura, Phys. Lett. B **609**, 317 (2005) [hep-ph/0411232]; S. Verma, Nucl. Phys. B **854**, 340 (2012) [arXiv:1109.4228 [hep-ph]]; S. Dev, S. Gupta, R. R. Gautam and L. Singh, Phys. Lett. B **706**, 168 (2011) [arXiv:1111.1300 [hep-ph]]; T. Araki, J. Heeck and J. Kubo, JHEP **1207**, 083 (2012) [arXiv:1203.4951 [hep-ph]];

[100] E. I. Lashin and N. Chamoun, Phys. Rev. D **78**, 073002 (2008) [arXiv:0708.2423 [hep-ph]].

[101] S. Dev, S. Verma, S. Gupta and R. R. Gautam, Phys. Rev. D **81**, 053010 (2010) [arXiv:1003.1006 [hep-ph]].

[102] P. A. R. Ade *et al.* [Planck Collaboration], arXiv:1303.5076 [astro-ph.CO].

[103] D. Meloni, A. Meroni and E. Peinado, Phys. Rev. D **89**, 053009 (2014) [arXiv:1401.3207 [hep-ph]].

[104] F. P. An *et al.* [Daya Bay Collaboration], Chin. Phys. C **37**, 011001 (2013) [arXiv:1210.6327 [hep-ex]].

[105] C. Adams *et al.* [LBNE Collaboration], arXiv:1307.7335 [hep-ex].

[106] E. I. Lashin and N. Chamoun, Phys. Rev. D **85**, 113011 (2012) [arXiv:1108.4010 [hep-ph]].

[107] S. Dev, R. R. Gautam and L. Singh, Phys. Rev. D **87**, 073011 (2013) [arXiv:1303.3092 [hep-ph]].

[108] R. N. Mohapatra and W. Rodejohann, Phys. Lett. B **644**, 59 (2007) [hep-ph/0608111]; A. Blum, R. N. Mohapatra and W. Rodejohann, Phys. Rev. D **76**, 053003 (2007) [arXiv:0706.3801 [hep-ph]]; A. S. Joshipura and W. Rodejohann, Phys. Lett. B **678**, 276 (2009) [arXiv:0905.2126 [hep-ph]]; B. Adhikary, M. Chakraborty and A. Ghosal, Phys. Rev. D **86**, 013015 (2012) [arXiv:1205.1355 [hep-ph]]; M. Yasue, Phys. Rev. D **86**, 116011 (2012) [arXiv:1210.7448 [hep-ph]].

[109] K. Abe *et al.* [T2K Collaboration],Nucl. Instrum. Meth. A **659**, 106 (2011) [arXiv:1106.1238 [physics.ins-det]].

[110] R. B. Patterson [NOvA Collaboration], Nucl. Phys. Proc. Suppl. **235-236**, 151 (2013) [arXiv:1209.0716 [hep-ex]].

[111] T. Akiri *et al.* [LBNE Collaboration], arXiv:1110.6249 [hep-ex].

[112] PINGU Collaboration, arXiv:1306.5846 [astro-ph.IM].

[113] N. K. Mondal [INO Collaboration], Pramana **79**, 1003 (2012).

[114] S. Kettell, J. Ling, X. Qian, M. Yeh, C. Zhang, C. -J. Lin, K. -B. Luk and R. Johnson *et al.*, arXiv:1307.7419 [hep-ex].

[115] R. N. Cahn, D. A. Dwyer, S. J. Freedman, W. C. Haxton, R. W. Kadel, Y. .G. Kolomensky, K. B. Luk and P. McDonald *et al.*, arXiv:1307.5487 [hep-ex].

[116] A. Osipowicz *et al.* [KATRIN Collaboration], hep-ex/0109033.

[117] R. de Putter, O. Zahn and E. V. Linder, Phys. Rev. D **79**, 065033 (2009) [arXiv:0901.0916 [astro-ph.CO]].

[118] J. Liao, D. Marfatia and K. Whisnant, Phys. Rev. D **87**, 013003 (2013) [arXiv:1205.6860 [hep-ph]].

[119] J. Liao, D. Marfatia and K. Whisnant, Phys. Rev. D **88**, 033011 (2013) [arXiv:1306.4659 [hep-ph]].

[120] J. Liao, D. Marfatia and K. Whisnant, JHEP **1409**, 013 (2014) [arXiv:1311.2639 [hep-ph]].

[121] J. Liao, D. Marfatia and K. Whisnant, Phys. Rev. D **89**, no. 1, 013009 (2014) [arXiv:1308.1368 [hep-ph]].

[122] V. Barger, D. Marfatia and K. Whisnant, Phys. Rev. D **65**, 073023 (2002) [hep-ph/0112119].

[123] J. Liao, D. Marfatia and K. Whisnant, arXiv:1407.0352 [hep-ph].

[124] V. Barger, D. Marfatia and K. Whisnant, Phys. Rev. D **66**, 053007 (2002) [hep-ph/0206038]; Phys. Lett. B **560**, 75 (2003) [hep-ph/0210428].

[125] P. Adamson, J. A. B. Coelho, G. S. Davies, J. J. Evans, P. Guzowski, A. Habig, J. Hartnell and A. Holin *et al.*, arXiv:1307.5918 [physics.ins-det].